LBL-35022
UC-404

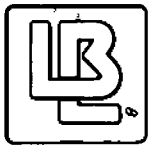

Lawrence Berkeley Laboratory
UNIVERSITY OF CALIFORNIA

Materials Sciences Division

Low-Frequency Noise in High-T_c Superconductor Josephson Junctions, SQUIDs, and Magnetometers

A.H. Miklich
(Ph.D. Thesis)

May 1994

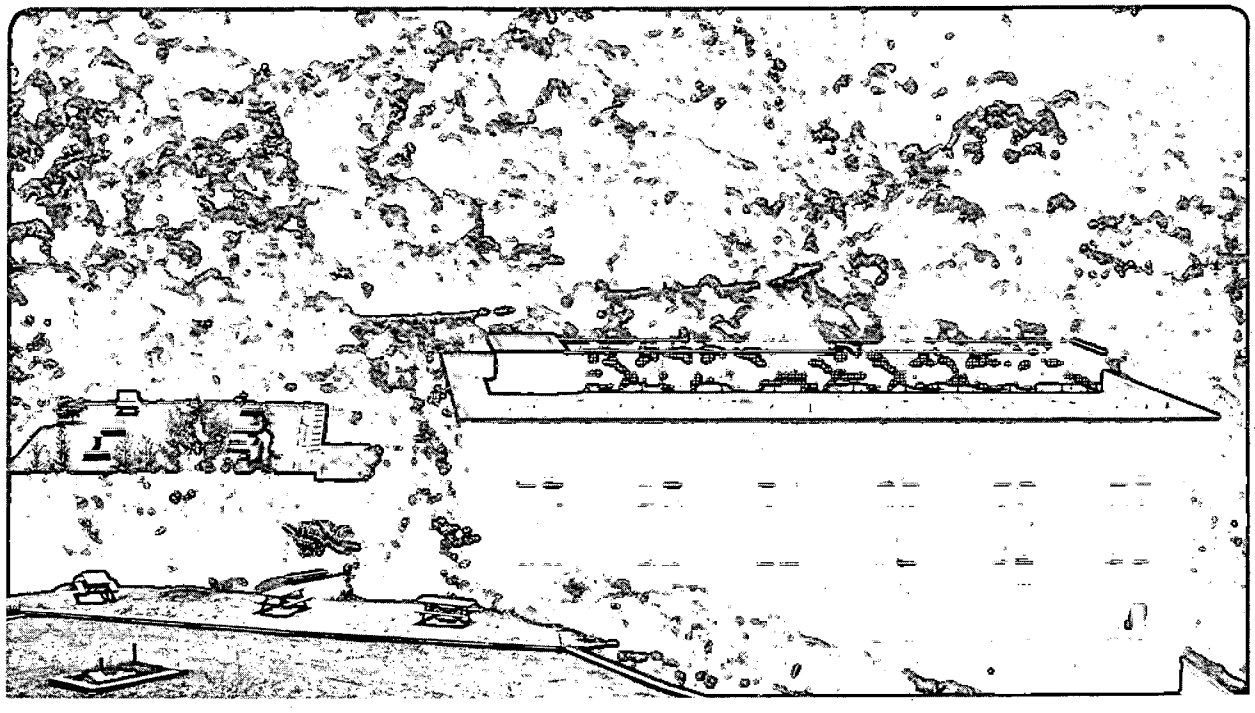

Prepared for the U.S. Department of Energy under Contract Number DE-AC03-76SF00098

DISCLAIMER

LBL-35022

Low-Frequency Noise in High-T_c Superconductor Josephson Junctions, SQUIDs, and Magnetometers

Andrew Hostetler Miklich
(Ph.D. Thesis)

Department of Physics, University of California
and
Materials Science Division,
Lawrence Berkeley Laboratory,
University of California,
Berkeley, CA 94720

May 1994

This work was supported by the California Competitive Technology Program and by the Director, Office of Energy Research, Office of Basic Energy Sciences, Materials Sciences Division of the U.S. Department of Energy under contract number DE-AC03-76SF00098.

Low-Frequency Noise in
High-T_c Superconductor Josephson Junctions, SQUIDs, and Magnetometers

by

Andrew Hostetler Miklich

Abstract

Low-Frequency Noise in High-T_c Superconductor Josephson Junctions, SQUIDs, and Magnetometers

by

Andrew Hostetler Miklich

Doctor of Philosophy in Physics

University of California at Berkeley

Professor John Clarke, Chair

The design and performance of high-T_c dc superconducting quantum interference devices (SQUIDs), the junctions that comprise them, and magnetometers made from them are described, with special attention paid to sources of 1/f noise. Biepitaxial junctions are found to have large levels of critical current fluctuations which make them unsuitable for low-noise SQUIDs. This noise suggests a poorly connected interface at the grain boundary junction. SQUIDs from bicrystal junctions, in contrast, have levels of critical current noise that are controllable using bias current reversal techniques which leave the noise white down to frequencies of a few Hz. A SQUID with an energy resolution of 1.5×10^{-30} J Hz^{-1} at 1 Hz is reported. Magnetometers in which a $(9\text{ mm})^2$ pickup loop is directly coupled to a SQUID body have achieved field resolutions of 93 fT $Hz^{-1/2}$ down to frequencies below 1 Hz, improving to 39 fT $Hz^{-1/2}$ at 1 Hz with the addition of a 50-mm-diameter single-turn flux transformer. Although the performance of these devices is sufficient for single-channel biomagnetometry or geophysical studies, their relatively poor coupling to the pickup loop makes it difficult to satisfy the competing goals of high field resolution and small detector size necessary for multichannel biomagnetic imaging. Improved coupling is demonstrated by the use of multiturn-input-coil flux transformers, and a resolution of 35 fT $Hz^{-1/2}$ in the white noise region is reported with a $(10\text{ mm})^2$ pickup loop. However, additional 1/f noise from the processed multilayer structures in the transformer limits the resolution at 1 Hz to 114 fT $Hz^{-1/2}$. High-T_c SQUIDs are shown

to exhibit additional 1/f noise when they are cooled in a nonzero static magnetic field because of the additional flux vortices trapped in the film, with the noise power at 1 Hz typically increasing by a factor of 10-20 in a field of 0.05 mT (0.5 G). Finally, a SQUID-based voltmeter with a resolution of 9.2 pV $Hz^{-1/2}$ at 10 Hz (24 pV $Hz^{-1/2}$ at 1 Hz) is described.

John Clarke — April 21, 1994

Chair — Date

Table of Contents

List of Commonly used Symbols and Abbreviations

Φ_0	the superconducting flux quantum = h/2e
k_B	Boltzmann's constant
YBCO	$YBa_2Cu_3O_{7-x}$
STO	$SrTiO_3$
GBJ	grain boundary junction
RSJ	resistively shunted junction
SQUID	superconducting quantum interference device
I_0 (or I_c)	critical current of a single junction
R (or R_N)	asymptotic resistance of a single junction
L	SQUID self inductance
β	SQUID inductance parameter $\equiv 2I_0L/\Phi_0$
S_Φ	flux noise power spectral density (or "flux noise power")
ε	energy resolution $\equiv S_\Phi/2L$ (L is the SQUID self inductance)
$S_B^{1/2}$	rms magnetic field resolution

Acknowledgements

First and foremost I wish to acknowledge my advisor, John Clarke, for giving me the chance to work on a timely experiment in an exciting field, and for his many insightful comments and useful suggestions.

With the exception of the noise in single junctions experiment and the picovoltmeter, this project has been a team effort. Often it is difficult in hindsight to separate out which parts of a given experiment were performed by which team members, but I shall endeavor to give proper credit to individuals at the appropriate places. At some time or another I have benefited from discussions with almost every member of the Clarke group, and many members of the extended family of former Clarke group researchers, of whom a few are listed below. Fred Wellstood and Jack Kingston were with the high-T_c effort from the beginning and together they pioneered the multilayer crossover technology necessary to make the flux transformers in the magnetometers I measured. Additionally, Fred served as my first mentor and taught me more about SQUIDs and life in general than I think he ever realized. Du Quan also helped with the fabrication of the devices described herein during his brief stay with the Clarke group. Mark Colclough joined the group after I did and provided me with some excellent hands-on training in the world of low-noise measurements and analog electronics. Many of my early experiments (most of which are not presented here) were done while working as an apprentice under Mark. Shortly after the departure of Fred and Jack, the thin-film deposition and multilayer processing were put in the capable hands of Frank Ludwig and David Nemeth. Gene Dantsker also joined the group at this time and has assisted with both the fabrication and measurement of the devices. I wish to especially acknowledge the contributions of Dieter Koelle who joined the group at about this time as well. Much of the later data on bicrystal SQUIDs, flux transformers, directly coupled magnetometers, and the magnetic field dependence of the noise was taken jointly with him. I also wish to acknowledge the participation of visiting

graduate students Lise Sagdahl and Rasmus Kromann in SQUID measurement and fabrication, respectively.

I have been fortunate as a graduate student to have benefited from the presence (albeit brief) of many postdoctoral researchers who gave me the opportunity to learn about physics while working on their projects. Chief among these were Philippe Lerch and Didier Robbes (who was primarily responsible for the electric spike method of making junctions I briefly mention). Nancy Missert was another postdoc to whom I am thankful for interesting discussions about x-ray crystallography and other things. Both Nancy and Mark Ferrari deserve special thanks for lending us time in their screen rooms during the early days of these experiments.

Many of these experiments have involved collaborations with members of other organizations. I thank Nate Newman of Conductus, Inc., for providing me with some grainy sputtered films with which we made our first SQUIDs. Our first magnetometers were made with thallium-based SQUIDs provided by Lincoln Bourne, Albert Cardona, W. L. Olson, and M. M. Eddy of Superconductor Technologies, Inc. Shortly thereafter we started using biepitaxial YBCO SQUIDs provided by Kookrin Char and Greg Zaharchuk of Conductus, Inc. Kookrin also provided the biepitaxial junctions for the experiments I did on critical current noise in single junctions. Kookrin and Ward Ruby (also of Conductus) were responsible as well for the 2-inch diameter single turn flux transformers which were used in our most sensitive magnetometers. The determination of the magnetic field dependence of the 1/f noise would not have been possible without the superconducting tube provided by Neil Alford and Tim Button of ICI Superconductors.

Special thanks go to Prof. Gene Commins and Steve Ross for lending us the high-permeability shields which enabled us to do the human magnetocardiogram experiment. Likewise, I wish to thank Prof. Erwin Hahn and Larry Wald for letting us use a screen room in their laboratory while we were finding a home for the high-T_c experiments.

The Physics Department at the University of California is in the fortunate position

of having available to it the expert assistance of a number of fine technicians. I have profited immensely from many fruitful discussions and the able assistance of both the electronics shop (especially John Davis and Levern Garner) and the machine shop (with special thanks to Andy Brocato for many fine welds, often done at a moment's notice, and for much good advice.) In particular I wish to thank Al Daft who ran the graduate student machine shop and taught me most of what I know about machining.

The hard work of John Clarke's administrative assistant, Barbara Salisbury, in preparing manuscripts and camera ready copies of papers is greatly appreciated.

The photolithographic processing described here was performed at the Electronics Research Laboratory of the Electrical Engineering and Computer Sciences Department (the "microlab"). I am thankful for the expert leadership of the facility provided by Katalin Voros, and for much useful advice, assistance, and effort provided by the members of the staff (in particular Dave Hebert and Marilyn Kushner).

Mats Gustafsson and Mark Ferrari deserve special thanks for advising me on the production of this manuscript.

I am grateful for the financial support of the Fannie and John Hertz Foundation, which sponsored me as a fellow through my first five years as a graduate student. This work was supported by the Director, Office of Energy Research, Office of Basic Energy Sciences, Materials Sciences Division of the U.S. Department of Energy under contract No. DE-AC03-76SF00098, and the California Competitive Technology Program.

The text portion of this document was prepared using MicroSoft Word version 4.0 on an Apple Macintosh IIsi computer, and printed on an Apple Personal LaserWriter printer.

Chapter I: Introduction and Overview

The recent discovery of superconductivity in the La-Ba-Cu-O system with transition temperatures, T_c, much higher than previously reported [BEM86], and the subsequent discovery of $YBa_2Cu_3O_{7-x}$ with T_c above the boiling point of nitrogen [WAT87], has sparked a frenzy of activity in both the pure and applied sciences. At a basic level there is considerable interest in understanding the mechanism behind superconductivity at such high temperatures. From a technological point of view, the prospect of superconducting devices operating without cumbersome and expensive liquid helium cryogenic systems has attracted unparalleled investment to this field.

The goal of the high-T_c project in Prof. Clarke's lab, of which this dissertation is a product, has been to make magnetometers based on dc superconducting quantum interference devices (SQUIDs) with very high field resolution at low frequencies (of order 1 Hz). The prototypical instrument in which we have envisioned using our detectors would be an array of sensors suspended just above a human patient to measure the magnetic activity of (for example) the heart or brain. By simultaneously recording the magnetic field at a large number of points (~30-100) it is possible (given certain assumptions) to work backwards to reconstruct the patterns of electrical current in the organ of interest [WIK81, ROM89, EHL81]. The accuracy with which this inversion can be done depends on two factors: the field resolution of the sensors, and the number of sensors over the organ in question. One sees immediately that the goals for our detectors will be low noise and small size. Several companies are presently marketing biomagnetic imagers using conventional ("low-T_c") superconductors in which the SQUID magnetometers typically have resolutions of better than 10 fT $Hz^{-1/2}$ at frequencies down to 1 Hz and occupy an area less than $(25\ mm)^2$ [VBB93, DDF93, YMM93, FPP93, CGL93, HDB91, AHK91, KCD91]. In the remainder of this section I will give a brief introduction to SQUIDs and SQUID magnetometers, and then outline the work I report on

in this dissertation.

A Review of SQUID Concepts[1]

The heart of the magnetometer is the dc SQUID shown schematically in Fig. 1.1(a). The SQUID is a loop of superconductor, of inductance L, cut in two places by Josephson junctions or weak links. Each junction has a critical current I_0 and a shunting resistance R. (The shunting capacitance shown in Fig. 1.1(a) is assumed to be negligible.) The interference of the wavefunction for the superconducting condensate as it divides between the two junctions causes the maximum zero-voltage current of the SQUID to oscillate with applied flux as shown in Fig. 1.1(b). The period of oscillation is one superconducting flux quantum, $\Phi_0 = h/2e$, where h is Planck's constant and e is the electron charge. In practice, one applies a static bias current to the SQUID and measures the voltage which oscillates periodically with applied flux as shown in Fig. 1.1(c). In this mode of operation, the SQUID acts as a flux-to-voltage transducer with a transfer function V_Φ defined as the maximum slope of the voltage-flux characteristic. Computer simulations [TEC77] show that for an inductance parameter $\beta \equiv 2I_0L/\Phi_0 = 1$, the transfer function is approximately given by R/L. (The same result can also be obtained by considering the screening current in the SQUID loop [CLA93].)

The simplest method of using a dc SQUID is to bias the SQUID with a static flux on the steepest portion of the V-Φ transfer curve and then read out the voltage. Flux feedback can be used to maintain the SQUID at its optimum bias point. At Berkeley, however, we use an ac flux modulation technique which makes the SQUID easier to operate. The static flux bias is set to one of the peaks or troughs in the V-Φ characteristic

---

[1]The basics of the dc SQUID are found in chapter 5 of ref. [DUT81]. John Clarke has written a number of excellent reviews of SQUIDs made of both high-T_c and conventional superconductors, the most recent of which is ref. [CLA93]. Also note the recent book edited by Barone [BAR92] and the fine review article by Ryhänen *et al.* [RSI89].

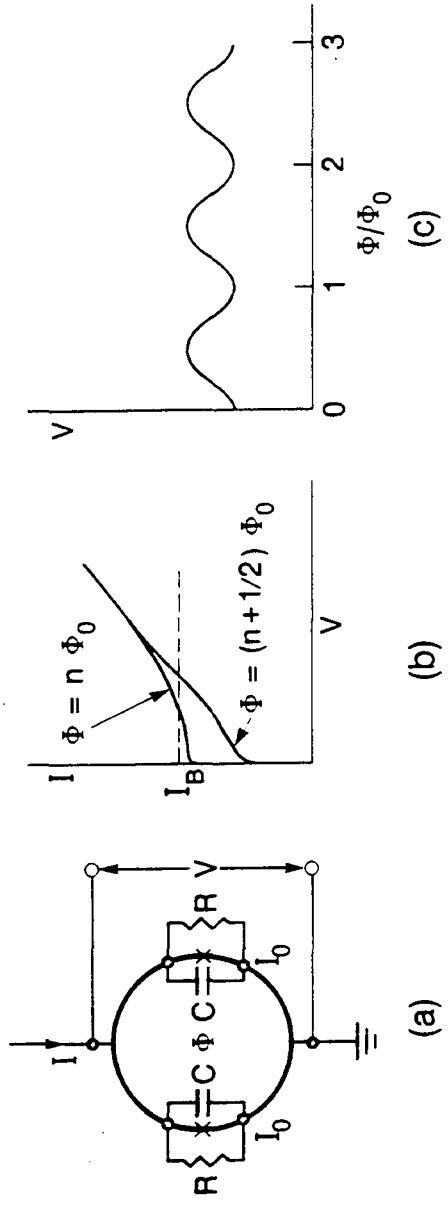

Fig. 1.1 Basic function of a dc SQUID. (a) Schematic representation. (b) I-V characteristics for integral and half-integral numbers of flux quanta threading the SQUID showing the modulation of critical current. I_B is the static biasing current. (c) Voltage-flux characteristic for the SQUID at a static bias current. (From ref. [CLA93].)

in Fig. 1.1(c) (i.e., either $n\Phi_0$ or $(n + 1/2)\Phi_0$). Then an ac squarewave flux of frequency 100 kHz and amplitude $\sim\pm 1/4\ \Phi_0$ is applied to the SQUID. The amplitude is adjusted so that the SQUID sees the steepest part of the V-Φ curve at all times. As long as the static flux remains at a peak or a trough, the V-Φ characteristic looks symmetric with respect to the bias point, so there is no voltage signal at the modulation frequency. If, however, a quasistatic flux is applied to the SQUID thereby shifting the static bias point, then there will be an alternating voltage generated. This alternating voltage is then amplified and demodulated back down to dc, then sent to a flux feedback circuit. It is this fed-back flux that is recorded as the SQUID output. This technique has several advantages: 1) the SQUID voltage can be amplified by a cooled transformer or tank circuit; 2) the signal of interest is moved to frequencies above the 1/f noise in the preamplifier; and 3) there is greater immunity from dc drifts in the amplifiers and current bias. The main disadvantage to this scheme is that the closed loop bandwidth of the system is limited to no more than half the modulation frequency and is typically less than that due to phase shifts in the various amplifiers. (Because of this, and because of the complexity involved with the modulation and demodulation, much progress has been made lately at other labs in developing techniques to read out the SQUID voltage directly. Most of these involve positive flux feedback at the level of the chip to increase V_Φ on one half of the V-Φ characteristic [DCP91].)

The smallest flux that a dc SQUID can measure is determined by noise properties intrinsic to the SQUID itself. The noise contributions of the amplifiers can be made negligible with proper engineering. In this dissertation, I will refer to this minimum detectable flux as the *resolution.* This should not be confused with the *sensitivity* of the instrument which is just the number of volts at the output per unit flux applied at the SQUID, and which can be increased almost arbitrarily by use of more amplifiers. The resolution is usually specified by the flux noise power spectral density, $S_\Phi(f)$, which is the amount of mean square noise power per unit bandwidth at a given frequency, f. At high

frequencies, this noise is frequency independent and is the result of the Nyquist voltages generated in the two resistive shunts in the SQUID. Computer simulations [TEC77] show that for a SQUID with $\beta = 1$ the voltage noise across the SQUID is approximately $16k_BTR$, and the corresponding flux noise is

$$S_\Phi(f) = \frac{16k_BTR}{(V_\Phi)^2} = \frac{16k_BTL^2}{R} \tag{1.1}$$

where I have used $V_\Phi \approx R/L$. It is important to note that this noise is properly described as a noisy SQUID *voltage* and not a noisy *flux*; the flux noise that one measures therefore depends on the magnitude of the transfer function of the SQUID. Experiments on low-T_c SQUIDs generally find excellent agreement with this theory. At low frequencies, however, SQUIDs show excess noise which is usually of the form $1/f^\alpha$ where $\alpha \approx 1$. High-T_c SQUIDs in particular have been plagued from their earliest days with copious amounts of 1/f noise, and it was recognized from the start that this noise would limit the resolution of any device at frequencies of 1 Hz and below.

1/f noise in SQUIDs is known to arise from two distinct processes. First, flux vortices may penetrate the body of the SQUID becoming pinned at places where the order parameter is depressed. These vortices can then hop at random between pinning sites producing a random flux in the SQUID. A vortex which hops between only two sites, with an average lifetime in either site of τ, will produce a flux in the SQUID which alternates between two values randomly in time, a so-called "random telegraph signal" (or RTS). It has been shown that a superposition of RTS sources with different lifetimes can yield a 1/f noise power spectrum if the distribution of lifetimes is logarithmic [DDH79, DUH81]. Mark Ferrari has extensively measured the hopping of flux vortices in unpatterned high-T_c films with a low-T_c SQUID, and has related it to models in which the hopping is due to thermal activation over the barrier between pinning sites [FJW94, FER91].

The other source of 1/f noise in SQUIDs is RTS fluctuations in the critical currents of the junctions. Fortunately, this source of noise can be eliminated by appropriate choice of biasing. To see how this is accomplished, we must recall that since there are two junctions, any arbitrary fluctuation of the critical currents can be thought of as consisting of two modes: a symmetric one in which the junctions fluctuate in phase resulting in a net change in the overall critical current of the SQUID, and an anti-symmetric mode where the junctions fluctuate out of phase creating a circulating current in the SQUID loop. One can think of the effect of the symmetric mode as to move the V-Φ characteristic of Fig. 1.1(c) up and down along the V axis, whereas the anti-symmetric mode moves the characteristic along the Φ axis. The ac flux modulation we use to operate our SQUIDs removes the symmetric noise in the same manner in which it counteracts bias current drifts (the critical current fluctuations are presumed to be much slower than the ac modulation frequency) but does not address the anti-symmetric component which appears as a flux noise in the SQUID. It is possible, however, to remove even this component of noise by using one of a number of techniques (first proposed by Koch *et al.* [KCG83]) in which the bias current is alternated between positive and negative values. The principle underlying all of these techniques is that the circulating current established by the fluctuating critical currents changes direction as the bias current is reversed. Therefore, by alternating the bias current, one changes a noisy quasistatic flux into a noisy amplitude modulation of a carrier signal at the bias current modulation frequency. In other terms, one has mixed the noise up to the bias current modulation frequency which is above the frequency range of interest. Because this technique requires an ac modulation for the bias current as well as the flux, members of the Clarke group often refer to it as "double modulation."

The noise in the SQUID is only one issue to consider in the construction of a magnetometer. SQUIDs made using thin-film technology must be kept small to reduce their inductance which directly effects the white noise in Eq. (1.1). Thus, almost paradoxically we find that the SQUIDs with the best flux resolution often have the worst

field resolution. The usual solution to the dilemma is to couple the SQUID to a superconducting *flux transformer* shown schematically in Fig. 1.2[2]. The flux transformer is a continuous thin-film circuit of superconductor which can be thought of as two parts, a large-area pickup loop and an input coil which is coupled to the SQUID body. The principle of operation is that a weak magnetic field applied uniformly to the flux transformer will produce a large amount of flux in the pickup loop by virtue of its large area. Since the total flux in the flux transformer must be conserved, a supercurrent will be established which will flow into the input coil and thus couple flux to the SQUID. Thus, the total effective sensing area of the magnetometer (flux in the SQUID per unit field applied) is

$$A = A_S \pm A_P \frac{M_i}{L_i + L_P} \tag{1.2}$$

where A_S is the effective area of the bare SQUID (including flux focussing), A_P and L_P are the pickup loop area and inductance respectively, L_i is the input coil inductance and M_i is its mutual inductance to the SQUID. One should note that the sign of the second term depends only on the sense of rotation of the input coil relative to the pickup loop. As the second term usually dominates the first, this is generally a minor consideration. The field resolution of the magnetometer is then $S_B^{1/2} = S_\Phi^{1/2}/A$ where S_Φ is the rms SQUID flux noise. This however assumes that the flux transformer itself adds no noise to the SQUID.

For low-T_c SQUIDs the input coil is usually fabricated as a flat thin-film spiral in a superconducting layer just above the layer containing the SQUID. Ketchen [KET81] has shown that for this geometry the input coil is tightly coupled to the SQUID, and the following limiting expressions are obtained:

$$M_i = n\,L \tag{1.3a}$$

---

[2]An alternative design is the "fractional-turn" SQUID first proposed by Zimmerman [ZIM71] and recently employed for biological imaging by Drung *et al.* [DCP91].

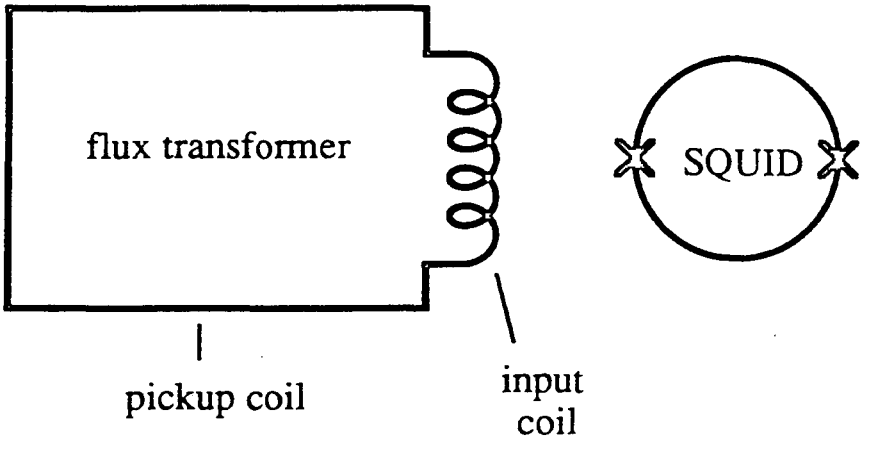

Fig. 1.2 A flux transformer coupled to a SQUID.

$$L_i = n^2 L + L_S. \tag{1.3b}$$

Here n is the number of turns on the input coil, L is the SQUID inductance, and L_S is the parasitic stripline inductance of the input coil on the ground plane provided by the SQUID washer. One sees that the prescription for maximizing A is to increase n, so as to enhance M_i, until L_i becomes as large as L_P. In fact, if one can neglect L_S, it is easy to show that for a given SQUID and pickup loop inductance, A is maximized when n is at its optimal value given by

$$n_{opt} = \sqrt{L_p/L} \tag{1.4}$$

at which point $L_i = L_P$. The total effective area can then be rewritten as

$$A_{opt} = A_S \pm A_P \frac{1}{2}\sqrt{\frac{L}{L_P}}. \tag{1.5}$$

It should be noted that A_P scales as the square of the radius of the pickup loop whereas L_P increases only linearly. Thus, by examining Eq. (1.2), it is clear that one can always increase the field resolution of the magnetometer by increasing the size of the pickup loop, provided the field to be measured remains uniform over the area of the loop. For many applications (such as geophysical surveys using the magnetotelluric effect) this is not unreasonable. However, for the biomagnetic imaging applications outlined above where the detector size is a premium, one wants to optimize the number of turns to achieve the maximum ratio of A/A_P.

Experimental Apparatus

The majority of this dissertation concerns noise measurements made on high-T_c SQUIDs and magnetometers. In this section I describe briefly the equipment used in these measurements. Often other probes were used for simple measurements such as resistance vs. temperature or I-V characteristics. The samples were cooled in one of several

superinsulated dewars which had previously been used for liquid helium experiments. Most of these had fiberglass bodies although one had an aluminum outer body. For the noise measurements, the samples were mounted on one of two probes of similar design. The samples were secured to a fiberglass stage with rubber cement, the type used for pasting up paper documents. This was found to be the best glue for low-temperature work as it would not crack or let go even after several thermal cycles, and yet it was non-permanent and could be removed easily by mechanical action or weak solvents (e.g., ethanol). The stage was permanently attached to a stainless steel tube (0.5 inch O.D., 0.01 inch wall) approximately 1 m long. Wires to the probe stage were threaded through the center of this tube, often in twisted pairs inside Cu-Ni tubes for rf shielding. Most of the wires were small-diameter Cu although occasionally manganin was used. At the top of the tube was an aluminum box with connectors for the wires to the probe. The tube was sent through a brass compression fitting which in turn was soldered into a 2 inch Kwik-Flange plate. The Kwik-Flange was secured to the top of the dewar to make an air-tight seal for the cryogen, and the compression fitting could be loosened to allow the probe to slide up and down in the dewar. In this way I could vary the temperature by adjusting the height of the probe above the level of the liquid cryogen (although temperatures adjusted this way were typically not stable to better than 2 or 3 K over the time required to bias the SQUID and measure the noise). Most of the experiments, however, were done at a fixed temperature of 77 K obtained by lowering the probe to near the bottom of a dewar filled with liquid nitrogen. All of the experiments were conducted in a Cu-mesh screen room in the second basement of Birge Hall where rf interference is minimal.

Magnetic shielding was accomplished with high-permeability cylinders as we were not able to obtain high-T_c superconducting shields whose noise properties were well-characterized. Attached to the stage was a concentric spiral of Co-Netic alloy[3], typically 5 to 10 layers of 0.004- or 0.01-inch-thick material. Although this alloy loses 90% of its

[3]Magnetic Shield Corporation, Bensenville, IL.

permeability at low temperatures, it is desirable to have the cold shield because the probe is not well-secured to the dewar and tends to wobble about. This creates noise if there is a residual field inside the dewar. Outside the dewar (at room temperature) I used one of several high-permeability shields which were available in the lab ranging from one to three concentric cylinders. I estimated the 60 Hz attenuation of these shields to be between several hundred and several thousand depending on the number of cylinders and their size. The residual field, measured with a flux gate magnetometer, was $\lesssim 10^{-7}$ T.

The SQUID control electronics was the standard Berkeley 100 kHz "SQUID box" which was last redesigned in 1980[4]. The 2 kHz bias reversal electronics was new and was designed by me. The 100 kHz signal voltage from the SQUID was amplified by a cold, Cu-wire transformer wound on the yoke of a common audio frequency transformer. A typical turns ratio was 15 which stepped up the SQUID noise above the preamplifier noise, although it generally left the SQUID undermatched to the preamplifier. A second, room-temperature transformer was not used. The modulation coil for the SQUID (which was used to couple the 100 kHz signal, the 2 kHz double modulation signal, the dc flux, and the flux feedback) was a small Cu-wire coil imbedded in the fiberglass stage directly under the SQUID. In addition, each probe had a second Cu-wire coil, typically a 1 to 2 inch square or rectangle, which was intended to provide a uniform magnetic field over both the SQUID and the $(1\ \text{cm})^2$ flux transformer. This was used to determine the field resolution of our devices with the current-to-field calibration of the coil computed analytically or numerically.

Outline of this Work

My dissertation research has been directed at measuring noise (in particular 1/f noise) in high-T_c junctions, SQUIDs, and magnetometers. The research has had two

[4]UCB Electronic Shop drawing number 80-18.

goals. First, I wanted to understand the causes of noise in this new technology and to study it as a means of learning about high-T_c devices and materials. Second, I was curious to see just how far this technology could be pushed and to see if one could actually make usable devices from it. Thus, the tone of the following research often switches from very basic physics to very goal-oriented applications. The account presented here is roughly chronological detailing the development of high-T_c technology from its infancy to its present state.

I begin in chapter 2 with some early work on high-T_c SQUIDs in which the junctions were made using a technique called "biepitaxy". I discuss a detailed study I made of the 1/f noise in single biepitaxial junctions, and then consider some of the shortcomings of this technology. In chapter 3 I discuss junctions and SQUIDs made using the "bicrystal" technique which has become the mainstay of our high-T_c program. In chapter 4 I discuss measurements I made on our earliest flux transformers and the implications of those measurements for high-T_c magnetometers. I briefly detail some of the problems our group has encountered in fabricating quiet multilayer structures before moving on in chapter 5 to discuss magnetometers made without multilayer structures. Chapter 6 discusses the behavior of our high-T_c SQUIDs when operated in static fields the size of the Earth's field, a situation necessary in geophysical applications. Finally, the last chapter concludes with a presentation of a different type of instrument, a SQUID-based voltmeter.

Chapter II: Biepitaxial SQUIDs and Junctions

Assuming one has a method of depositing thin films of high-T_c superconductor, the next thing one needs is a method of making junctions in these thin films. A tremendous amount of work has been done in the past 7 years trying to make junctions with a variety of techniques so vast I cannot begin to list them all. Broadly speaking, all of the methods rely on coupling two regions of superconductor together with one of the following types of intermediaries: damaged superconducting regions, artificial barriers, or grain boundaries. (See section 6.1 of ref. [CLA93] and references therein for an overview.)

Some of the first experiments I participated in as a student concerned making junctions of the first type by applying brief electrical pulses to narrow bridges patterned in otherwise epitaxial superconductor [RMK90]. With some care, this method could controllably reduce the critical current of a single bridge from that of the as-patterned film to some arbitrary value, typically between 10 μA and 10 mA. These junctions typically had I_0R products of ~30 μV at 77 K, and constant-voltage steps were clearly visible on the I-V characteristic when irradiated with microwaves indicating that a periodic current-phase relation had developed. However, we were never able to ascertain the mechanism responsible for the formation of the damaged region, and the I-V curves never accurately replicated the predictions of the resistively shunted junction model [STE68, MCU68] even with thermal noise rounding [AMH69]. Also, a significant number of trials resulted in destroyed junctions, not surprisingly. More importantly, we were never able to reliably extend this technique to the case of the SQUID where one has two junctions in parallel. We often found that any imbalance in the critical currents of the junctions would cause the energy from the pulse to be preferentially deposited in the junction with the lower critical current. A runaway effect would ensue in which one junction would be destroyed while the other was unaffected. After some considerable effort we were never able to produce a working SQUID this way, and the haphazard nature of the process led us to abandon it.

Biepitaxial SQUIDs

Of the three types of junctions outlined above, grain boundaries are usually the easiest to make. In fact, the first thin-film high-T_c SQUID that I am aware of was made by patterning two narrow constrictions in a polycrystalline film of YBCO [KUG87]. Of course what one would really like is an epitaxial film with just two grain boundaries placed at specified locations. One method of doing just that, called "biepitaxy," was developed by Kookrin Char at Conductus. A version of this method (which I will call "biepitaxy-1" [CCG91]) is illustrated in Fig. 2.1. One starts with a substrate of r-plane sapphire and then covers it with an epitaxial seed layer of MgO. Then the MgO layer is patterned photolithographically and removed by ion milling from a portion of the substrate. The entire chip is then covered with $SrTiO_3$ and then c-axis YBCO. The $SrTiO_3$ grows epitaxially on both the sapphire and the seed layer but with its in-plane axes rotated by 45° with respect to one another; hence the name biepitaxy. The YBCO follows the local epitaxy of the $SrTiO_3$ thereby yielding a 45° grain boundary at the edge of the patterned seed layer. In the second version ("biepitaxy-2" [CCL91]) the sapphire is replaced with a $SrTiO_3$ substrate or base layer ([001] axis vertical). Again MgO is used as the seed layer, but the 45° rotation is produced in a layer of CeO_2 deposited in place of the $SrTiO_3$. YBCO is then grown as before. Typically, all layers are grown via pulsed laser deposition.

A typical biepitaxial SQUID (version biepitaxy-1), fabricated by Kookrin Char, is shown in Fig. 2.2. The SQUID is patterned in a YBCO layer 200-nm-thick by photolithography and acid etch. The two junctions are formed in the necks at the top of the SQUID body, each ~40 μm wide. At the center of the washer is a hole ~$(20\ \mu m)^2$ which would give the SQUID a nominal inductance of 30 pH. However, the long slit leading up to the junctions and the bridges containing the junctions contributes substantially to the inductance, and I have estimated the total inductance of the structure to be 96 pH (see

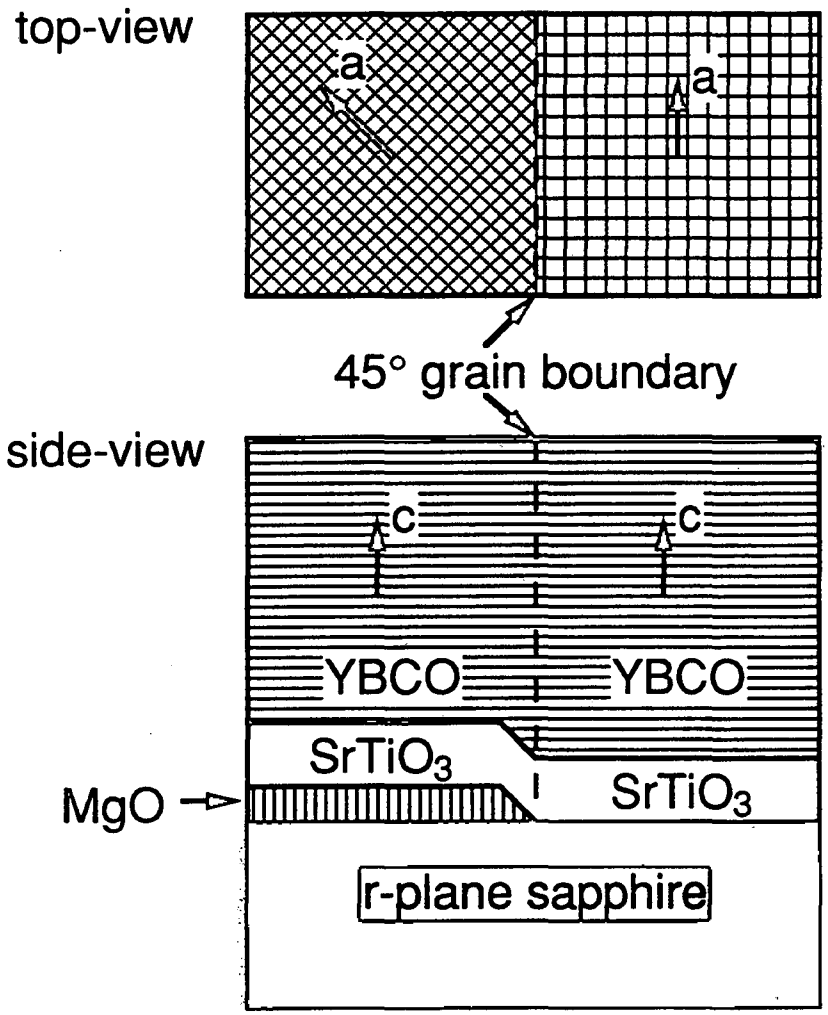

Fig. 2.1 Diagram of the interface of a biepitaxial junction (version biepitaxy-1). A cross-section is shown below and a top view is above. (Redrawn from ref. [CCG91].)

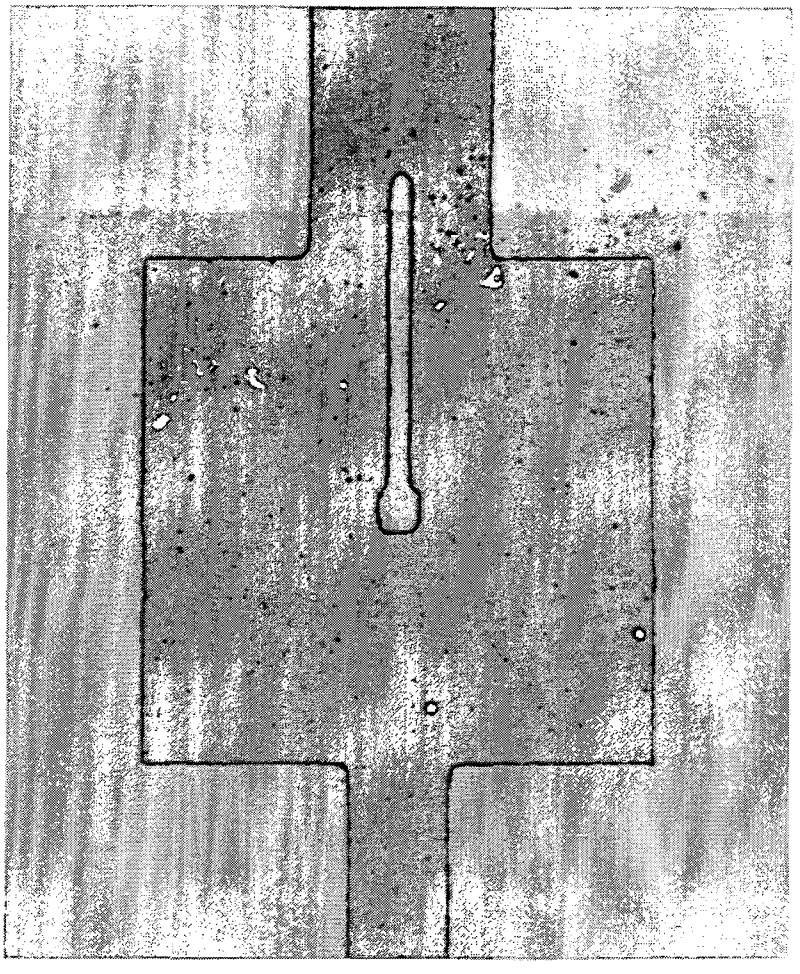

Fig. 2.2 A biepitaxial SQUID. Dark material is YBCO. The boundary of the seed layer is apparent in the change in the hue of substrate. The SQUID washer is 250 μm on a side.

Appendix A). Mark Colclough and I extensively studied a biepitaxial SQUID of the same design as that shown in Fig. 2.2. We observed voltage modulation with magnetic field at temperatures up to 88 K, and operated it in a flux-locked loop at temperatures up to 83 K. The I_0R product was typically 0.4 mV at 4.2 K and the junction resistance, R, was approximately 8 Ω. I note, however, that many biepitaxial SQUIDs would stop functioning at temperatures far below liquid nitrogen or wouldn't work at all. More distressing is that this biepitaxial SQUID (like all high-T_c grain boundary junction SQUIDs) showed copious amounts of 1/f noise as illustrated in Fig. 2.3. Since finding ways to control this noise is certainly a technological priority, I embarked on a project to see how much of this noise was due to critical current fluctuations in the biepitaxial junctions.

Noise in Single Biepitaxial Junctions[1]

I investigated the noise of three junctions (version biepitaxy-2), provided by Kookrin Char, all of which exhibited current-voltage (I-V) characteristics at 4.2 K that were close to the predictions of the resistively shunted junction model [STE68, MCU68]. The junction width w, critical current I_0, asymptotic resistance R, I_0R product, and temperature T_0 above which no critical current was discernible are listed in Table 2.1. I show the noise measurement circuit in the inset of Fig. 2.4. Each junction had four contacts to it, two to supply current and two to pick up the voltage. The static voltage across the junction was nulled out by means of a current I' through a cold 1 Ω resistor, thereby ensuring that very little current flowed through the voltage contacts to the film and eliminating them as a source of noise. The noise voltage was amplified by a room temperature transformer[2] followed by a low noise preamplifier connected to a spectrum

[1]Most of the following section has appeared previously as ref. [MCC92].

[2]Subsequent to the first publication of this work, Chris Muirhead of the University of Birmingham pointed out a difficulty with this method: a transformer has a very small impedance at low frequencies, and therefore

Table 2.1. Parameters of biepitaxial junctions in the single junction noise experiment.

Sample (Device)	w (μm)	I_0 (4.2 K) (μA)	R (4.2 K) (Ω)	I_0R (μV)	T_0 (K)
A (K355-2-4)	20	5.3	3.17	16.8	73
B (K355-2-3)	15	25.8	3.89	100.4	78.5
C (K336-1-1)	5	19.0	4.72	89.7	70.5

analyzer; the background voltage noise due to the Nyquist noise of the transformer referred to the input of the transformer was 0.35 nV $Hz^{-1/2}$. The preamplifier had a low-frequency 3 dB roll-off of 0.5 Hz; therefore I chose to quote all noise measurements at 10 Hz where the frequency response was flat. When the junctions were biased above their critical current (so that a nonzero static voltage existed across the junction), the spectral density of the noise from the junction scaled approximately as 1/f at the measured frequencies (below 500 Hz) at all temperatures.

Figure 2.4 shows the rms noise, $S_V^{1/2}$(10 Hz), vs. bias current, I, for junction A at four temperatures. At the highest temperature, there was no detectable critical current, and $S_V^{1/2}$(f) is proportional to I. At the lower temperatures, the noise shows a sharp peak at low bias currents and a linear dependence on I at high bias currents. Kawasaki *et al.* [KCG92] had earlier performed a similar set of experiments on single bicrystal GBJs and found a similar behavior (see chapter 3 for a description of bicrystal junctions). As they concluded, we ascribe the noise peak predominantly to critical current fluctuations and the linear region predominantly to resistance fluctuations. One can understand this qualitatively as follows. At bias currents just above the critical current the dynamic resistance is very large so that small changes in the critical current cause large voltage fluctuations. As the bias current is increased, critical current fluctuations become less important. Resistance fluctuations,

large scale fluctuations in I_0 at quasistatic frequencies can effectively shift the bias point during data taking.

however, cause a change in the asymptotic slope of the I-V characteristic; therefore they produce a noise voltage whose rms value increases linearly with bias current.

It is difficult to analyze quantitatively how much noise voltage critical current and resistance fluctuations give unless one knows *a priori* how the I-V curve depends on I_0 and R. To make progress, I assume that the I-V characteristic can be expressed in the form

$$V = I_0 R v(i), \tag{2.1}$$

where v is a dimensionless function and $i = I/I_0$. I then assume that voltage fluctuations can be written as $\delta V = \delta I_0 (\partial V/\partial I_0)_I + \delta R (\partial V/\partial R)_I$, where δI_0 and δR represent fluctuations in I_0 and R, respectively. The spectral density of the voltage noise is thus

$$S_V(f) = S_i(f)\,(V\text{-}IR_d)^2 + S_r(f)\,V^2 + S_{ir}(f)\,(V\text{-}IR_d)V. \tag{2.2}$$

Here, $R_d = \partial V/\partial I$, $S_i(f) \equiv S_{I_0}(f)/I_0^2$, $S_r \equiv S_R(f)/R^2$ and $S_{ir}(f) \equiv S_{I_0R}(f)/I_0R$ is the cross-spectral density of the fluctuations δI_0 and δR, which may be correlated. Equation (2.1) is certainly correct for the case of a true Josephson junction with no capacitive shunting at zero temperature in which the I-V characteristic has the solution $V = I_0R[(I/I_0)^2\text{-}1]^{1/2}$ [STE68, MCU68]. However, the essential premise of this expression, that there are no other current scales in the problem except for I_0, breaks down at nonzero temperatures where there is an rms thermal noise current proportional to k_BT/Φ_0 [AMH69]. Therefore, Eq. (2.2) underestimates the noise at low biases ($I \lesssim 6\pi k_BT/\Phi_0$) where noise rounding of the I-V characteristic is significant, and I excluded data in this region from further analysis.

I separated the data into those taken at high currents, where critical current fluctuations contribute negligibly to the voltage noise, and those taken at low currents, where critical current fluctuations dominate the voltage noise although there is still some contribution from resistance fluctuations. In Fig. 2.5(a) I plot S_V(10 Hz) vs. V^2 for the high current data for junction A at 4 temperatures; these data are representative of all three junctions. At each temperature I used a least squares fit to a straight line through the origin to obtain the slope, S_r(10 Hz). To analyze the low current data I subtract $S_r(10\text{ Hz}) \times V^2$ from S_V(10 Hz) and plot the result vs. $(V\text{-}IR_d)^2$ using measured values of R_d. Figure

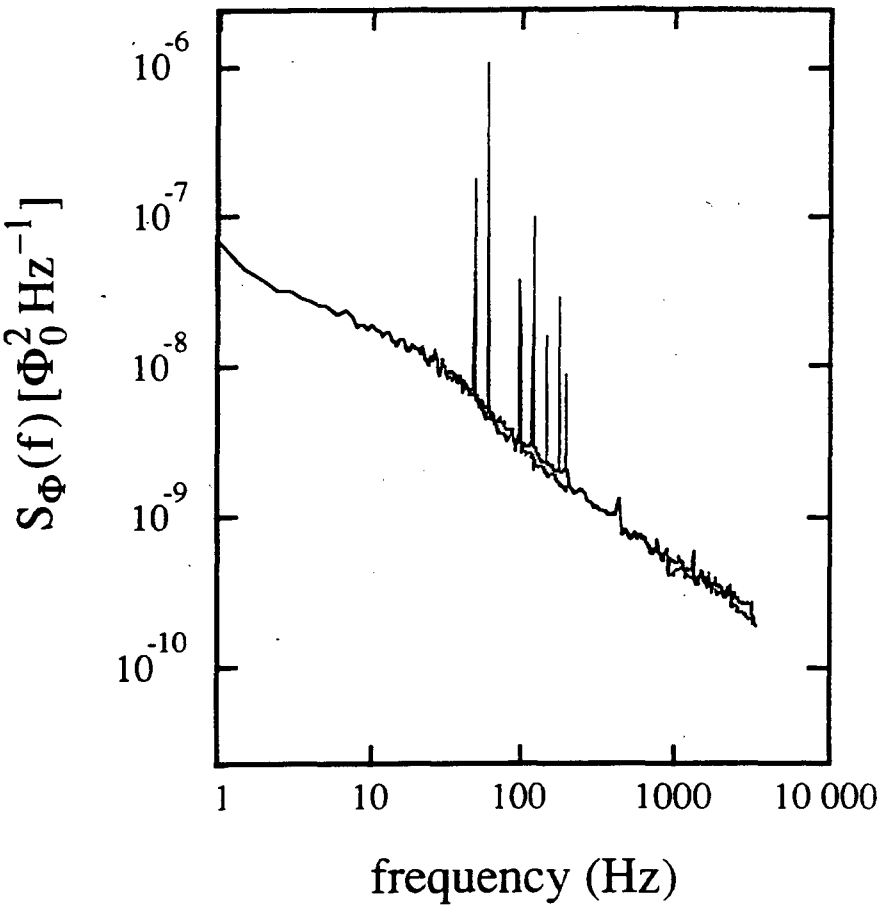

Fig. 2.3 Flux noise spectrum of a biepitaxial SQUID similar to the one shown in Fig. 2.2 taken at 4.2 K. The discrete spectral lines near 100 Hz are predominantly due to external 60 Hz pickup (the room-temperature shields described in chapter 1 were not used at this time).

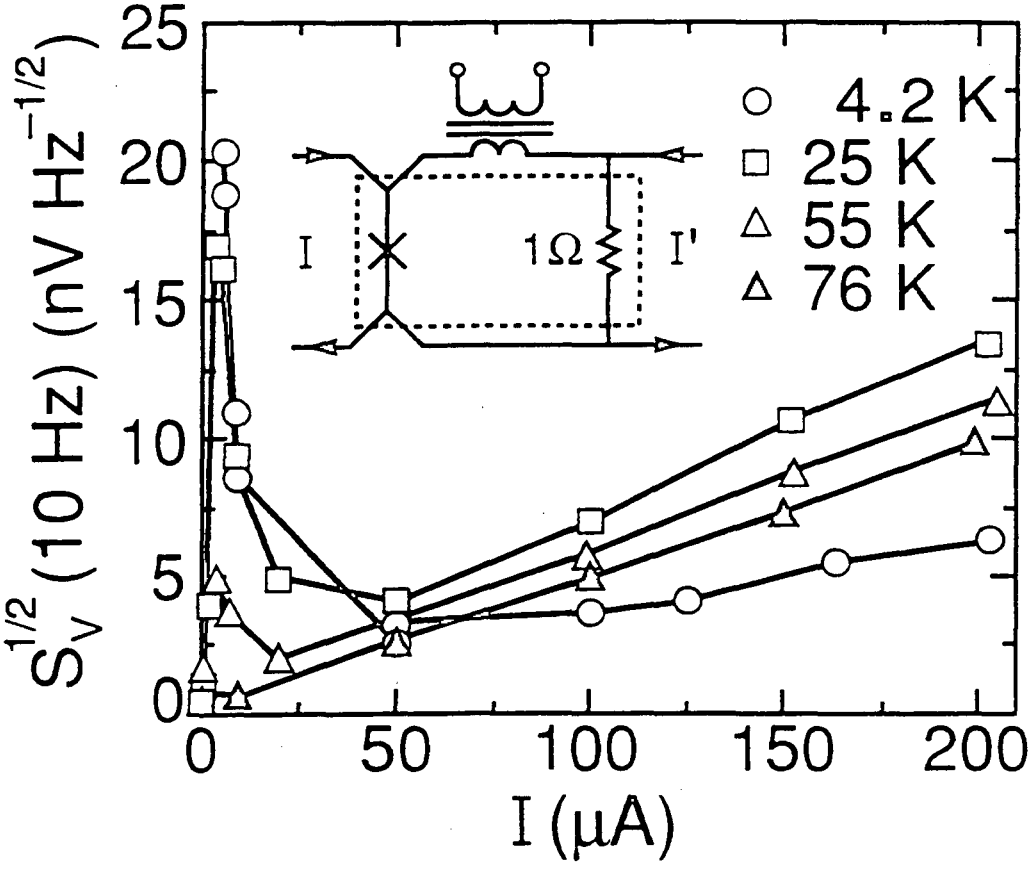

Fig. 2.4 $S_V^{1/2}$(10 Hz) vs. I for junction A at 4 temperatures. Solid lines are guides to the eye. Inset shows noise measurement circuit; components in dashed box are cold.

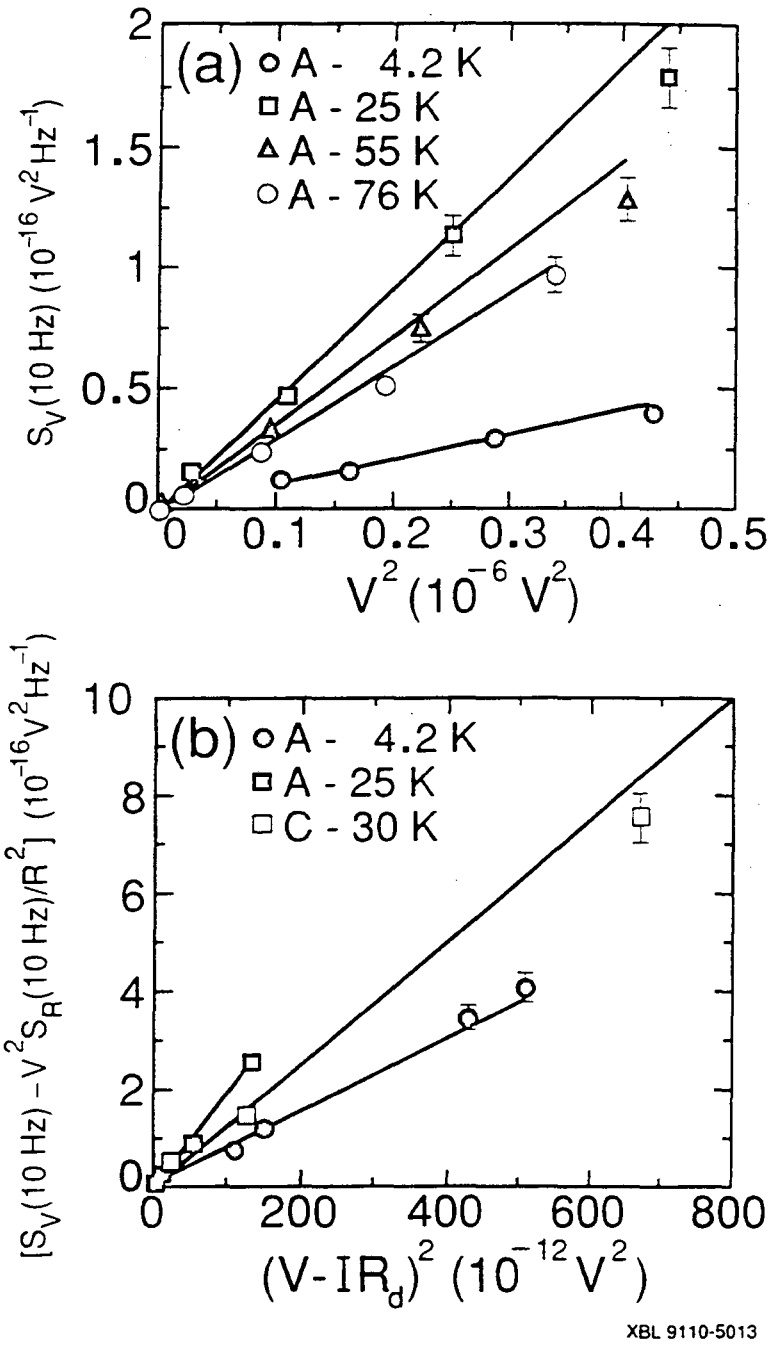

Fig. 2.5 (a) $S_V(10\ Hz)$ vs. V^2 for junction A at 4 temperatures, and (b) $S_V(10\ Hz) - V^2S_R(10\ Hz)/R^2$ vs. $(V\text{-}IR_d)^2$ for junctions A and C. Fitted line for C includes a data point at higher voltage not shown here.

2.5(b) shows the result for two junctions. I have ignored the cross-correlation term in Eq. (2.2), which is negligible because the prefactor $(V\text{-}IR_d)V$ is small at all bias currents. This does not imply that the cross-spectrum is negligible; merely that I could not measure it with this experiment. The slope of lines fitted to these data using a similar procedure is $S_i(10\ Hz)$. In Fig. 2.6 I plot $S_r(10\ Hz)$ and $S_i(10\ Hz)$ vs. T for all three junctions. One sees that $S_r(10\ Hz)$ is remarkably similar for all three junctions, rising slightly as the temperature is raised from 4.2 K to about 20 K, and then remaining more or less constant at about $4\times10^{-10}\ Hz^{-1}$. Thus, it appears that $\delta R/R$ is relatively constant for this junction technology. By contrast, $S_i(10\ Hz)$ varies widely for the three junctions. Junction A exhibits the highest noise, which increases slowly with temperature, junction B has much less noise at 4.2 K but a stronger temperature dependence, and junction C has a higher noise level at 30 K than at 4.2 K or 53 K. Above 53 K the small-bias region of the I-V curve was completely noise-rounded so that it was impossible to infer S_i.

However, all three junctions have a common feature: the values of $S_i(f)$ are very much greater than $S_r(f)$, that is, $|\delta I_0/I_0| \gg |\delta R/R|$. This observation is inconsistent with the expectations for the uniform flow of current through a *tunnel* junction. In this case, the same matrix element is involved in the tunneling of both electrons and electron pairs, so that $I_0 \propto 1/R$, and one expects $\delta I_0/I_0 = -\delta R/R$. However, I have observed that these types of junctions usually do not exhibit a Fraunhofer-like modulation pattern in a magnetic field, but rather produce an interference-like response suggesting that the supercurrent is carried by a small number of filamentary paths. Transmission electron microscope studies on biepitaxial junctions also support this conclusion [RCZ91] as does a large body of work by Moeckly *et al.* [MLB93] on electromigration of oxygen defects in high-T_c superconductor grain boundary junctions. To give a possible explanation of these results I assume a simple model in which the junction consists of N identical parallel channels, each with the same shunting conductance σ_1, of which only some fraction, F, support a supercurrent I_1. The conductivity of the junction is then $\sigma = N\sigma_1$, and the mean square fluctuation in σ is

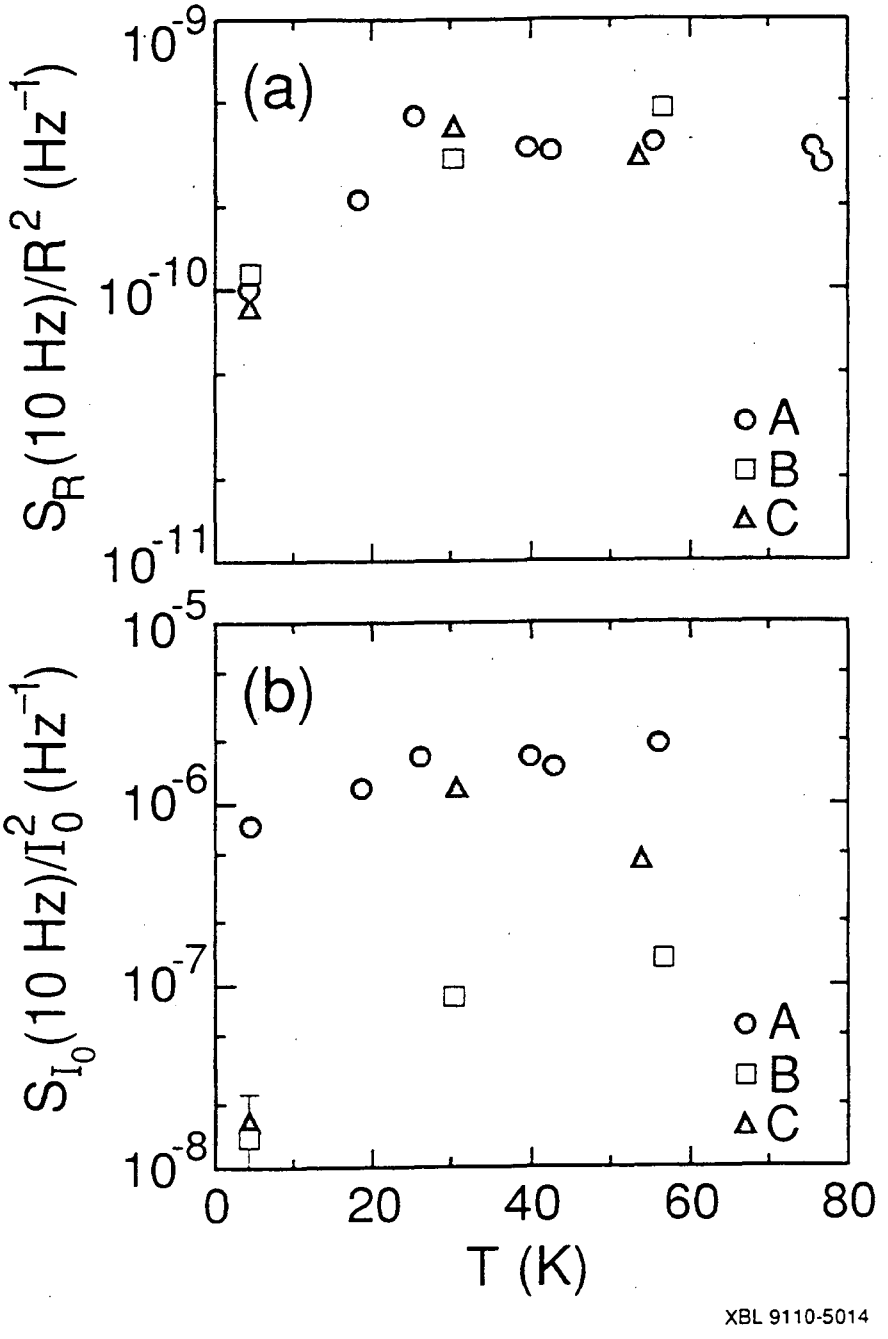

Fig. 2.6 $S_R(10\ Hz)/R^2$ and $S_{I_0}(10\ Hz)/I_0^2$ vs. T for three junctions.

$\langle(\delta\sigma)^2\rangle = N\langle(\delta\sigma_1)^2\rangle$, provided each channel fluctuates independently. Likewise, the critical current of the junction is $I_0 = FNI_1$ and its mean square fluctuation is $\langle(\delta I_0)^2\rangle = FN\langle(\delta I_1)^2\rangle$. If I assume finally that $|\delta I_1/I_1| = |\delta\sigma_1/\sigma_1|$ for the channels that support both a supercurrent and a normal shunting current, one finds $\langle(\delta I_0)^2\rangle/I_0^2 = (1/F)\langle(\delta\sigma)^2\rangle/\sigma^2$. It is straightforward to show that $\langle(\delta\sigma)^2\rangle/\sigma^2 = \langle(\delta R)^2\rangle/R^2$. Thus, the relative fluctuations in I_0 can greatly exceed those in R if F is sufficiently small ($\sim 10^{-3}$).

In contrast to these results, Kawasaki *et al.* [KCG92] in their study of single bicrystal GBJs found that $|\delta I_0/I_0| = 2.5\ |\delta R/R|$ implying that the current distribution was relatively uniform. Moreover, they found that annealing the samples in ozone caused a reduction in both $|\delta I_0/I_0|$ and $|\delta R/R|$, but the ratio between the two remained the same. Furthermore, it is known that if one varies the critical current of a high-T_c GBJ by varying the critical current density of the junction (say by changing the tilt angle in a bicrystal junction), then the critical current and junction resistance follow a scaling relation given by $I_0 \propto R^{-x}$, where $2 \lesssim x \lesssim 2.5$ [GCK90, DCM90, GRM91, RLM90, MLB93]. If one postulates that the critical current and resistance fluctuations occur because of some fluctuation in the barrier transmittance, which nevertheless preserves the above scaling relation, then one finds $\delta I_0/I_0 = -x\ \delta R/R$ in excellent agreement with experiment. All of this is, again, suggestive that the tunneling in bicrystal GBJs is uniform across the junction, and that the same path that carries the supercurrent also carries the normal shunting current. The ultimate test for this would be to alternate the bias current between regions where the noise is dominated by critical current fluctuations and regions where it is dominated by resistance fluctuations, and then measure the correlation in the noise voltages. This has been done for biepitaxial junctions [HHM93] with the expected result that the critical current and resistance fluctuations are uncorrelated.

Bias Reversal

Whatever the origin of the 1/f noise is in the junctions, a key question is whether or not the noise can be reduced by an appropriate bias reversal scheme. To examine this issue, I applied a 2 kHz square-wave current to a potentiometric arrangement [inset in Fig. 2.7(b)] to switch the junction bias between +I and -I. I adjusted the variable resistors to minimize the square-wave signal detected by a preamplifier connected in place of the transformer. Consider a fluctuation δI_0, with a characteristic time much greater than one switching cycle, that reduces the magnitude of both the positive- and negative-going critical currents. This fluctuation produces a voltage fluctuation of $+\delta V$ for +I and $-\delta V$ for -I. Thus, *provided the fluctuation remains coherent as the current is switched*, the average voltage fluctuation is zero. Figure 2.7(a) shows $S_V^{1/2}(f)$ for junction A measured with both static and modulated bias currents. Modulation reduces the 1/f noise dramatically, for example, by a factor of about 10 at 10 Hz. Figure 2.7(b) shows $S_V^{1/2}(10\ \text{Hz})$ vs. I for sample C for static and modulated currents. Again, we see that the 1/f noise is greatly reduced, for both critical current and resistance fluctuations. Comparable reductions in 1/f noise were observed for junctions A and B.

The fact that the junction fluctuations remain coherent as the bias current is reversed implies that bias reversal schemes applied to SQUIDs should reduce their flux noise. The bias and readout circuitry for our SQUIDs with a modulated bias is shown in Fig. 2.8. The 100 kHz square-wave generator provides a flux modulation with an amplitude of $\pm 1/4\ \Phi_0$ and the static flux bias keeps the SQUID operating at either an integral or half integral number of Φ_0. The transformer (which is cooled along with the SQUID) amplifies the 100 kHz voltage across the SQUID before sending it to an amplifier and a lock-in detector referenced to the 100 kHz source. The demodulated output of the lock-in is sent to an integrator and then a ballast resistor and the modulation coil coupled to the SQUID,

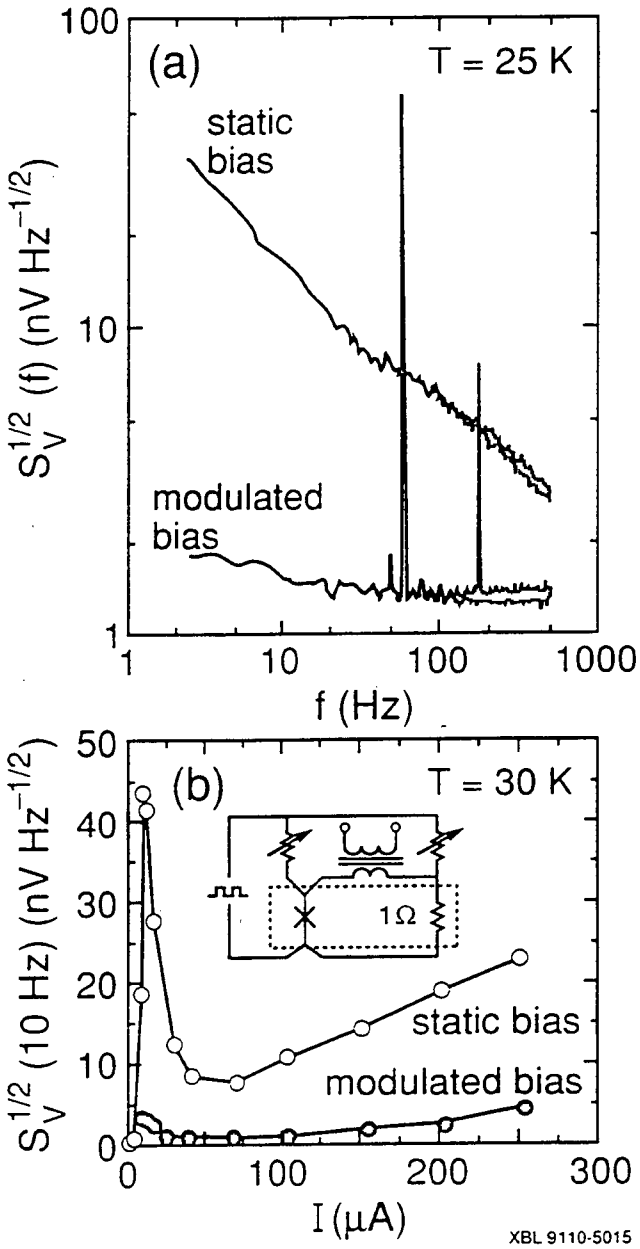

Fig. 2.7 (a) $S_V^{1/2}(f)$ vs. f for junction A and (b) $S_V^{1/2}(10\ Hz)$ vs. I for junction C with static and modulated bias currents. Inset in (b) shows circuit for modulated current.

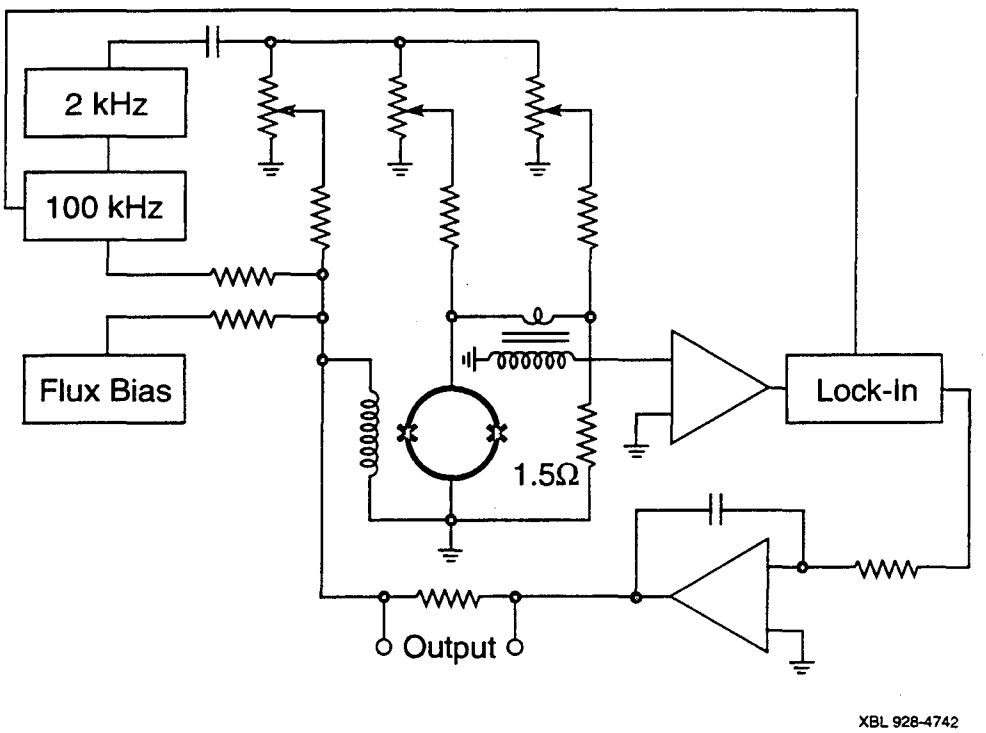

Fig. 2.8 Schematic of biasing and readout circuitry for SQUID with bias modulation.

thereby completing a feedback loop which keeps the SQUID at its proper flux bias point. The recorded output of the SQUID is just the fedback flux to the SQUID. All of the above procedure is the same as with standard modulation (static current biasing). The modulated bias current is provided with a 2 kHz square-wave generator *phase locked* to the 100 kHz source. The 2 kHz generator provides three current sources. The middle source in Fig. 2.8 provides a square-wave bias current such that the SQUID is operated between bias currents of equal magnitude and opposite polarity. The one on the far right sends a current to a cooled 1.5 Ω resistor which is used to produce a voltage equal to the biased voltage of the SQUID. In practice, one adjusts the current to this resistor to minimize the 2 kHz transient voltage picked up by the transformer. The current source on the far left adds an extra flux bias to the SQUID which is synchronous with the 2 kHz current bias. This is necessary in our bias reversal scheme because when the bias current is reversed the peaks in the V-Φ curve become troughs and vice-versa. Thus, if the bias flux is left unchanged one finds that the voltage for an applied *signal* flux becomes averaged to zero over many cycles of the bias current. To correct this, the left-hand current source provides a flux bias of 1/2 Φ_0 as the bias current is reversed so that the peaks and troughs line up [KCG83]. The signal voltage is then read out in the same way as with standard modulation.

Figure 2.9 shows the flux noise spectrum of a biepitaxial SQUID made at Berkeley using a variation of the biepitaxy-2 process. The bias reversal clearly improves the low-frequency noise, reducing the 1/f noise power by an order of magnitude. Unfortunately, there is still quite a bit of 1/f noise remaining on the spectrum. This noise may be due to flux motion in the superconducting film, or it may be that our bias reversing procedure does not remove all of the 1/f critical current noise. In particular, one should note that the effect of bias reversal is to mix the quasistatic critical current noise up to the bias reversal frequency (2 kHz). At the same time, any noise at the reversal frequency will be mixed down to dc. Thus, if the SQUID has a large amount of 1/f noise to begin with (such that the spectrum is 1/f at 2 kHz) then there will still be 1/f noise at low frequencies. I have

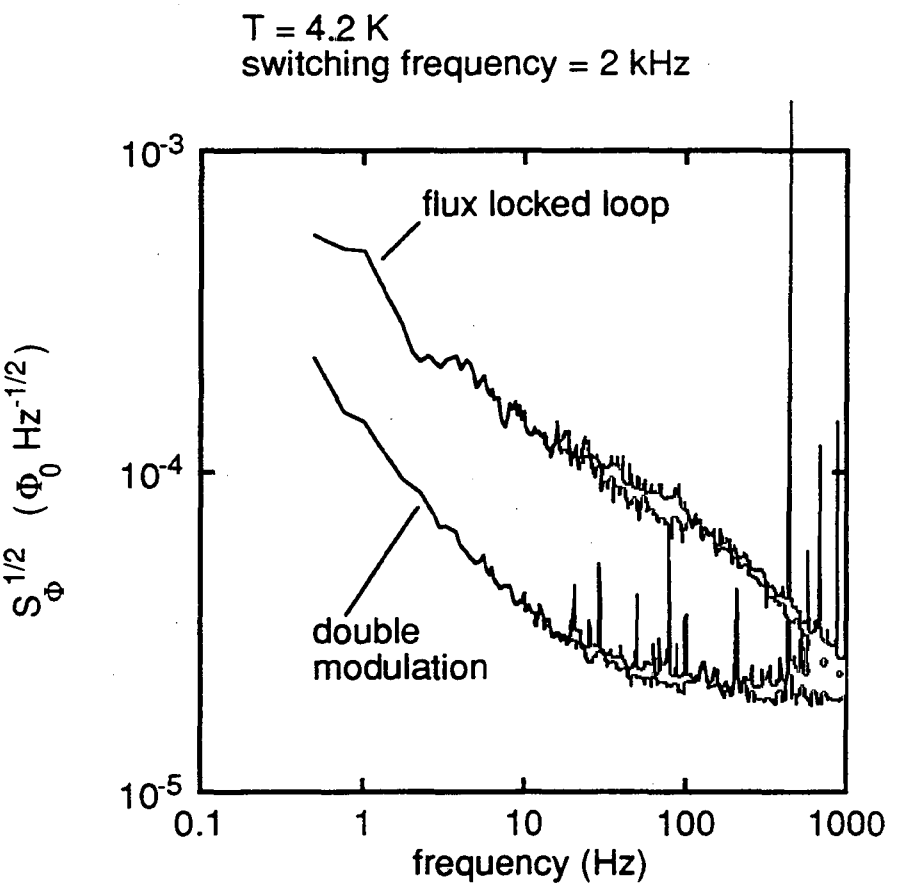

Fig. 2.9 Rms flux noise spectrum for a biepitaxial SQUID at 4.2 K with standard modulation (upper trace) and bias reversal at 2 kHz (lower trace).

tried increasing the reversal frequency to 5 kHz, but at that switching rate, the transient response to the current switching occupies a large fraction of the duty cycle. Consequently, not much improvement in the low-frequency noise was found. Also I note that the 2 kHz generator was *not* phase locked to the 100 kHz source as discussed above. The beating between the two sources produced many of the discrete spectral lines between 10 Hz and 1 kHz.

Eventually the Clarke group abandoned biepitaxial junctions in favor of the bicrystal technique discussed in the remainder of this thesis. There were two main reasons for this. First, as my noise measurements indicated, the biepitaxial junctions never showed the characteristics of a well-connected tunneling barrier. This is evidenced by the exceptionally small critical current densities across the junctions (notice the junction widths shown in Table 2.1 are 5 to 20 μm whereas for our bicrystal SQUIDs shown in the next chapter they were 2 to 3 μm). A likely related issue is that the biepitaxial junctions I measured were noisier than their bicrystal counterparts; Kawasaki reported $S_i^{1/2}(1\ \text{Hz}) = 1.0\times10^{-4}\ \text{Hz}^{-1/2}$ at 77 K whereas I found $S_i^{1/2}(1\ \text{Hz})$ ranging from 1.0 to $4.5\times10^{-3}\ \text{Hz}^{-1/2}$ at the highest temperatures I could reliably measure it. (In both cases, I have extrapolated the data to 1 Hz from the measured frequency assuming a 1/f frequency dependence.) One can argue that improvements in processing with time would improve matters. However, one should recall that studies on bicrystals with variable grain boundary angles have shown that the critical current falls off very rapidly with angle and reaches a minimum at 45° [DCM88, DCM90, GRM91]. The second reason is that creating a biepitaxial junction requires at least one seed layer and then a rotation layer before putting down the YBCO; often an assortment of epitaxial buffer layers is also required. The complexity in being able to deposit all of these layers sequentially resulted in long production times to make single devices, and a small yield of devices operating at 77 K. The principle advantage of biepitaxy is the ability to put an arbitrary number of junctions at arbitrary locations on a chip, but for a SQUID which only requires two junctions this is a null issue. Once

bicrystal substrates became commercially available, it was possible to make junctions by patterning a single superconducting film and biepitaxy was given up.

Chapter III: Bicrystal SQUIDs[1]

Following our bad experiences with biepitaxial junctions, we began looking for an alternative junction technology. The method we eventually decided upon is the bicrystal technique developed at IBM [DCM88]. In this process, one starts with a boule of single-crystal substrate material. We have always used $SrTiO_3$ although YSZ [OKN93] and MgO [LHW93] substrates have been reported. The substrate boule is then cut along a plane oriented $\Theta/2$ degrees away from the (100) plane. The boule is fused and sintered back together such that at the interface the [100] vectors meet with a net misorientation of Θ degrees. The boule is then cut and polished into [001] axis vertical substrates in the usual way. YBCO is then grown on top of the substrate replicating the grain boundary. It is interesting to note that the bicrystal process results in a *symmetrical* grain boundary whereas the biepitaxial process is asymmetric; that is, with the bicrystal process the [001] vectors on either side of the grain boundary intersect the interface plane with the *same* angle ($\Theta/2$ degrees), whereas with the biepitaxial process the [001] axis is rotated only on one side of the grain boundary (see chapter 2). It is not known if this is important in terms of the microstructure of the interface, but it may well contribute to the sparsely connected nature of the biepitaxial GBJ. It is clear, however, that the bicrystal process requires far fewer epitaxial depositions than biepitaxy. Not only does this make them easier to produce and improve the yield, but by reducing the height of the epitaxial stack one generally improves the film quality and probably reduces the number of weak flux pinning sites in the YBCO. When bicrystal substrates became commercially available[2] it became clear that they were the best way to go.

---

[1]Portions of this chapter were published earlier as ref. [MKD93].
[2]Wako Bussan Co., Ltd., Tokyo.

Fabrication

In the summer of 1992 I began making bicrystal SQUIDs out of films grown by other members of the Clarke group. The original fabrication procedure is outlined below. YBCO films 200 to 300 nm thick were deposited on 10 mm × 10 mm (100) $SrTiO_3$ bicrystal substrates with a 24° misorientation angle. Subsequently, an Ag film was laser deposited to a thickness of 100-200 nm through a shadow mask over the part of the YBCO film to be used for contact pads. The faint line of YBCO grains along the grain boundary of the substrate allows one to align a mask for photolithographic patterning. I first ion-milled the Ag through the photomask and then etched the SQUID in 0.05-0.1% nitric acid. The acid undercuts the photoresist in a controllable way, enabling me to make a bridge 2-4 μm wide for the junctions. Finally, I made electrical connections to the SQUIDs by ultrasonic bonding 25 μm diameter Al wires to the Ag-covered contact pads.

The procedure above produced SQUIDs working at 77 K on the third sample I tried. The first two trials failed only because I had designed the junctions too wide, not knowing *a priori* what the critical current of our junctions would be. In the intervening two years since this first test numerous improvements to the process have been made, many of them due to the hard work of the other members of the high-T_c group. It was found that a thin (~10 nm) buffer layer of $SrTiO_3$ on the substrate often improved the quality of the YBCO. The Ag layer for the contacts is now deposited by thermal evaporation in a separate deposition chamber to prevent the windows in the laser chamber from becoming covered with Ag. Also, the acid undercutting method is not used anymore in favor of ion milling the YBCO with a 2-4 μm photomask. We then optionally undercut the YBCO slightly ($\lesssim$ 1 μm) which is believed to remove damaged, nonsuperconducting material from the edges of the bridges, thereby increasing the resistance of the junctions. Finally, our bicrystal substrates are now of sufficiently high quality that we cannot in general see

the grain boundary. Therefore, before patterning the YBCO we scrape or etch slightly the edges of the substrate which is scratched preferentially along the crystal axes. We can thus see where the axes change direction, and we align this to alignment marks at the outside of the photomask.

Figures 3.1 and 3.2 show photographs of two square-washer SQUIDs, called type A and B respectively. Both have inner holes of 25 μm × 25 μm. The type A washers have an outer dimension of 250 μm × 250 μm, while the type B were either 250 μm × 250 μm or 500 μm × 500 μm. In the type A design, the junctions are placed outside the washer, to maintain a high coupling efficiency to a multiturn input coil. However, the extra inductance associated with the slit reduces the signal available from the SQUID (see Appendix A). In the type B design, the junctions are placed at the inner edge of the washer, thereby eliminating the inductance of the slit. On the other hand, the junctions are now in the relatively high magnetic field region produced by the flux focusing [KGK85] of the SQUID body, which introduces additional single-junction modulation effects in the earth's field.

Performance

I tested 9 type A SQUIDs and 3 type B SQUIDs on one chip. I first studied the properties of the SQUIDs by cooling them, in the earth's magnetic field, in liquid nitrogen. The current-voltage (I-V) characteristics have well-defined upward curvature, expected from the resistively shunted junction model [MCU68, STE68], as shown in Fig. 3.3 for one type B SQUID. In Fig. 3.4 I show the V-Φ modulation pattern for that SQUID as a function of static biasing current. The transfer function rises smoothly as I increase the bias current above the critical current, reaching a maximum at roughly 250 μA. Notice that the V-Φ curve for 290 μA is inverted from those at smaller bias currents (peaks have become troughs and vice-versa). I have observed this in a number of SQUIDs and I

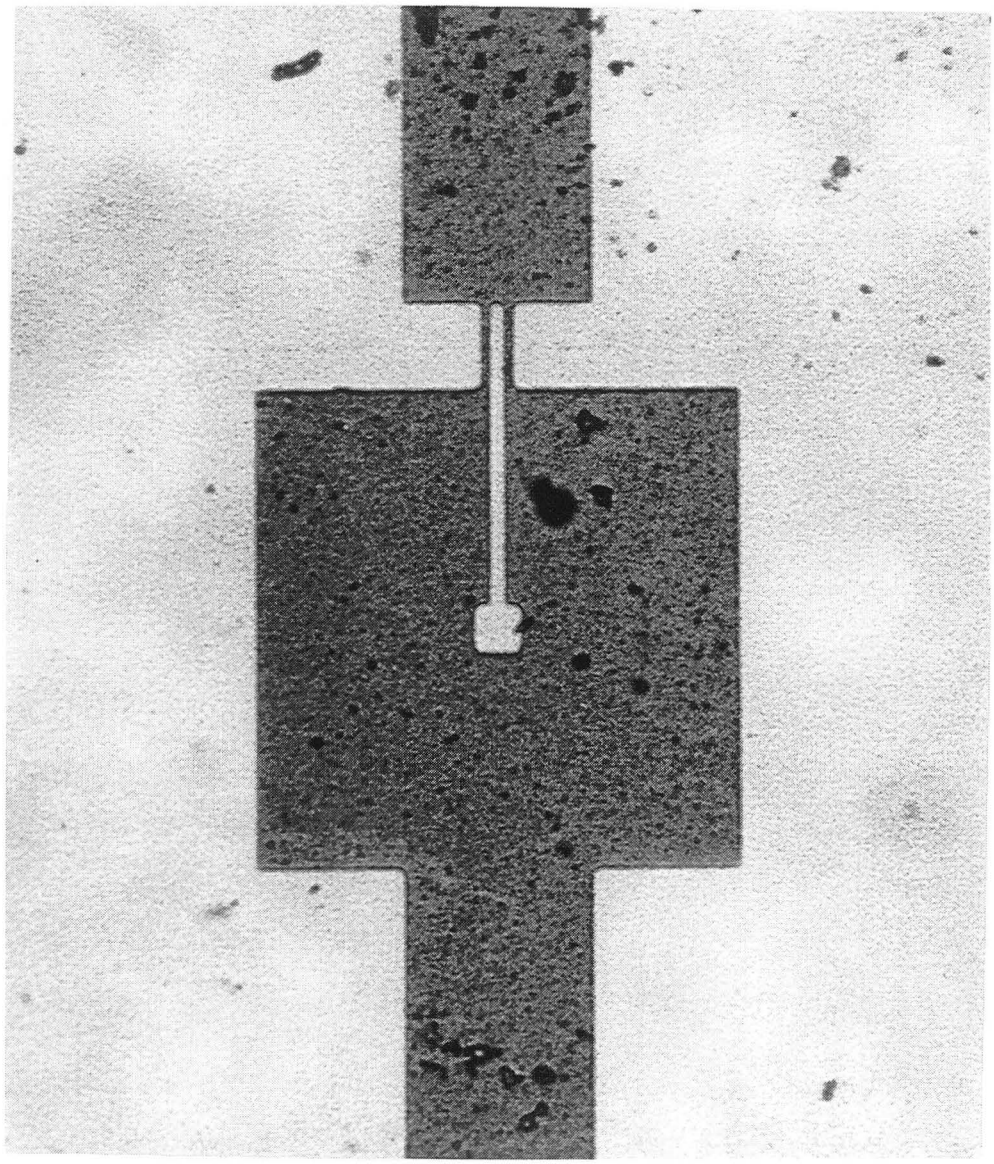

Fig. 3.1 Photograph of a type A bicrystal SQUID. The grain boundary junctions are formed in the narrow bridges at the top of the square washer body. The square washer body is 250 μm across.

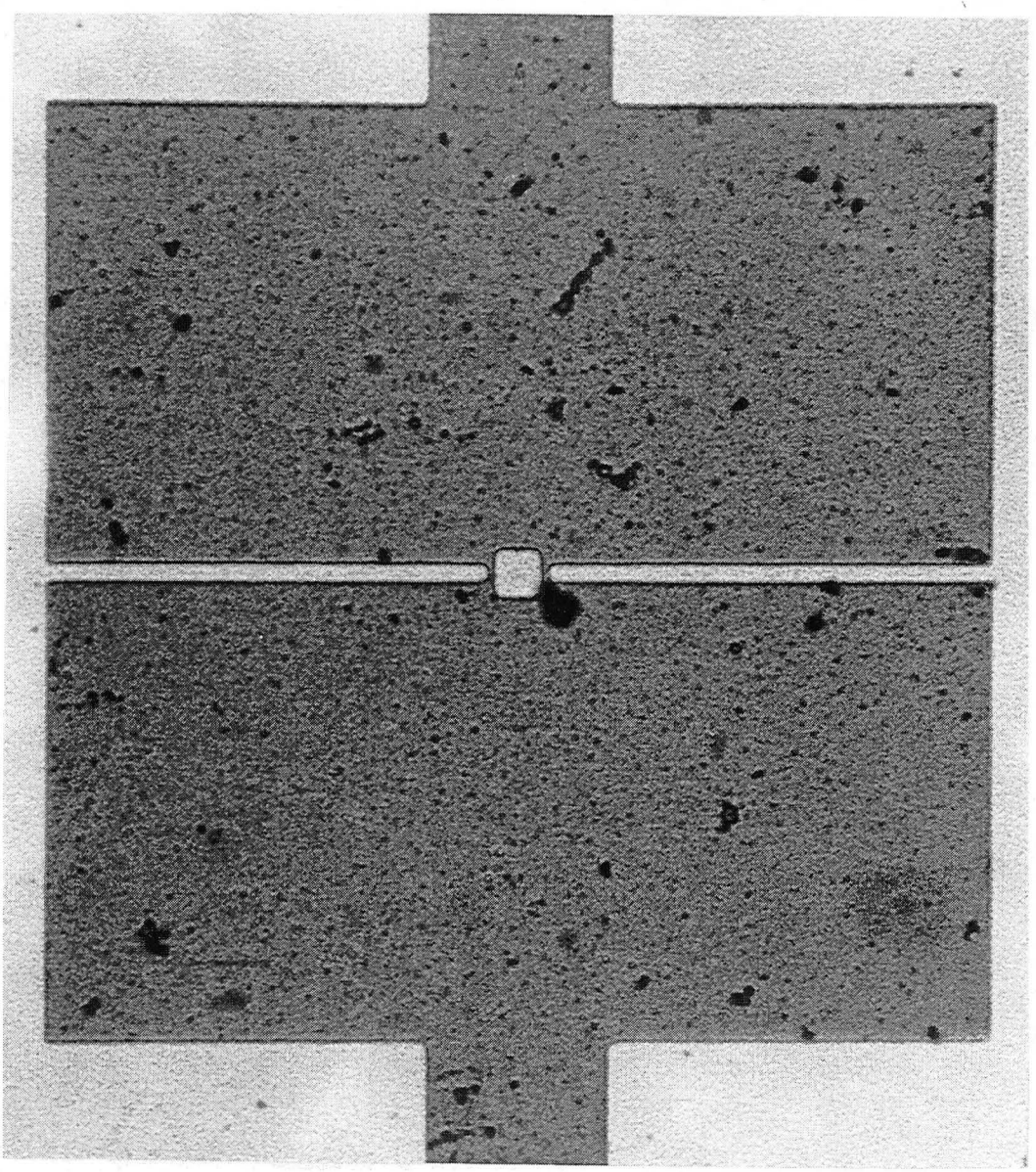

Fig. 3.2 Photograph of a type B bicrystal SQUID. The grain boundary junctions are formed in the narrow bridges in the center of the square washer body. The square washer body is 500 μm across.

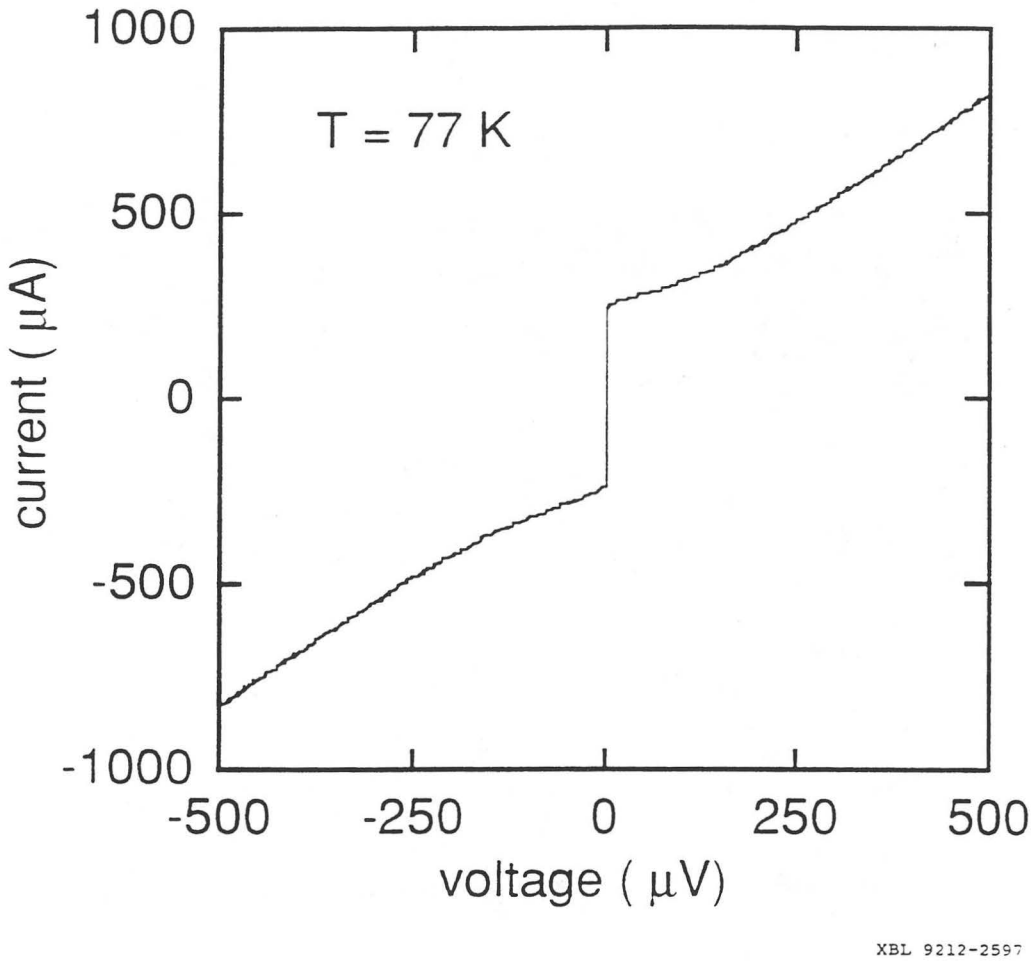

Fig. 3.3 I-V characteristic of the SQUID in Fig. 3.2 at T = 77 K.

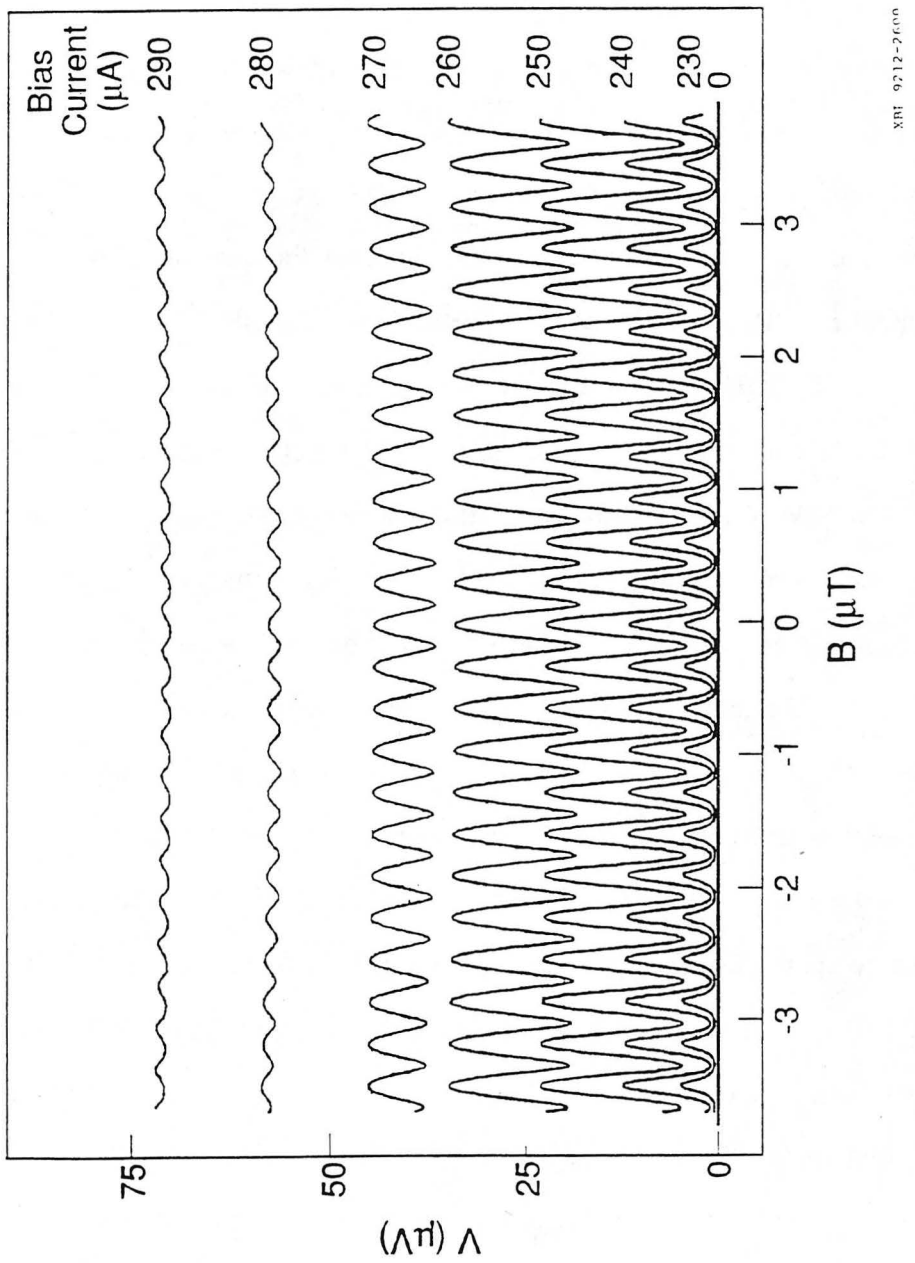

Fig. 3.4 V-Φ characteristic for the SQUID in Fig. 3.2 at T = 77 K at various bias currents.

believe it is correlated with the appearance of bumps at certain places in the I-V. These may be because of rf resonances in the SQUID bodies or asymmetries in the critical currents of the two junctions [CLF69].

Figure 3.5 summarizes the critical currents ($2I_c$), maximized by rotating the probe in the ambient magnetic field, and asymptotic resistances ($R_N/2$) for all 12 SQUIDs on a single chip with nominally identical junction widths of 3 μm; I_c and R_N refer to single junctions. Also shown is the maximum peak-to-peak voltage modulation, ΔV, obtained when the magnetic flux is varied at the optimum bias current. The average values of these parameters are $2I_c$ = 185 μA, $R_N/2$ = 0.78 Ω, and ΔV = 1.8 μV and 15 μV for type A and type B SQUIDs, respectively. The standard deviation in $2I_c$ corresponds to about ±30% of the average value and in $R_N/2$ to about ±20% for both type A and type B devices. For the type A devices, the standard deviation in ΔV corresponds to about ±20%. We note, however, that the standard deviation in I_cR_N corresponds to about ±18%, suggesting that some of the scatter in I_c and R_N may well be due to small variations in the widths of the junctions. An additional variation in I_c may arise from the flux trapped in the junctions. The scatter in $\Delta V/R_N$ is only ±11% in type A and ±9% in type B, implying that the modulation depth in critical current is constant to this level.

All SQUIDs of the same type have remarkably similar effective magnetic flux capture areas. For the type A SQUIDs this was $\Phi_0/0.14\ \mu T = 1.5\times10^{-8}\ m^2$; neglecting the slit, we expect an effective area [KGK85] A_s of 25 μm × 250 μm = $6.3\times10^{-9}\ m^2$. Thus the slit increases the effective area by a factor of about 2.5. For the type B SQUIDs, the measured effective area for the 250 μm washer was $\Phi_0/(0.48\ \mu T) = 4.3\times10^{-9}\ m^2$ compared with the predicted value, neglecting the slits, of $6.3\times10^{-9}\ m^2$, while for the 500 μm washer the measured value was $\Phi_0/(0.32\ \mu T) = 6.5\times10^{-9}\ m^2$ compared with the predicted value of $1.25\times10^{-8}\ m^2$. Thus, for the type B SQUIDs the presence of the slits reduces the effective area by 32% and 48% for the 250 μm and 500 μm washer, respectively.

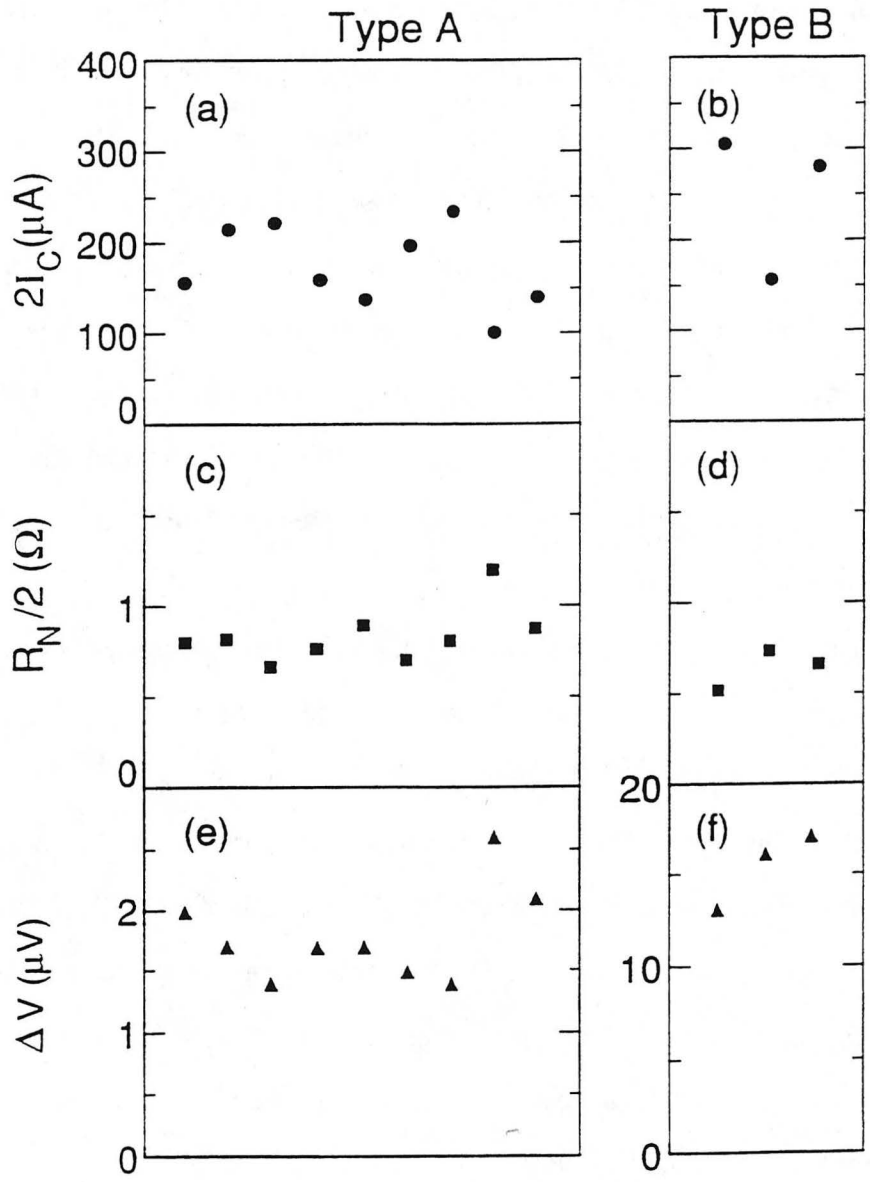

Fig. 3.5 Critical current (a) and (b), asymptotic resistance (c) and (d), and peak-to-peak voltage modulation, ΔV, (e) and (f) at 77 K for 12 SQUIDs on a single bicrystal. Abscissa enumerates the SQUIDs.

For the one type B SQUID that I studied in detail, the measured flux-to-voltage transfer coefficient was $dV/d\Phi = (65 \pm 10)\ \mu V/\Phi_0$ corresponding to a peak-to-peak modulation of 17 μV. This SQUID had an inner hole diameter of d = 26 μm from which I estimate an inductance of L = 41 pH (see Appendix A). Using the measured asymptotic resistance $R_N = 1.28\ \Omega$, one expects [TEC77] $dV/d\Phi \approx R_N/L \approx 65\ \mu V/\Phi_0$, an agreement that is excellent but undoubtedly fortuitous, given the uncertainties in the parameters. Also, the above prediction is strictly true only for the case of $\beta = 1$, and this SQUID had a critical current of 105 μA yielding $\beta \approx 5$. In the case of the type A SQUIDs, however, the transfer coefficients are much smaller, ranging up to $6\ \mu V/\Phi_0$ in a device with $R_N \approx 2.4\ \Omega$. I estimate the inductance of this type of SQUID (including the slit) to be 145 pH. Thus, I would expect $dV/d\Phi \approx 37\ \mu V/\Phi_0$, considerably larger than the observed transfer coefficient. The reason for the reduced response of the type A SQUIDs is not clear, but it appears now to be a general phenomenon associated with SQUIDs operated at high temperatures. Figure 3.6 shows the transfer function, normalized to the junction resistance, for many YBCO bicrystal SQUIDs made in the Clarke group and tested at 77 K. The crosses are the SQUIDs described above plus two others made with the same pattern on different chips. The squares are 40 pH and 145 pH directly coupled SQUID magnetometers (described in chapter 5); the SQUID elements of these are similar to the type A SQUIDs presented in this chapter. The circles are large area square-washer SQUIDs (~1 cm O.D.) of either type B or type C (described in chapter 5). The solid line is the prediction for $\beta = 1$ SQUIDs (although I note that all of the SQUIDs in this figure have $3 < \beta < 65$). For L > 40 pH the transfer function falls off as $1/L^{(2\pm0.2)}$.

The fact that this behavior has been seen for a number of SQUID geometries indicates that it is likely not an artifact of the way we estimate the SQUID inductance nor some peculiar resonance with the electromagnetic modes formed by the SQUID body. Furthermore, Roger Koch [KOC93, KOC93b] has duplicated qualitatively this rapid decay of transfer function with inductance using computer simulations, although the predicted

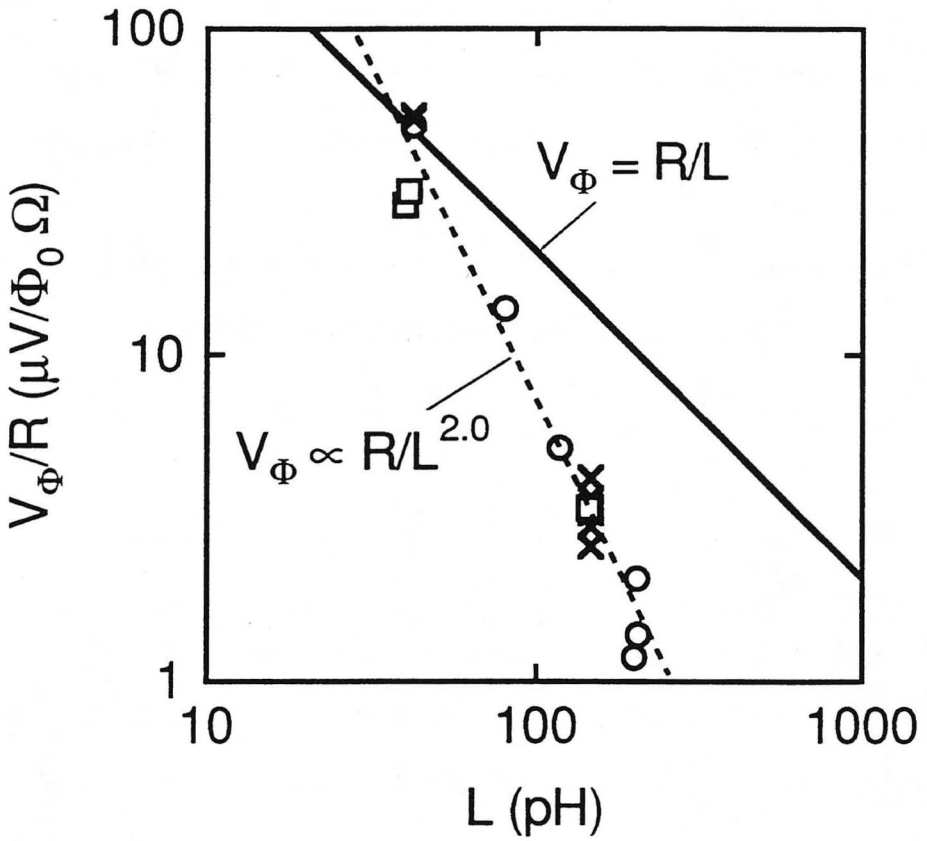

Fig. 3.6 Transfer coefficient V_Φ normalized to asymptotic SQUID resistance R vs. inductance L for large washer SQUIDs (O) [KML93], directly coupled SQUIDs (□) [KML93], and small washer SQUIDs (x) with outer dimension of 250 μm or 500 μm [MKD93]. Dashed line is least squares fit to the data.

values are still a factor of ~3 greater than those I have observed. It is important to note that the clear scaling seen in Fig. 3.6 does not appear if one plots the data as a function of β rather than L. My feeling is that the appropriate inductance parameter for this situation is not Φ_0/I_0 but rather $(\Phi_0)^2/k_BT$, indicating that this behavior is largely a result of having more thermal energy in the SQUID washer. Enpuku *et al.* [ESK93] have used numerical models to show that the transfer function decreases at large L as $\sqrt{k_BTL}/\Phi_0$ for *fixed* β. The data shown here are in qualitative agreement, but again tend to fall below the predictions especially at the larger inductances [KOE94]. Some possible explanations for this include parasitic inductances in the junctions themselves due to a non-sinusoidal current-phase relation, or extra damping via capacitive coupling across the SQUID body which is enhanced because of the high dielectric constant and large loss tangent of the $SrTiO_3$ substrate. Nevertheless, it is clear that operation of the SQUID at higher temperatures places a constraint on the size of the SQUID inductance, which in turn limits how well one can couple signals to it.

Noise Measurements

Having determined the parameters of the SQUIDs, I measured the flux noise in one of them at 77 K, first using a static current bias and a flux modulation frequency of 100 kHz. The flux noise power spectrum, $S_\Phi(f)$, and the noise energy, $\varepsilon(f) \equiv S_\Phi(f)/2L$, are shown as the upper trace of Fig. 3.7 for the type B SQUID discussed in the paragraph above with an outer dimension of 500 μm. At frequencies above 5 kHz the spectral density becomes white with a value of $S_\Phi(10\text{ kHz}) = 3.5\times10^{-11}\ \Phi_0^2\ \text{Hz}^{-1}$, corresponding to $\varepsilon(10\text{ kHz}) = 1.8\times10^{-30}\ \text{J Hz}^{-1}$. By comparison, using $R_N = 1.3\ \Omega$ and L = 41 pH, we predict [TEC77] $\varepsilon \approx 9k_BTL/R \approx 3\times10^{-31}\ \text{J Hz}^{-1}$, a factor of 6 smaller.

Between 0.1 Hz and 1 kHz, the power spectrum scales closely as 1/f. In an attempt to reduce this noise, we used the bias current reversal scheme described in chapter

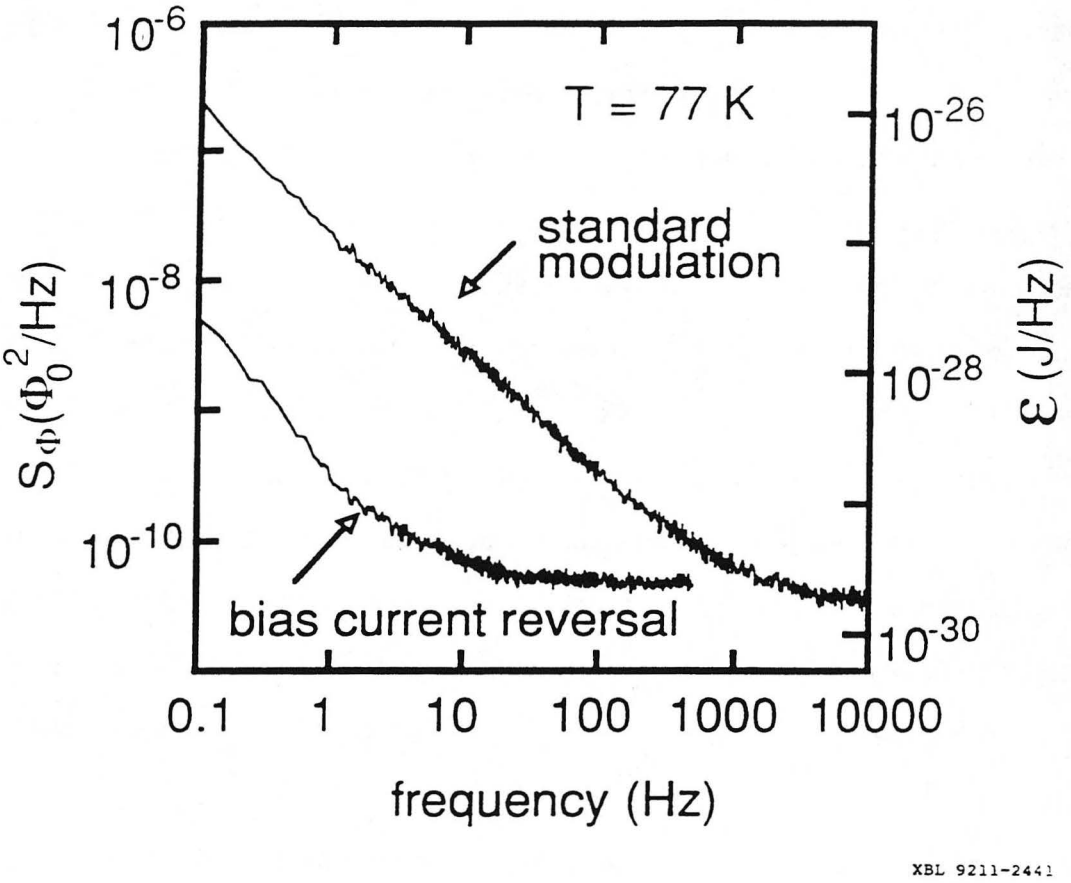

Fig. 3.7 Flux noise spectral density, $S_\Phi(f)$, and noise energy, $\varepsilon(f)$, for type B SQUID (500 μm outer dimension) at 77 K. Upper trace is for conventional flux-locked loop with static current bias, lower trace is for bias reversal scheme.

2. The resultant noise spectral density (lower trace in Fig. 3.7) is reduced by two orders of magnitude at 1 Hz. This large reduction demonstrates that the 1/f noise in the upper trace of Fig. 3.7 arises from critical current fluctuations rather than from flux noise. The bias reversal scheme has caused the white noise to increase slightly, to 2.5×10^{-30} J Hz^{-1}. The residual noise, $S_\Phi(1\text{ Hz}) = 2.9\times10^{-10}\,\Phi_0^2$ Hz^{-1}, may be due to flux noise within the body of the SQUID, or may represent the limit to which we have thus far been able to suppress the critical current fluctuations. I have noted that the amount of 1/f noise remaining after bias reversal is rather insensitive to the exact settings of the bias reversal controls, but there can be considerable spread in the noise between cool downs (say a factor of 2 in the rms). Also the remaining noise appears to be highly sensitive to any changes in the ambient magnetic field after the SQUID has cooled through T_c. Because of this, we have adopted the following procedure for cooling the SQUIDs. First we move the dewar into the screened room and set it in the place where it will be for noise measurements. Then the probe with the SQUID is lowered into the dewar such that the stage with the Co-Netic foil is just above the level of the liquid nitrogen. The probe is left for ~1 hour to cool to a temperature of ~100 K. This slow cooling allows the Co-Netic foil (and possibly the magnetic domains in it) to relax to its equilibrium position so that no shifting of the residual magnetic field will occur when the sample is cooled through T_c. Finally, the probe is lowered into the liquid nitrogen. Once the SQUID is cold, the dewar is not moved until the experiment is over.

At the time these data were taken, the measured noise energy at 1 Hz, 1.5×10^{-29} J Hz^{-1}, was the lowest value obtained for a dc SQUID operating at 77 K. Since then, the Clarke group has made much progress in improving the noise of our SQUIDs, primarily by reducing their inductance. At present our best energy resolution is achieved with a 10 pH SQUID, 1.5×10^{-30} J Hz^{-1} at 1 Hz falling to 5.5×10^{-31} J Hz^{-1} at 1 kHz. We believe the lowest inductance we can reasonably make our bicrystal SQUIDs is 10 pH because of the difficulties in aligning junction bridges < 4 μm long to the grain

boundary in the substrate with the procedure outlined above. Several other groups have made YBCO dc SQUIDs working at 77 K with energy resolutions in the white limit between 6×10^{-31} J Hz^{-1} and 10^{-29} J Hz^{-1} [FDV93, DYY93, SGC93, KCN91]. The 1/f knee for these devices is typically 1 to 10 Hz. It is interesting to note that commercially available dc SQUIDs operating at *4.2 K* from companies such as Quantum Design, Conductus, or BTi, are specified with energy sensitivities of 5×10^{-31} J Hz^{-1} to 10^{-30} J Hz^{-1} and 1/f knees as low as 0.1 Hz. Rf SQUIDs, which were the mainstay of the SQUID market for many years, are typically specified at 5×10^{-29} J Hz^{-1}. Although the actual devices are often much better than this guaranteed performance, it is clear that high-T_c technology is close to the point where it would be considered adequate for many of the tasks now done with low-T_c devices.

Chapter IV: Flux Transformers and Early High-T_c Magnetometers[1]

In parallel with the effort to develop the SQUIDs discussed in chapters 2 and 3, our group was also vigorously pursuing a high-T_c interconnect technology including superconducting wiring in two separate electrically insulated layers with superconducting vias between the layers at chosen places. The immediate goal of this project was to make a superconducting flux transformer which is the second half of a magnetometer. However, it should be stated that a Josephson junction technology combined with a superconducting interconnect technology provides one with the ability to make almost any superconducting circuit of interest. In this vein, the superconducting flux transformer is the simplest practical device that demonstrates all of the elements of a superconducting interconnect technology. The pioneering work on high-T_c interconnects was conducted primarily by Fred Wellstood and Jack Kingston who made the flux transformer reported here. Their work is recorded in refs. [KWL90, WKC90, WKF90, KWQ91, TGK91] and in the review by Wellstood *et al.* [WKC94].

Fabrication

Rather than try to build a flux transformer and SQUID integrated together on the same chip, we decided that we would first make the SQUIDs and flux transformers on separate substrates. Magnetometers could then be formed by pressing the input coil face-to-face with the SQUID body in a "flip chip" arrangement. This would allow us to develop our junction and interconnect processes independently, use our flux transformers with many different SQUIDs (including some from other groups), and reduce the overall complexity of the device. Our first magnetometers used $Tl_2Ba_2CaCu_2O_{8+y}$ SQUIDs

[1]Portions of this chapter were published previously as refs. [MKW91, MKD93, MWK91].

provided by Superconductor Technologies, Inc., with junctions formed in narrow bridges in a polycrystalline film [MWK91]. Shortly thereafter we started using the Conductus SQUID described in chapter 2 fabricated with the biepitaxy-1 process. By determining the magnetic field (perpendicular to the SQUID) required to induce one flux quantum, we estimated the effective pickup area A_S to be 12,000 μm^2; this value exceeds the geometrical area of the hole and slit by a factor of 6, and is due to focussing of the flux by the body of the SQUID [KGK85].

Although I completed and tested magnetometers made with several different flux transformers, I made extensive use of one of them in particular. The input coil of a similarly designed device is shown in Fig. 4.1. Jack Kingston and Fred Wellstood fabricated the flux transformer on an MgO substrate using the following procedure which is described in the references listed above. They first laser deposit a 300-nm-thick film of YBCO and pattern it to form the crossunder, the line that connects the inner turn of the input coil to the pickup loop, using a photomask and a 0.1% nitric acid etch. In the second step, they deposit 450 nm of $SrTiO_3$ and open two windows, one at the inner end of the crossunder and a second at the outer end [see Fig. 4.1]. The windows in the $SrTiO_3$ are patterned with photoresist, and etched with an Ar ion mill at an angle of 30° to the substrate; this procedure produces an edge along one side of the window beveled at about 8°. They also allow the ion mill to remove roughly 100 nm of the YBCO in the window, to ensure that no $SrTiO_3$ remains and so that the two YBCO films make contact both in the ab-plane and along the c-axis. The angled-ion milling yields an optically smooth contact surface, and allows the top layer of YBCO to grow in a highly oriented manner on the flat surfaces of YBCO and $SrTiO_3$ as well as on the beveled $SrTiO_3$ edge. Separate experiments on patterned window contacts of this kind indicate that the critical current density of the upper YBCO strip deposited on the beveled edge can be well over 10^4 A cm^{-2} at 77 K. The upper layer of YBCO is subsequently patterned with photolithography and the acid etch to produce the five-turn coil, shown in Fig. 4.1, and the

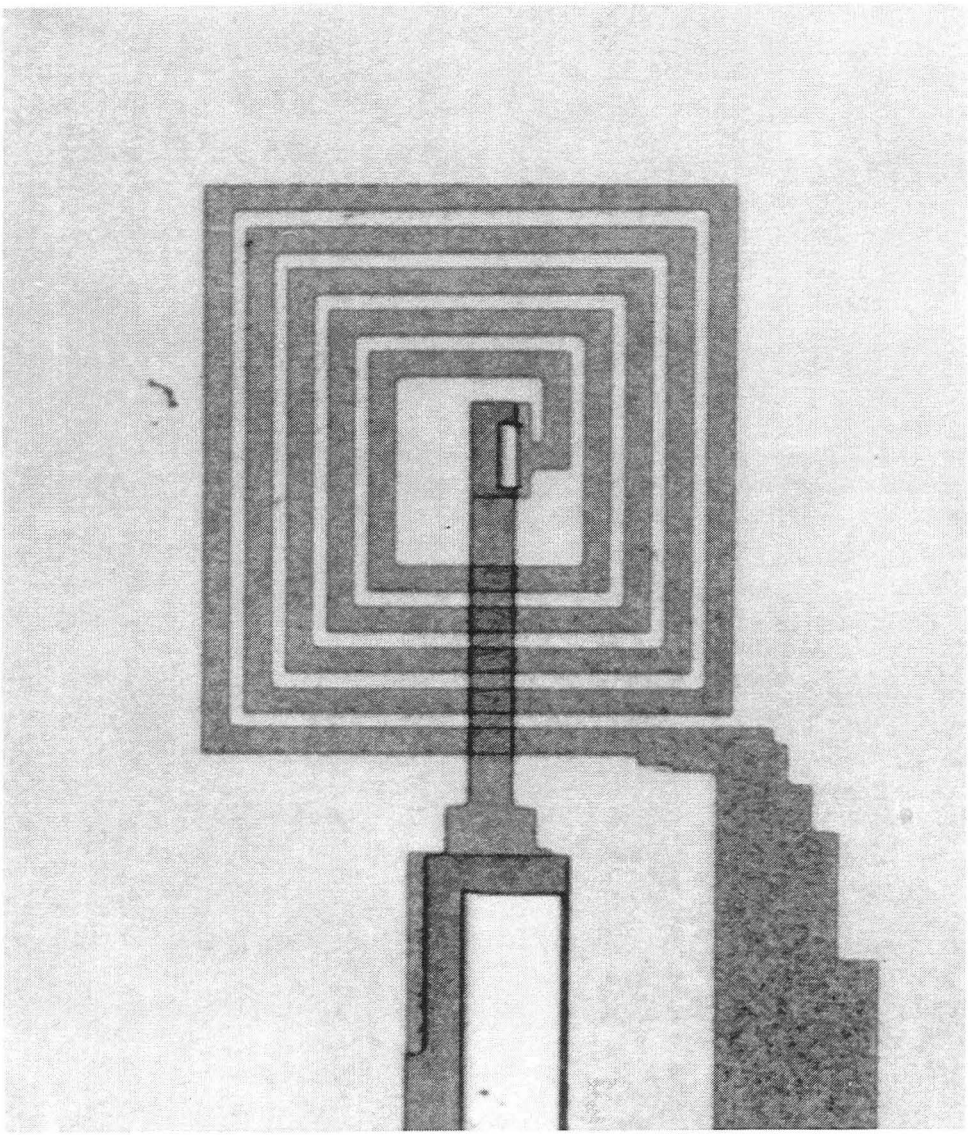

Fig. 4.1 Photograph of 5-turn spiral input coil. The two leads at the lower edge of the figure connect to the single-turn pickup loop (not shown).

single-turn pickup loop (not shown) which is approximately 10 mm across and has a pickup area of 81 mm^2. We deliberately broadened the linewidth of the turns of the input coil (to 11 μm) compared with our earlier transformers in an attempt to improve the coupling efficiency to the SQUID. I estimate the inductance of the pickup loop, L_p, to be about 20 nH. The input coil inductance is harder to estimate because both its coupled self inductance and its stripline inductance depend critically on the separation between it and the SQUID. Assuming a separation of 10 μm, I calculate a stripline inductance of ≈2.3 nH; however, the formulas used here assume that the stripline is much wider than its distance to the SQUID groundplane [DUT81]. Also, if the flux transformer were perfectly coupled to the SQUID, then one would expect a coupled self inductance of n^2L where n is the number of turns and L is the SQUID inductance [KET81]; for our SQUID this is roughly 2.4 nH. However, the reasoning behind this formula assumes that all of the SQUID's geometrical inductance is located inside the innermost turn of the input coil. For the present case where the SQUID inductance is largely in the slit, it is unclear how much of the SQUID inductance the transformer actually couples to. In the absence of more precise computer modeling, I assume for the present discussion that the transformer is moderately well coupled to the SQUID, but that the pickup loop still dominates the inductance of the transformer.

Performance

To test the magnetometer, I carefully aligned the SQUID and the input coil and clamped them together, with a 3-μm-thick mylar sheet between them. The magnetometer was mounted on a variable temperature insert in a liquid ^4He cryostat surrounded by a mu-metal shield as described in chapter 1; in some experiments, I immersed the magnetometer directly in liquid N_2.

I determined the critical current of the flux transformer by applying a known

magnetic field and noting the value at which the period of the oscillations in the SQUID voltage abruptly changed as the field was increased. At this point, the transformer evidently entered a critical state, and further increases in the magnetic field produced no increase in the induced supercurrent. From these measurements, I inferred the critical current from the area of the pickup loop and the uppermost value of the estimated transformer inductance. This procedure gives a lower bound on the critical current, which is plotted as a function of temperature in Fig. 4.2; the true values may well be somewhat higher. However, for magnetometer applications, the measured values are entirely adequate for temperatures up to at least 85 K. At 77 K, the critical current density referred to the cross-sectional area of the turns of the input coil is about 5×10^4 A cm^{-2}. We believe that in this sample the critical current density was limited by the point at which the upper YBCO film climbs the film rise in the $SrTiO_3$ that occurs at the edge of the lower YBCO film.

We define the gain g of the transformer as the ratio of the effective area of the magnetometer (defined in chapter 1) to the effective area of the bare SQUID. We deliberately chose the sense of the windings of our transformers to produce a flux in the SQUID opposite in sign to the direct flux; hence g is negative. It is straightforward to show that

$$g = 1 - \frac{A_p}{A_s} \frac{M_i}{L_i + L_p}, \tag{4.1}$$

where the mutual inductance $M_i = \alpha(LL_i)^{1/2}$, and I have neglected the area of the input coil compared to that of the pickup loop. The measured gain, shown in Fig. 4.3, is -83 ± 3 over the temperature range 4.2 K to 80 K. Taking the values $A_p = 81$ mm^2, $A_s = 1.2\times10^{-2}$ mm^2, $L_p = 20$ nH and assuming $L_i \ll L_p$, we find from Eq. (4.1) $M_i = (0.25 \pm 0.01)$ nH, which is approximately 0.5 nL. Subsequent to this work, Dieter Koelle [KOE94b] made a more extensive study of the coupling of high-T_c flux

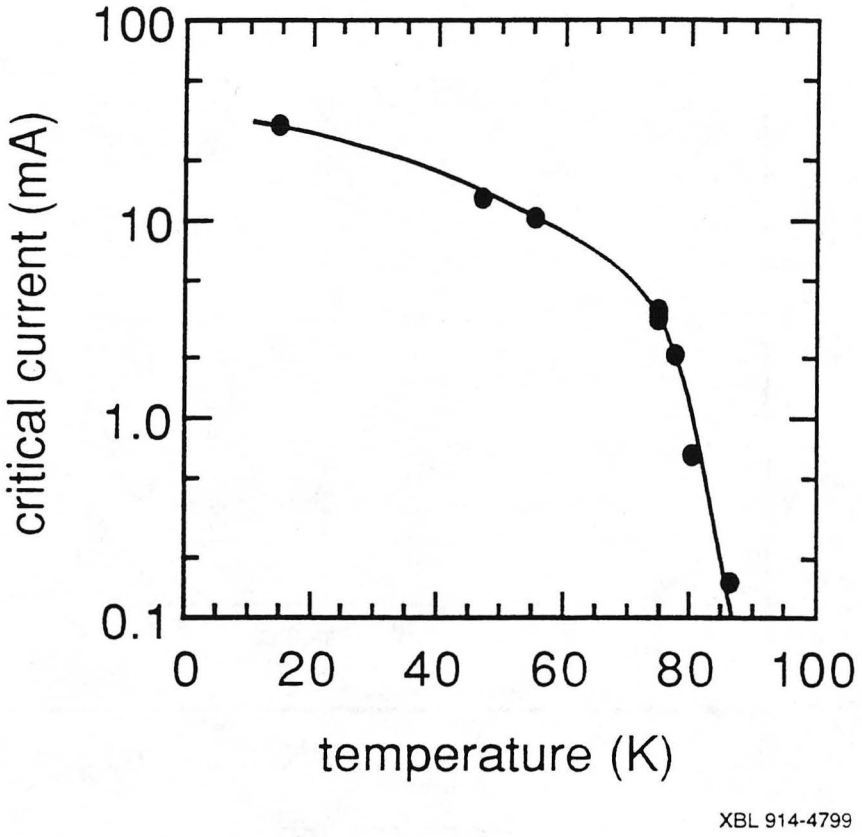

Fig. 4.2 Lower bound on critical current of flux transformer vs. temperature.

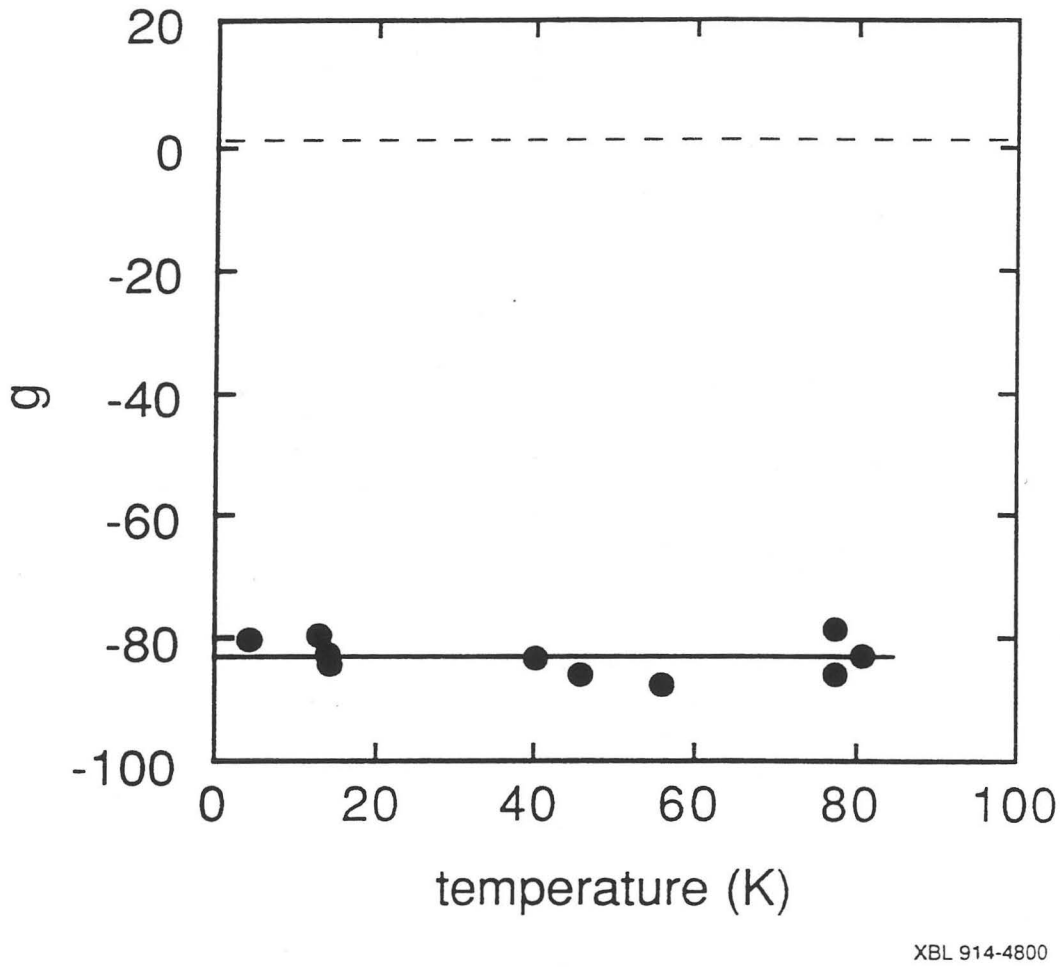

Fig. 4.3 Gain g of the magnetometer vs. temperature. The dashed line at g = +1 refers to the gain of the SQUID without a flux transformer.

transformers to high-T_c SQUIDs in which he measured M_i directly by cutting open the pickup loop and feeding current directly to the input coil. He found that M_i generally lies in the range (0.5 - 0.85) nL with corresponding coupling coefficients of $0.25 < \alpha < 0.52$.

I measured the noise of the magnetometer using our standard modulation technique (static current bias) and a flux-locked loop. The alternating voltage across the SQUID was amplified by a cooled transformer. Figure 4.4(a) shows the rms magnetic field noise, $S_B^{1/2}(f)$, vs. frequency when the magnetometer is immersed in liquid ^4He and in liquid N_2. At 4.2 K, the spectral density scales approximately as 1/f from a few Hz to several kHz. At 77 K, the noise begins to flatten off above 200 Hz, indicating that the white noise generated by the junctions is beginning to dominate in this frequency range. However, at lower frequencies, the rms noise has increased over that at 4.2 K by only a factor of 2. The magnitude of the noise at 77 K is $S_B^{1/2}(1\ Hz) = 2.6\ pT\ Hz^{-1/2}$ and $S_B^{1/2}(1\ kHz) = 0.09\ pT\ Hz^{-1/2}$. I also measured the temperature dependence of the noise of our magnetometer surrounded by ^4He gas. Figure 4.4(b) shows an example of the observed noise at 68 K. The noise is about a factor of two lower than that at 77 K in Fig. 4.4(a).

Magnetocardiology

Despite the large amount of 1/f noise in the magnetometer, we felt that the performance was sufficiently impressive to allow us to make an actual measurement with it. Fred Wellstood and I decided to demonstrate the capability of the device by using it to measure the magnetic signature of the beating of a human heart. A magnetocardiogram is the easiest biomagnetic signal to obtain; the peak signal can be many tens of pT since it arises from the coherent propagation of the electrochemical signal along the heart muscle, and the signal is unmistakably periodic. Although a magnetocardiogram had previously been obtained with a bulk YBCO rf SQUID [LPU90], our experiment was the first to apply a thin-film high-T_c magnetometer to a practical problem.

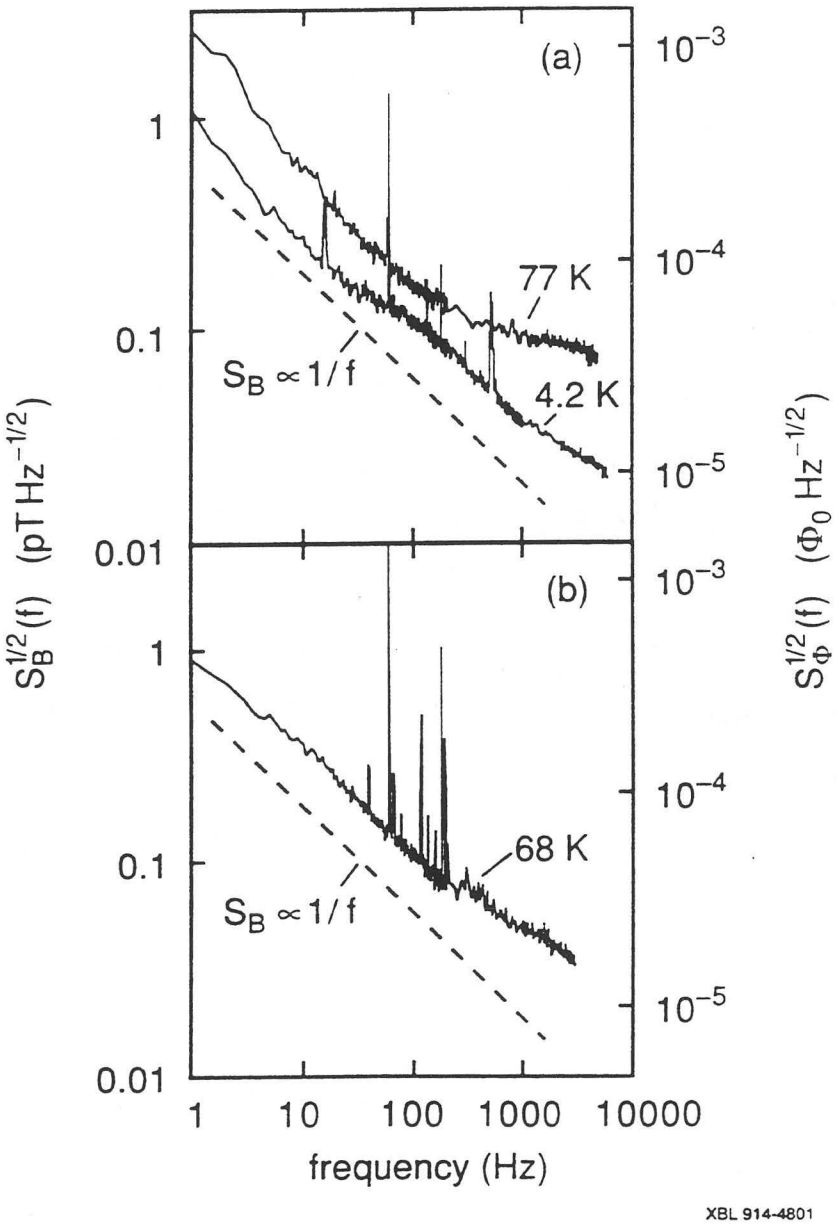

Fig. 4.4 (a) Rms magnetic field noise, $S_B^{1/2}(f)$, and rms flux noise, $S_\Phi^{1/2}(f)$, vs. frequency for flip chip magnetometer with biepitaxial SQUID at 4.2 K and 77 K. Dashed line is $S_\Phi \propto 1/f$. (b) Same for magnetometer at 68 K.

A photograph of the experimental apparatus is shown in Fig. 4.5. We immersed the magnetometer in liquid nitrogen contained in a thin-walled glass dewar extracted from a household thermos flask. The flask was rigidly supported in our shielded room, so that the plane of the magnetometer was parallel to the chest of a standing subject, and within about 25 mm of the chest wall. All of the support structures, including a brace for the subject to lean against, were made of wood with brass screws. The dewar and subject were surrounded by two high-permeability cylinders (kindly loaned by Professor Eugene Commins) which attenuated the ambient magnetic fields by a factor of ~300. The entire experiment was constructed inside the Cu-plate rf screened room in B275 Birge. By the time this experiment was performed, the white noise of the SQUID had deteriorated to 0.35 pT $Hz^{-1/2}$ when measured in the new environment, but the resolution at 1 Hz remained at 2.3 pT $Hz^{-1/2}$.

We measured the magnetocardiograms from three healthy male subjects ranging in age from 27 to 32. Each subject removed metallic objects from his person, and was not in contact with the dewar. The waveforms in Fig. 4.6 were obtained at grid locations [WIK81] D3 and D5, over the lower-right and lower-left chest of one subject. The bandwidth was 2-50 Hz; residual 60 Hz pickup is still evident in both traces as is noise from the magnetometer itself. The two cardiograms differ significantly from each other, but each is similar to that previously seen by others [WIK81] using low-T_c SQUID magnetometers placed at the same grid locations.

Although we were able to clearly resolve the heart beat (and perhaps some of the structure associated with it), for clinical use one would like an order of magnitude reduction in the rms magnetometer noise. At both 4.2 K and 77 K, the measured flux noise $S_\Phi^{1/2}(f)$ of the magnetometer [right-hand axis of Fig. 4.4(a)] was very close to that observed in the SQUID alone, implying that the noise contribution of the transformer was negligible at both temperatures. Unfortunately, we did not have our double modulation electronics at this time, so we could not say for sure how much of the noise was coming from critical current

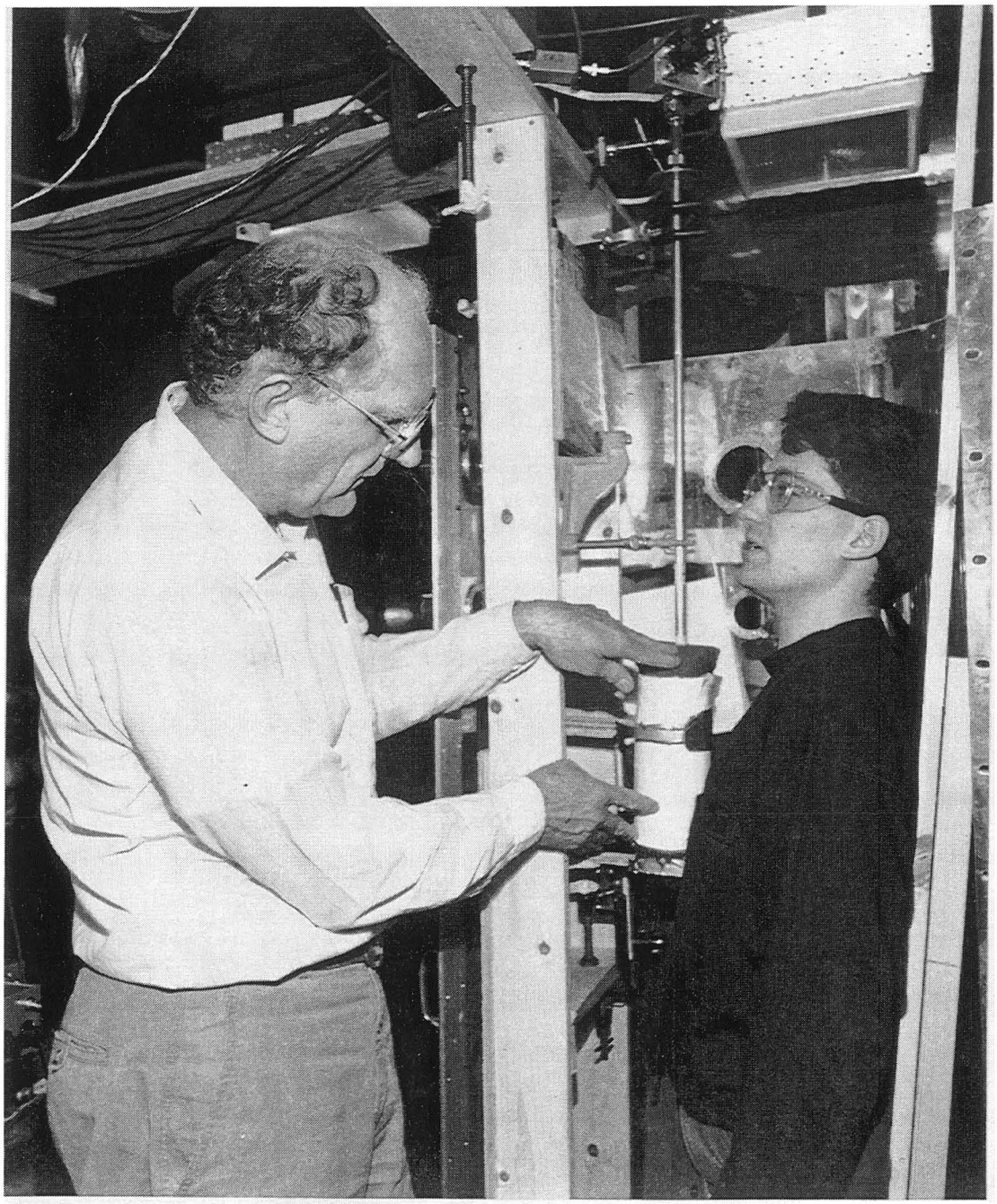

Fig. 4.5 John Clarke (left) and the author (right) in the magnetocardiography apparatus. I am leaning against the wooden brace as our subjects did. Prof. Clarke is adjusting the thermos flask which served as our dewar. The shiny metal visible behind me is part of the high-permeability shield.

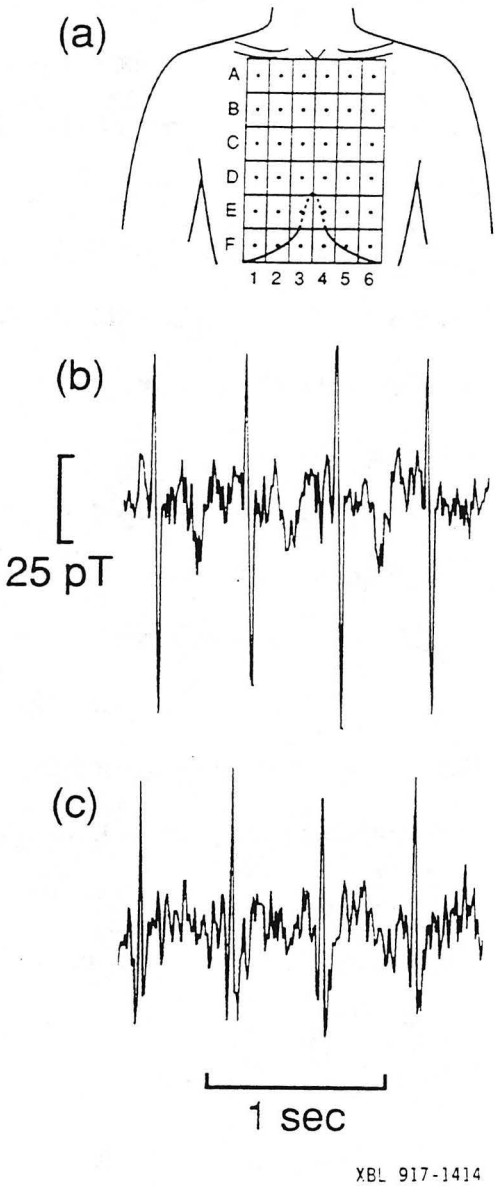

Fig. 4.6 (a) Rectangular reference grid on front of chest (redrawn from ref. [WIK81]). (b) and (c) Magnetocardiograms obtained from the same subject at D3 and D5, respectively.

fluctuations in the biepitaxial SQUID. Once we had developed bicrystal SQUIDs with low noise, we decided to test our ideas by making a flip-chip magnetometer using the same flux transformer but with the 40 pH type B SQUID described in chapter 2. Figure 4.7 shows the rms field resolution and the flux noise of this magnetometer. At 1 Hz the field noise of the magnetometer was 1.7 pT $Hz^{-1/2}$, which is not significantly better than the performance of the magnetometer with the biepitaxial SQUID. More importantly, the magnitude of this noise was not measurably reduced by our bias reversal scheme, indicating that it arose from the motion of flux vortices in the flux transformer.

At the time of this writing, it is unclear exactly where in the flux transformer the noise originated. The fact that we can make quiet SQUIDs means that we can make single layers of YBCO that are relatively noise free. In fact, we have demonstrated [LDN94] that superconductor-insulator-superconductor multilayer sandwiches can be grown which have no more noise than a single layer provided that all of the layers are deposited *in situ*. This leads us to believe that processing our multilayers creates defects in the upper YBCO film, the edges of the crossovers, and/or the superconducting via which act as weak pinning sites for vortices. Despite much hard work on both improving the quality of multilayer high-T_c structures [LDN94] and understanding the effects of transformer noise on magnetometer performance [FKW91, WKF91], the noise of flip-chip magnetometers remains an issue. Our best flip chip magnetometer to date [KOE94b] uses 16 turns on the input coil to achieve a resolution of 35 fT $Hz^{-1/2}$ in the white noise region, but the 1/f flux noise power is still an order of magnitude greater than that of the bare SQUID yielding 114 fT $Hz^{-1/2}$ at 1 Hz. Because of this we decided to try some alternatives to flip-chips which are discussed in the next chapter.

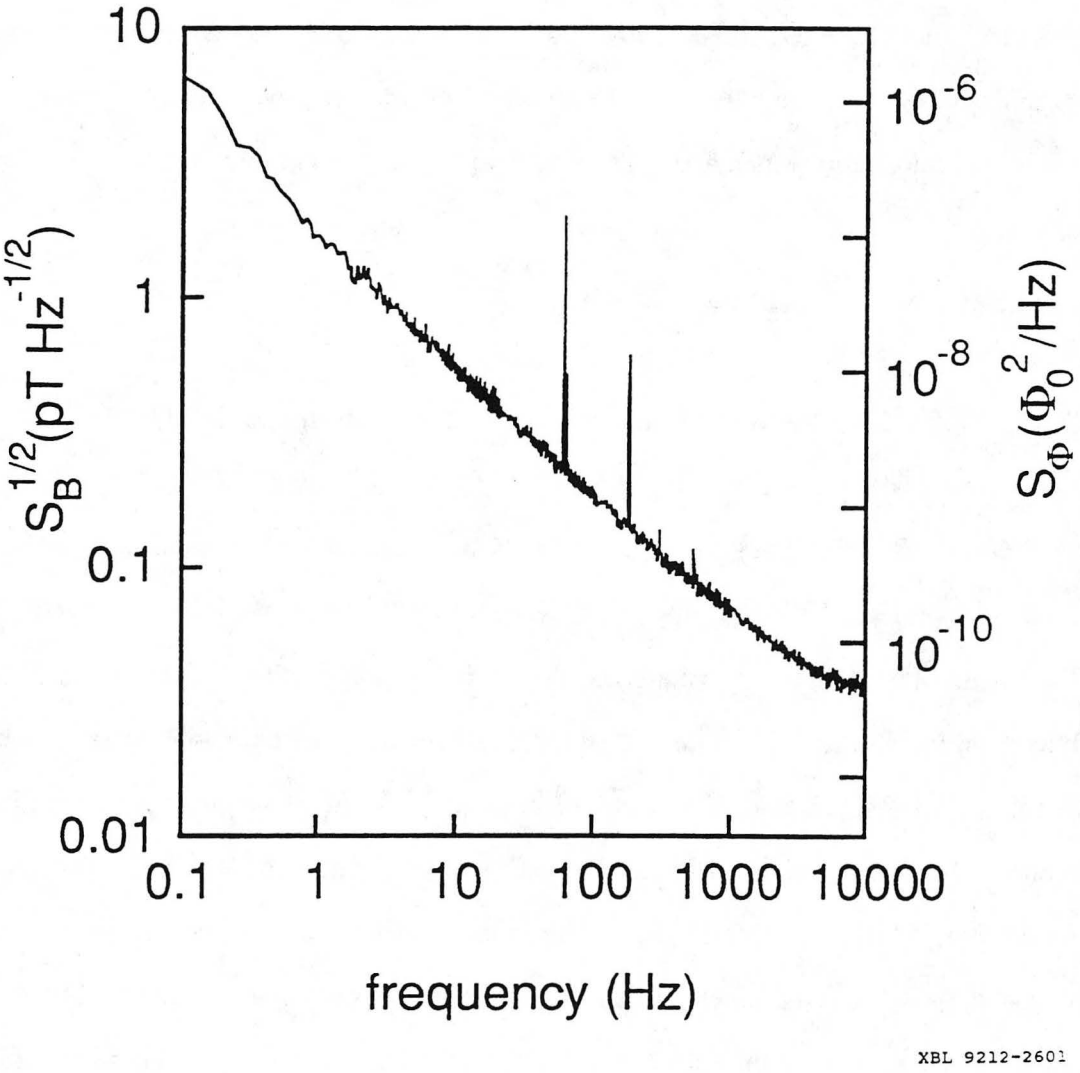

Fig. 4.7 Rms magnetic field noise, $S_B^{1/2}(f)$, and flux noise power, $S_\Phi(f)$, vs. frequency for flip chip magnetometer with bicrystal SQUID at 77 K.

Chapter V: Magnetometers with Single Superconducting Layers[1]

The work on magnetometers with flip-chipped flux transformers left us with many interesting but challenging materials and processing issues. While Frank Ludwig, David Nemeth, and Gene Dantsker were working to improve our multilayer processing technology, John Clarke, Dieter Koelle, and I decided to see how much progress one could make with magnetometers made out of single layers of superconductor.

Large-Area Square Washer SQUIDs

Figure 5.1 shows the configuration of our first design, a dc SQUID with a large area washer, which resembles the rf SQUIDs of Zhang *et al.* [ZMH93]. We call this our type C SQUID. Our film growers used a pulsed excimer laser to deposit 200- to 300-nm-thick c-axis oriented $YBa_2Cu_3O_{7-x}$ (YBCO) films on 10×10 mm^2 $SrTiO_3$ bicrystals with a 24° misorientation angle. We patterned the films using wet etching as described in chapter 3 to produce 2-3 μm wide junctions with typical resistances R of 1.5 Ω and critical currents I_0 of 150 μA at 77 K. The effective area for a square washer with no slit in it has been measured to be $A_w \approx 1.1$ dD, where D and d are the outer and inner dimensions of the washer [KGK85]. With the slit in the square washer, some of the applied flux will be focussed away from the inner SQUID hole. We thus expect that the area will be given by $A_w = \alpha_w dD$ where α_w is a numerical coefficient less than unity. We have fabricated several SQUIDs with D = 8.5 mm and various values of d, ranging from 27 to 107 μm, including one device (3) in which the inner hole was widened in successive steps by wet etching. We list the measured values of A_w in Table 5.1. To a reasonable approximation we find $A_w \approx 0.5$ Dd, a result comparable to that found for rf SQUIDs [ZMH93]. We

[1]Portions of this chapter have appeared previously as refs. [KML93] and [KMD93].

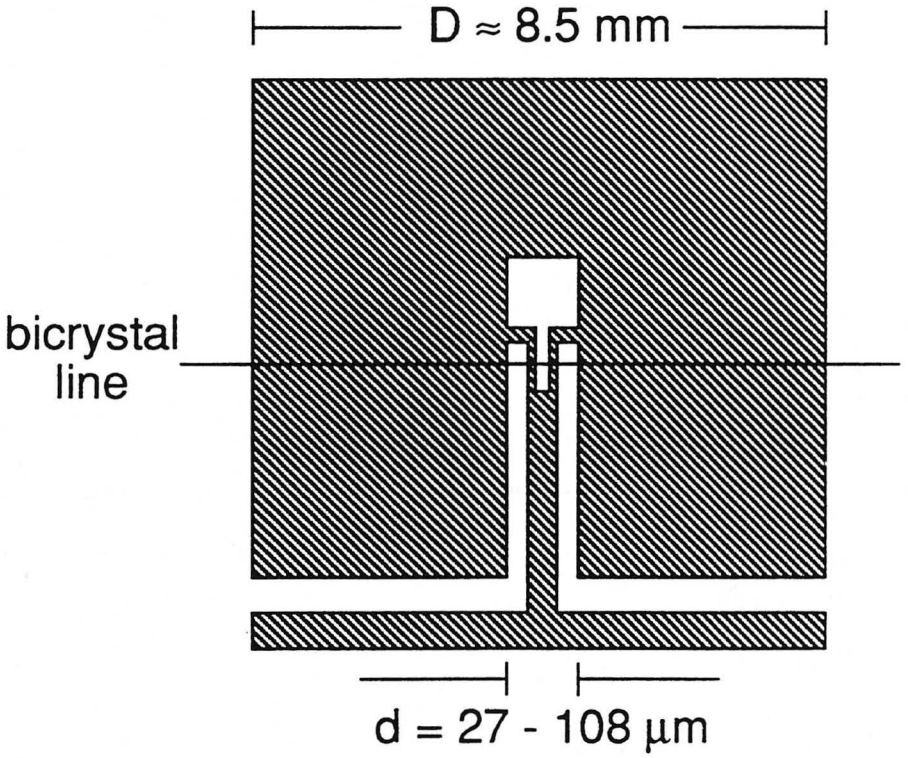

Fig. 5.1 Configuration of our type C, large-area square washer bicrystal SQUIDs (not to scale).

Table 5.1. Hole size, inductance, and effective areas for large-area type C SQUIDs (samples 1-3) and directly coupled magnetometers (4-7).

Sample (Device)	d (μm)	L (pH)	$A_{w,d}$ (mm^2)	A_w/dD	α_d
1 (897)	107	210	0.45	0.49	—
2 (943)	106	210	0.49	0.55	—
3C (951)	27	80	0.11	0.47	—
3B (951)	51	120	0.22	0.50	—
3C (951)	103	200	0.48	0.55	—
4 (833)	—	145	0.29	—	0.6
5 (981)	—	40	0.13	—	0.9
6 (984)	—	40	0.14	—	0.9
7 (1019)	—	20	0.086	—	0.8

tried covering the slit with a film of YBCO deposited on a second chip, but we were only able to obtain an improvement in the effective area of ~30%. Experiments with large type B SQUIDs (which have slits on two sides of the square washer) yielded even poorer performance, $A_w \approx 0.11$ Dd with the slits uncovered and $A_w \approx 0.23$ Dd with the cover.

Directly Coupled Magnetometers

A different approach to the problem, which we call the "directly coupled magnetometer" is shown in Fig. 5.2. It consists of a pickup loop of YBCO [Fig. 5.2(a)] connected to opposite sides of the body of a SQUID. The junctions are placed outside the SQUID washer which, in the version shown in Fig. 5.2(b) (sample 4), has inner and outer dimensions of 26 μm and 250 μm. It's based on the type A SQUIDs of chapter 3. The

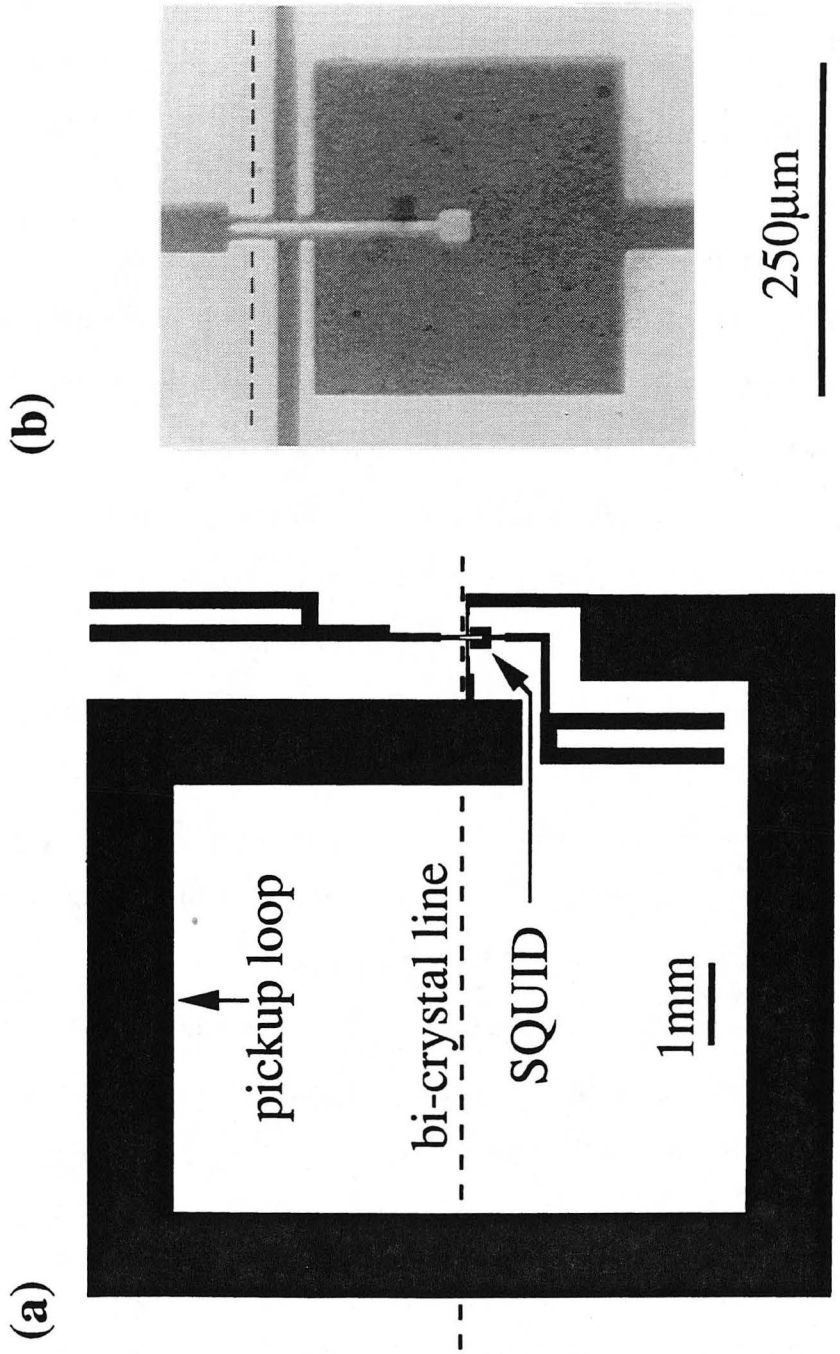

Fig. 5.2 (a) Configuration of directly coupled magnetometer (device 4); (b) detail of coupling to bicrystal SQUID. Dashed line indicates grain boundary.

principle of operation is similar to that of the early SLUGs (superconducting low-inductance undulatory galvanometers) [CLA66]. A magnetic field applied to the magnetometer induces a supercurrent in the pickup loop which is injected directly into the body of the SQUID. (Recall that for a dc SQUID the junctions are biased in the voltage state at all times so that no supercurrent flows through them.) Neglecting the mutual inductance between the pickup loop and the SQUID, we find an effective area $A_d = A_s + \alpha_d A_p L/L_p$, where A_p and L_p are the area and inductance of the pickup loop, L is the SQUID inductance, and α_d is the fraction of L to which the supercurrent couples. By comparison, the optimized effective area of a transformer with a multiturn input coil inductively coupled to a SQUID with coefficient $\alpha_m \approx 1$ is $A_m = A_s + \alpha_m A_p (L/L_p)(n/2)$, where we have set $n = \sqrt{L_p/L}$ as described in chapter 1. We see that A_d is a factor of approximately n/2 smaller than A_m, reflecting the advantage gained in the multiturn transformer by matching the pickup loop inductance to the SQUID inductance. For device 4 we estimate $L_p = (2/\pi)\mu_0 l[\ln(l/w) + 0.5] = 15$ nH [KET87], $A_p = 56$ mm^2, L = 145 pH (see Appendix A), and $\alpha_d = 0.6$. Neglecting A_s, we find $A_d = 0.34$ mm^2, in reasonable agreement with the measured value listed in Table 5.1. A rough estimate shows that this discrepancy can be accounted for by the stray inductive coupling between the pickup loop and the SQUID.

It is interesting to note that on the basis of simple arguments, both types of single layer devices, although different in design, are expected to have similar performance. For the large washer SQUID the inductance is given by $L = 1.25\,\mu_0 d + L_J$, where L_J is the inductance of the bridges containing the junctions (see Appendix A). With $A_w \approx 0.5$ Dd, we find $A_w \approx 0.4\, D(L-L_J)/\mu_0$. For the directly coupled SQUID with a pickup area $A_p = D^2$ and inductance $L_p \approx 1.6\,\mu_0 D$, we find a similar result, $A_d \approx \alpha_d A_p (L/L_p) \approx 0.3\, DL/\mu_0$, assuming $A_s \ll A_d$. This is not as surprising as one might think at first if one considers the distribution of currents in the large washer SQUIDs as discussed by Ketchen *et al.* [KGK85]. Figure 5.3 shows roughly the pattern of circulating supercurrent established in

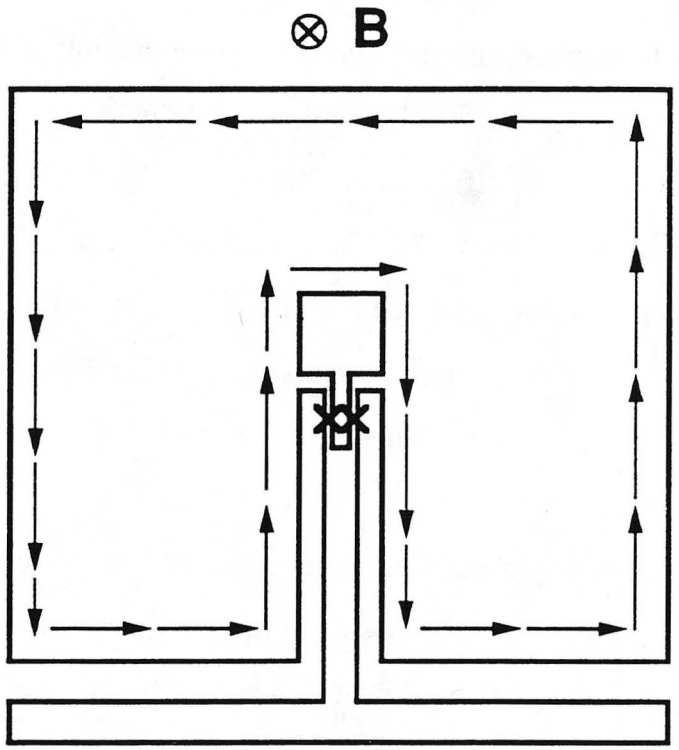

Fig. 5.3 Schematic representation of the flow of supercurrent in a large type C SQUID in response to an applied uniform field. (Redrawn after Fig. 2 of ref. [KGK85].)

the washer in response to an applied field, which, intuitively, we would expect to be concentrated primarily at the edges of the structure. As the current flows along the outer edge it cancels all of the applied flux to the washer body; it then reapplies some of that flux to the SQUID as it flows along the inner edge. The current flow suggested by this diagram is nearly identical to that in the directly coupled magnetometer, and thus we would expect them to have similar effective areas, apart from factors of order unity.

Since D is limited by the size of the substrate, one can attempt to increase the magnetometer area by increasing L. As a result, one expects the flux-to-voltage transfer coefficient, V_Φ, to decrease, and hence the spectral density of flux noise in the white noise limit, $S_\Phi^{(w)}(f)$, which is proportional to $1/V_\Phi^2$, should increase. However, because the magnetic field resolution, $S_B^{(w)}(f)$, scales inversely with A_w^2 (or A_d^2), it will not be affected as much by this. As discussed in chapter 3, one usually assumes that $V_\Phi \approx R/L$; since for both types of SQUIDs $A \propto L$[†] in the limit $L \gg L_J$, we expect the field resolution to be independent of L. Unfortunately, as discussed in chapter 3 the transfer function in fact falls off as $1/L^2$ at large values of inductance rather than 1/L so that the field resolution in the white limit should become *worse* as L is increased. It is therefore advantageous to reduce L as much as possible as long as the transfer function increases at least as fast as 1/L. (In the low β limit ($\beta \lesssim 1$), however, the transfer function becomes independent of L and saturates at a value given by the I_0R product of the junctions. For typical junction critical currents of 50-100 μA, this occurs at $L \approx$ 10-20 pH.) In contrast, if we assume that an appropriate bias current reversal scheme eliminates the 1/f noise due to critical current fluctuations, we expect the remaining 1/f flux noise, due to the motion of vortices in the body of the SQUID, to be approximately independent of L. Therefore, it is best to increase the inductance as much as possible so as to increase the effective area; the spectral density of the magnetic field noise in the 1/f regime, $S_B^{(1/f)}(f)$, should be reduced as $1/L^2$.

[†]We are in the undercoupled limit for the directly coupled magnetometer so $A \propto L$ and not $\sqrt{L}$.

We measured the noise of our SQUID magnetometers using our standard 100 kHz flux modulation and a flux-locked loop with both a static current bias and our 2 kHz bias reversal scheme. The SQUIDs were immersed in liquid nitrogen and surrounded by three mu-metal shields. In all cases the bias current was chosen to maximize V_Φ. The results are summarized in Table 5.2. Figure 5.4 shows both the rms field resolution, $S_B^{1/2}(f)$, and the equivalent flux noise power, $S_\Phi(f)$, for directly coupled magnetometer sample 4, shown in Fig. 5.2. With a static bias current the noise power scales approximately as 1/f for frequencies below 100 Hz and then becomes nearly white at higher frequencies. The use of bias current reversal reduces the 1/f noise power by almost 2 orders of magnitude at 1 Hz to the white noise limit of 290 fT $Hz^{-1/2}$. The sharp upturn in the noise at lower frequencies probably arises from drift, for example in the ambient field, rather than 1/f noise in the device. We note that when we reversed the bias current to any big washer SQUID the voltage at the output of the 100 kHz mixer circuit changed sluggishly, suggesting that flux trapped in the large area body of the SQUID moves slowly and possibly irreversibly. We believe that the SQUID is forced off the steepest part of the voltage-flux characteristic for a large fraction of the 2 kHz bias reversing cycle, thus resulting in the generally observed increase in white noise seen during bias reversal with big washer SQUIDs. We have not observed this behavior in any of our SQUIDs with washer sizes up to 500 μm.

Improvements to the Directly Coupled Magnetometer

Dieter Koelle continued with this project after I began the experiments described in the next two chapters, and produced many of the refinements which led to the improved performance of magnetometers 5-7 over that of device 4. Chief among these was reducing the SQUID inductance to increase the transfer function as described above. For device 4 (Fig. 5.2) 54% of the total inductance (79 pH) is in the narrow strips which contain the

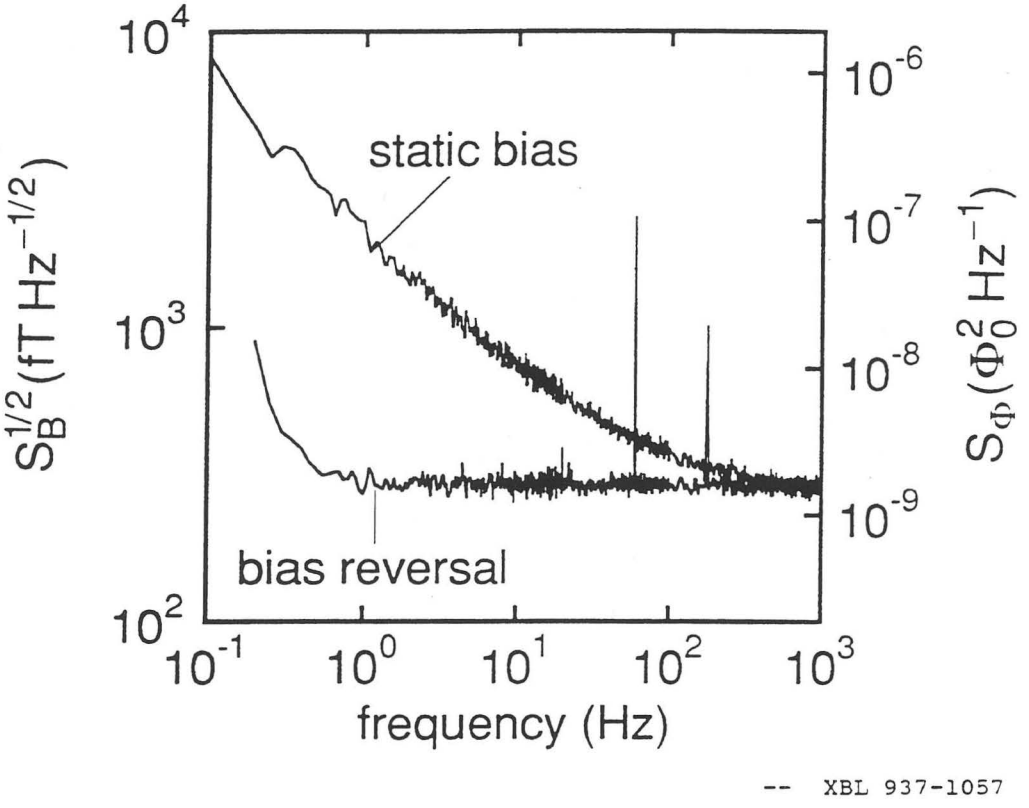

Fig. 5.4 Rms magnetic field field noise, $S_B^{1/2}(f)$, and flux noise power, $S_\Phi(f)$, vs. frequency for directly coupled magnetometer 4 for static current bias and current bias reversal.

Table 5.2. Performance and relevant parameters for large-area type C SQUIDs (samples 1-3) and directly coupled magnetometers (4-7).

Sample (Device)	L (pH)	R (Ω)	I_0 (μA)	V_Φ ($\mu V/\Phi_0$)	$[S_\Phi^{(w)}]^{1/2}$ ($\mu\Phi_0$ Hz$^{-1/2}$)	$[S_B^{(w)}]^{1/2}$ (fT Hz$^{-1/2}$)
1 (897)	210	1.3	14	1.8	—	—
2 (943)	210	1.0	320	1.8	107	450
3C (951)	80	2.0	135	28	15	280
3B (951)	120	1.4	185	7.3	40	380
3C (951)	200	1.4	180	1.7	210	900
4 (833)	145	2.1	45	7.1	40	290
5 (981)	40	3.2	70	93	6	105
6 (984)	40	2.3	70	73	14	210
7 (1019)	20	3.4	45	220	3.9	93

junctions. Also, 2/3 of this strip length is above the leads to the pickup loop which accounts for the poor coupling factor (α_d). Our best directly coupled magnetometer (sample 7) is shown in Fig. 5.5(a and b). The necks above the coupling leads have been made as short as possible (4 μm) while still allowing us to align the bridges to the grain boundary in the substrate. The inductance (20 pH) is formed entirely by the slit in the SQUID body; there is no central hole. Also, the pickup loop has been widened to reduce its inductance. The performance of this magnetometer and two others with slightly larger SQUIDs (40 pH) is summarized in Tables 5.1 and 5.2. With bias reversal, the 20 pH magnetometer achieved a resolution of 93 fT Hz$^{-1/2}$ at frequencies down to 1 Hz.

Another innovation [KMD93] was the use of a thin-film flux transformer fabricated on a 50 mm wafer by Kookrin Char and Ward Ruby of Conductus, Inc. [Fig. 5.5(c)]. The flux transformer has a single-turn input coil which is designed to match the pickup

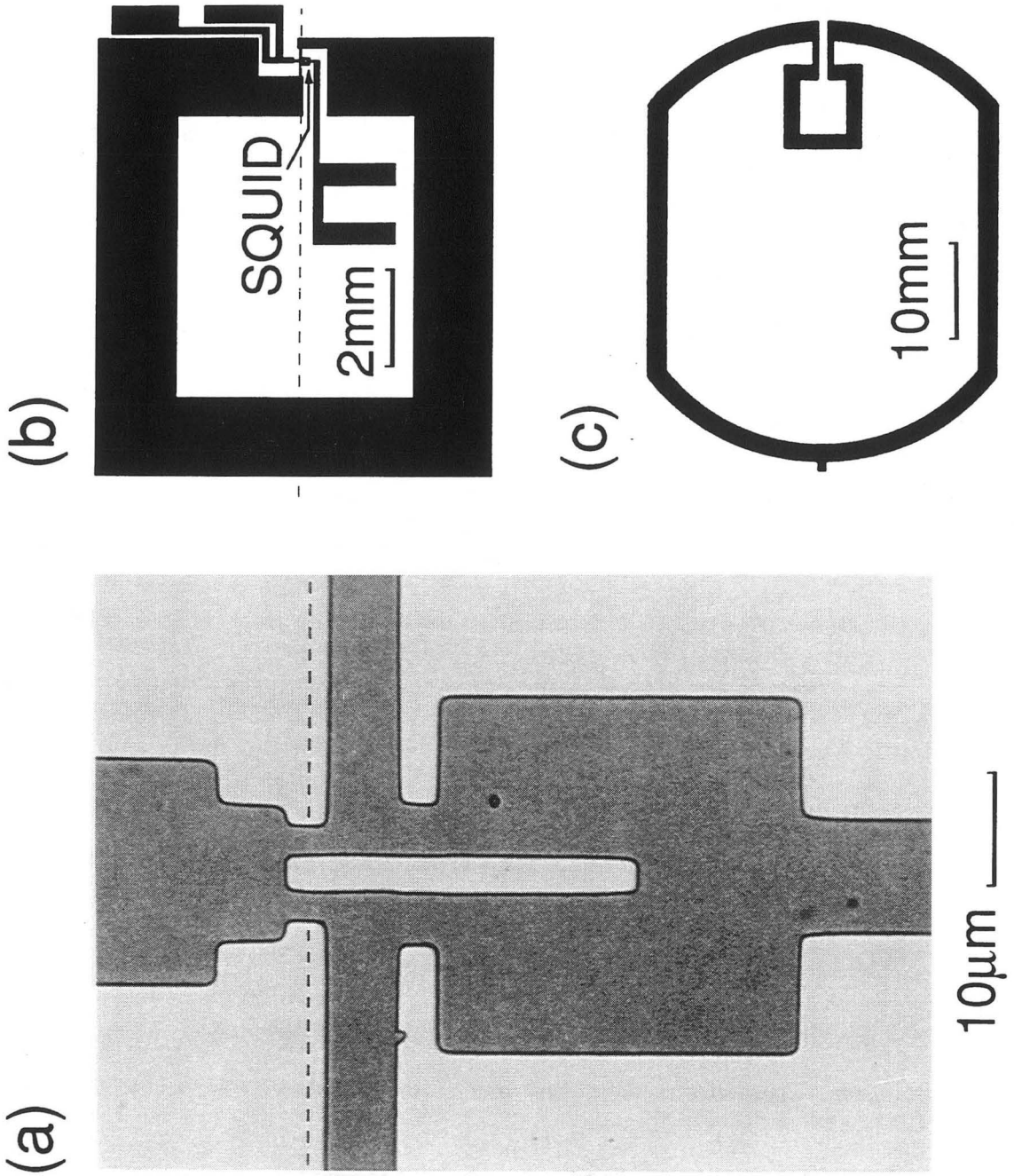

Fig. 5.5 Directly coupled magnetometer (sample 7). Photograph of a 20 pH SQUID (a) which is connected to the coupling loop as shown in (b). Dashed lines indicate grain boundary. (c) Configuration of single layer YBCO flux transformer.

loop on the directly coupled magnetometer. The increase in the pickup area is partly offset by the increase in the inductance of the large pickup loop, especially because the single-turn input coil is not well matched to the pickup loop. Nevertheless, this device achieved a net increase in the effective area of a factor of 3.4 over the directly coupled magnetometer alone. The coupling coefficient of the input coil to the pickup loop on the directly coupled magnetometer was estimated to be $\alpha_m = 0.9$ indicating that flip-chip coupling with structures that are much wider than the spacing between the chips can be very efficient.

More important is the fact that the flux transformer did not contribute any substantial amount of 1/f noise to the SQUID, and in fact, our estimates show that it would not be expected to. According to the model of Ferrari *et al.* [FKW91], flux noise in the large transformer will couple to the SQUID by inducing noisy screening currents in the flux transformer which then couple to the SQUID along with the screening currents induced by the applied magnetic field. The noise flux coupled to the flux transformer can be expressed as $S_\Phi(f) \approx S_r(f) N \Phi_0^2 l/w$, where $S_r(f)$ is the spectral density for the radial motion of a flux vortex and N is the number of uncorrelated vortices per unit area of film patterned into a total length l and width w. The corresponding magnetic field noise is

$$S_B(f) \approx \frac{S_r(f) N \Phi_0^2 \, l}{w A_p^2} . \qquad (5.1)$$

To investigate the noise contribution of the flux transformer, in a separate experiment we determined the noise in the YBCO film of the transformer by placing it directly over the 40 pH type B SQUID described in chapter 3 and measuring the flux noise coupled into the SQUID. We found $S_\Phi^{1/2}(1\ \text{Hz}) = 34\ \mu\Phi_0\ \text{Hz}^{-1/2}$, the same value that we measured for the SQUID alone.[2] This noise sets an upper limit of $S_r(1\ \text{Hz}) N \Phi_0^2 \approx S_\Phi(1\ \text{Hz}) / 4 \approx 3\times10^{-10}\ \Phi_0^2\ \text{Hz}^{-1}$ on the noise produced by the film [FKW91]. Inserting this value in Eq. (5.1), together with $l \approx 132$ mm, $w = 2$ mm and $A_p = 1.33\times10^{-3}\ \text{m}^2$, we find $S_B^{1/2}(1\ \text{Hz})$

[2]The SQUID had deteriorated somewhat by the time this measurement was made.

$\approx 2\times10^{-1}$ fT $Hz^{-1/2}$. Thus, the predicted 1/f magnetic field noise power created by the film is more than 4 orders of magnitude below that measured for our magnetometer. Evidently, one could fabricate these large flux transformers from films of much poorer quality and/or include noisy multilayer input coils in them without degrading the low frequency performance of the magnetometer.

The field resolution of our 20 pH directly coupled magnetometer is shown in Fig. 5.6(b) along with the noise of the directly coupled magnetometer with the 50 mm flux transformer (trace c). For comparison, I have also displayed the noise of our best flip-chip multiturn flux transformer.(trace a). At high frequencies the better coupling to the SQUID afforded by the multiturn input coil gives the flip chip the best field resolution per unit of pickup loop area. However, below ~1 Hz, the 1/f noise of the flux transformer makes the single layer device more attractive. With the flux transformer, the single layer device achieved a resolution of 39 fT $Hz^{-1/2}$ at 1 Hz, falling to 31 fT $Hz^{-1/2}$ at frequencies above 5 Hz. The current world's record for a high-T_c magnetometer of any kind is presently held by the group at Jülich [MUC94] who achieved 24 fT $Hz^{-1/2}$ at frequencies down to below 0.5 Hz with a thin film rf SQUID and a large area (~ 50 mm × 50 mm), single-turn flux transformer similar to the one described here. Certainly none of these devices has met the rather rigorous standards outlined in chapter 1 for biomagnetic imaging, but nevertheless there are many applications where they might be useful. For example, monitoring the heart activity of a developing fetus with a single channel magnetometer could be done with a 100 fT $Hz^{-1/2}$ device. This is a problem that is well-suited to magnetic detection since it is not feasible to place electrodes inside the womb. Another area that has attracted much interest recently is in using the magnetotelluric method [CLA83, NMC88, CGG83, GGC79] to study geophysical and geological processes. These applications generally require resolutions of ~100 fT $Hz^{-1/2}$, and since the fields to be studied are uniform over large distances, a detector size of 50 mm is not a problem. Also, geophysical studies, which are often conducted at remote locations in inaccessible

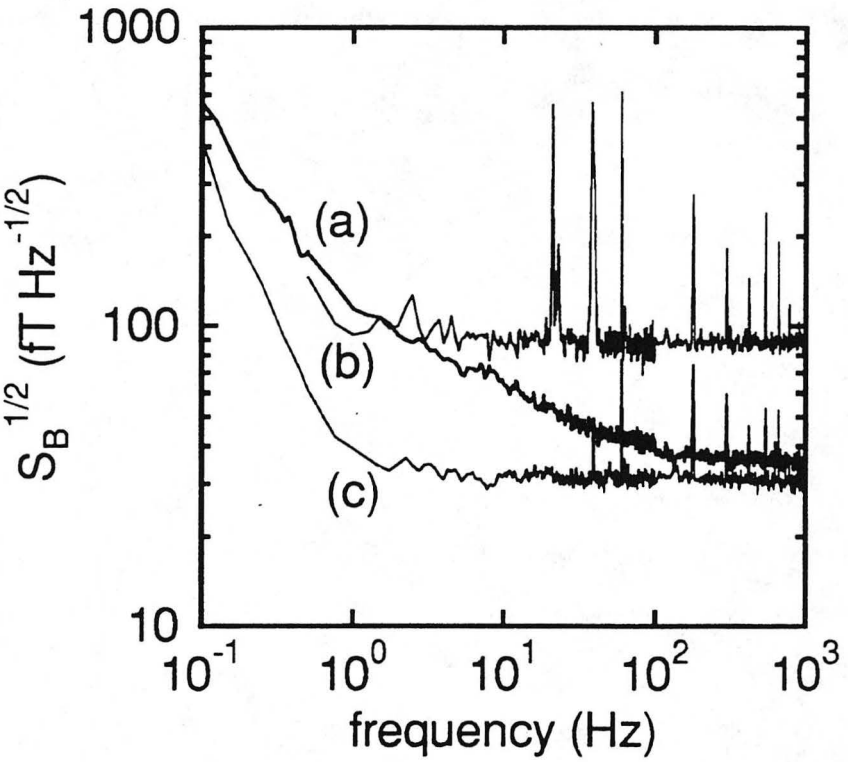

Fig. 5.6 Rms magnetic field resolution for our best examples of three different types of magnetometers. In descending order of noise at 1 Hz: (a) 16-turn input coil flip-chip flux transformer with a $(9\ \text{mm})^2$ pickup loop on a 40 pH SQUID; (b) 20 pH directly coupled magnetometer of Fig. 5.5(a and b); (c) 50 mm flux transformer on the 20 pH directly coupled magnetometer of Fig. 5.5. Spikes in the spectrum are from microphonic noise and 60 Hz pickup.

areas, would benefit greatly from the slower boil-off rate of liquid nitrogen as opposed to liquid helium. Gene Dantsker recently demonstrated a prototype 3-axis magnetometer system which used three of our directly coupled magnetometers. All three channels operated simultaneously in a field environment with the SQUIDs cooled in a dewar filled with liquid nitrogen [DKM94]. We were not able, however, to measure the noise of the devices in the field. It is likely that the presence of the Earth's static magnetic field increased the noise of the devices over that measured in the laboratory for reasons described in the following chapter.

Chapter VI: Behavior of SQUIDs in the Earth's Magnetic Field[1]

This chapter may well be subtitled "When Good SQUIDs Do Bad Things." The applications outlined in the previous chapter for geophysical magnetometry (and to a certain extent biological magnetometry) all presume that the SQUID maintains its good performance even when operated in the harsh environment outside of the laboratory. Roger Koch has performed extensive studies of one problem associated with this, the large amounts of rf interference present in large urban areas [KOC93b, KFS94, KFR94]. Another problem is that the SQUID must be cooled in the Earth's static magnetic field. In this chapter, I discuss experiments I performed with the assistance of Dieter Koelle to determine what effect this has on the performance of our bicrystal SQUIDs, and in particular on their noise.

Noise of High-T_c Films in a Static Field

This work was largely motivated by a series of experiments conducted by Tim Shaw [FER91, FJW94] in which he measured the random motion of flux vortices in thin films of YBCO cooled in a static magnetic field B_0. The apparatus is shown in the upper half of Fig. 6.1. A low-T_c SQUID was placed ~100 μm from the film in a specially designed cryostat in which the SQUID was kept at 4.2 K while the sample temperature was adjusted independently up to 100 K. The random hopping of flux vortices in the high-T_c film produces 1/f noise which is measured by the low-T_c SQUID. A stable magnetic field was provided by a superconducting Nb wire coil. Shielding of external fields was accomplished by use of a mu-metal shield at room temperature plus a

[1]Portions of this chapter were reported previously at the OE/LASE '94 conference [MKS94b] and the 4th International Superconductive Electronics Conference [MKS93], and are scheduled to be published as ref. [MKS94].

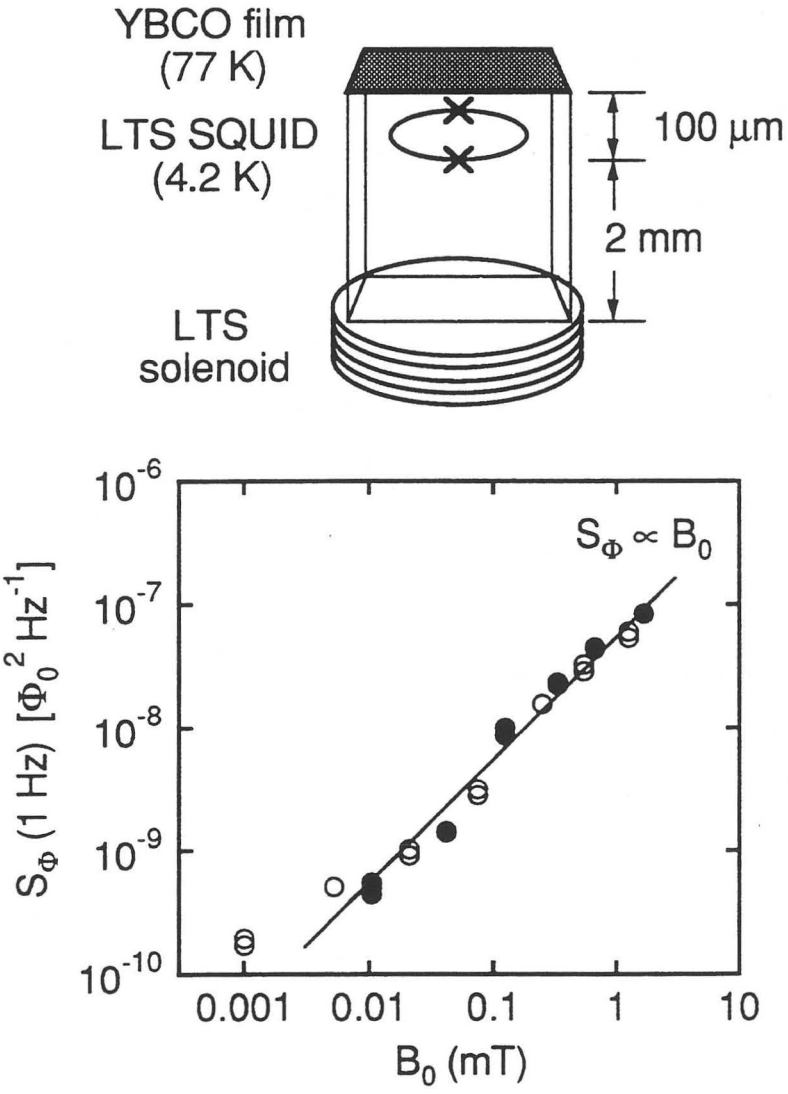

Fig. 6.1 (top) Apparatus for measuring the hopping of vortices in a high-T_c film. (bottom) Noise spectral density $S_\Phi(1\ \text{Hz})$ for a YBCO film at 77 K, as measured by a low-T_c SQUID, vs. magnetic field B_0 in which the film was cooled. Line is a least squares fit to $S_\Phi(1\ \text{Hz}) \propto B_0$. Filled and open symbols indicate reversed directions of B_0. "Zero-field" cooled data are shown at 0.001 mT.

superconducting can surrounding the experiment. When the films were cooled in low fields, typically below a few μT, the 1/f magnetic flux noise was more or less independent of field[2]. At higher fields, however, the spectral density of the flux noise, $S_\Phi(f)$, increased linearly with B_0 as shown in Fig. 6.1 for one of our quietest YBCO films at 77 K. This behavior has a simple explanation. In low cooling fields, the vortices trapped in the high-T_c film are generated spontaneously as the film is cooled through T_c. At higher fields, since the number of vortices is proportional to B_0, we expect $S_\Phi(f)$ to be proportional to B_0 provided the hopping of the vortices is, on the average, uncorrelated. We note that the data in Fig. 6.1 is from an exceptionally quiet film; most YBCO films have $S_\Phi(1\ \text{Hz}) \sim 10^{-9}\ \Phi_0^2\ \text{Hz}^{-1}$ when zero field cooled at 77 K. Given these effects in films, one might expect similar increases in the 1/f noise of high-T_c SQUIDs operated in nonzero static fields. Indeed, Koch reported significant increases in the 1/f noise of a SQUID after applying and removing a magnetic field [KOC93b].

A Stabilized Field at 77 K

For the high-T_c SQUID experiments, the devices were immersed in liquid nitrogen. To obtain a stable magnetic field we wound a copper wire solenoid around a hollow tube of yttria stabilized zirconia (73 mm long, 17.5 mm outer diameter) coated with a 50- to 100-μm-thick layer of sintered, polycrystalline YBCO [BAW91, ABA91] as shown in Fig. 6.2. The SQUID under test was placed in the center of the solenoid with its sensing axis along the axis of the solenoid. We applied the appropriate current to the solenoid with the YBCO shield and SQUID above their transition temperatures, and lowered the probe into liquid nitrogen. When the YBCO tube became superconducting, it trapped the ambient field, stabilizing it against fluctuations in the solenoid current which was usually maintained

[2]In this chapter I plot "zero-field" cooled data (i.e. cooled with no applied field) at 0.001 mT, which I feel is a conservative estimate of the residual field generated in the superconducting shield as it passes through T_c.

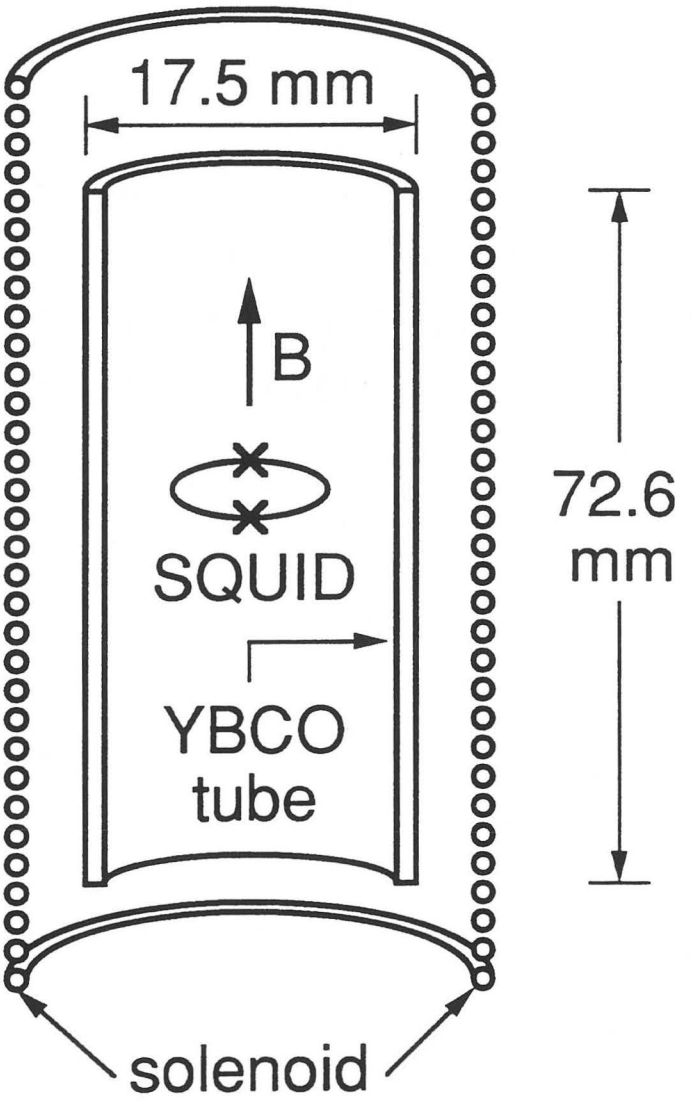

Fig. 6.2 Cross section view of Cu-wire solenoid and YBCO tube used to produce a stabilized field in a dewar of liquid nitrogen. The YBCO SQUID is oriented with its sensing axis parallel to the axis of the tube.

throughout the course of the experiment. This procedure enabled us to make measurements in fields up to 1 mT, well above the maximum field the tube could support with the field from the solenoid removed. To provide shielding from the external magnetic environment, a multilayer cylinder of high permeability foil was mounted around the solenoid, and two concentric mu-metal shields were placed around the cryostat.

To measure the shielding factor of the YBCO tube we cooled it in zero field and then applied a slowly varying current to the solenoid and measured the field inside the tube with the SQUID. Two such traces, taken with the same SQUID but different amplitudes of solenoid current, are shown in Fig. 6.3. From the slope of the lower trace I deduced a shielding factor of 22,000. For applied fields $\gtrsim 0.18$ mT the shielding broke down as shown in the upper curve, implying a critical current in the tube of 140 - 290 A/cm^2. Also, hysteresis is evident in the lower curve in Fig. 6.3 suggestive of flux motion into and out of the tube. This particular tube was made two years ago and had been used previous to this experiment, so the admittedly poor quality may not be representative of the state of the art. I note that YBCO tubes with screening factors of 10^6 have been reported [SYZ89]. Despite these difficulties, the measured screening factor was sufficient to attenuate noise in the current source to a level below that observed in our SQUIDs.

We made measurements on both a type A bicrystal SQUID (see chapter 3) and a directly coupled SQUID magnetometer (device 4 of chapter 5). For the remainder of this chapter I will refer to these as "the SQUID" and "the magnetometer," respectively. Figure 6.4 is a photograph of the SQUID which has a 250 μm outer diameter. Because of a mishap during patterning of the SQUID, a superconducting bridge shorted together the lines containing the junctions outside the main SQUID body producing a SQUID approximately 30 μm long and 15 μm wide. In fact, this short was rather fortuitous, since it reduced the estimated SQUID inductance to 39 pH thereby reducing the white noise. The pertinent parameters of both devices are listed in Table 6.1.

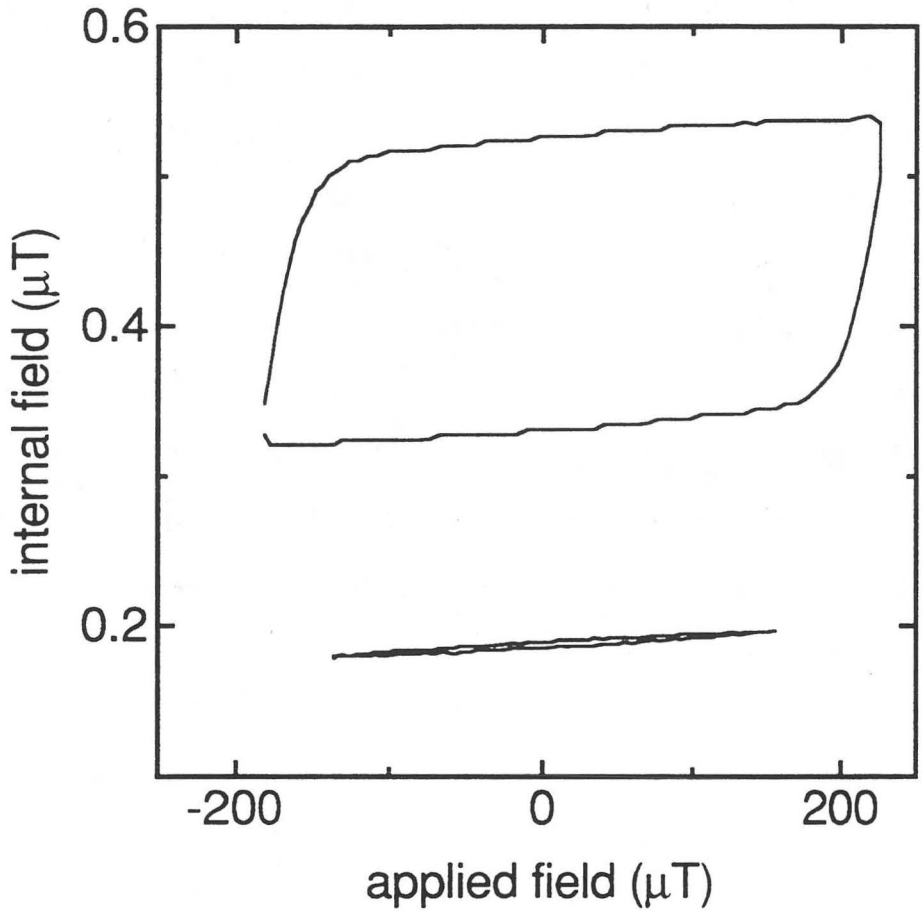

Fig. 6.3 Field measured inside the YBCO tube after zero-field cooling in response to a field applied with the solenoid. Upper trace is for larger amplitude of applied field and shows the effects of exceeding the critical current of the tube. Note the different scales.

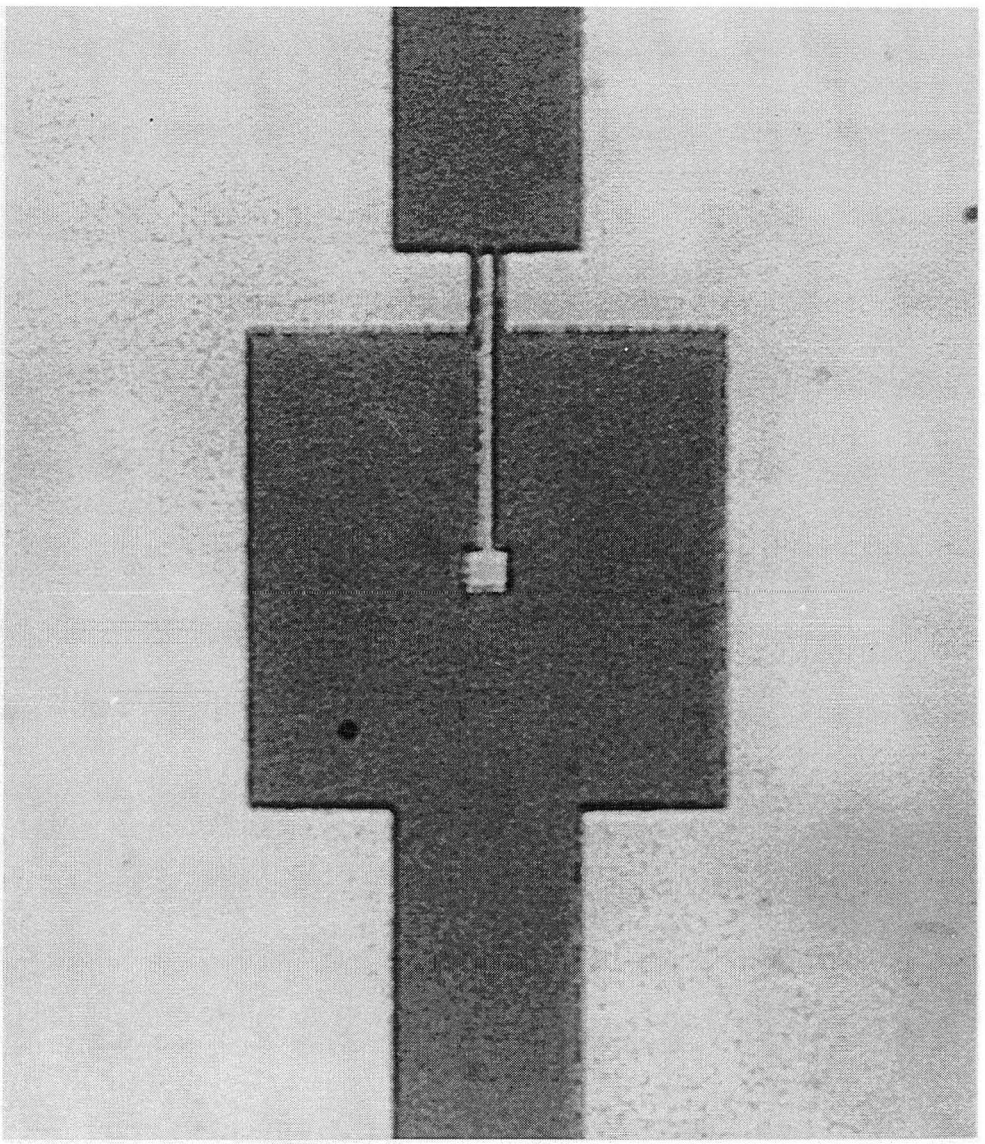

Fig. 6.4 Photograph of "the SQUID," a type A bicrystal SQUID. Square washer body is 250 μm along the outside.

Table 6.1. Parameters for SQUID and SQUID magnetometer. I_0 and R are the critical current and asymptotic resistance per junction (in zero field) at 77 K, L is the SQUID self inductance, and A is the effective area of the device.

Sample (Device)	I_0 (μA)	R (Ω)	L (pH)	A (mm^2)
SQUID (912-2)	1225	0.3	39	0.0013
magnetometer (833)	45	2.1	145	0.29

Critical Currents of the SQUIDs in a Magnetic Field

When we cooled the SQUID in a magnetic field the critical current of the junctions was reduced, as shown in Fig. 6.5(a); we observed similar effects for the magnetometer. The work of Rosenthal *et al.* [RBC91], which accounts for the flux focusing effects of a zero-field cooled superconductor in an applied field, predicts that the first minimum in critical current should occur at a field $\Phi_0 / (0.543\ w^2) \approx 0.42$ mT for our junction width $w = 3\ \mu m$, in surprisingly good agreement with our measurements. This can create a problem for SQUID operation because drifts in the ambient field will cause significant changes in the critical current. This effect is shown dramatically in Fig. 6.5(b) for the SQUID field cooled in 0.15 mT. Here I have plotted the output of the demodulator in the SQUID electronics vs. applied field, a rough measure of the V-Φ curve of the SQUID. SQUID-type voltage modulation persists for only a few periods before the critical current changes to the point that the SQUID is no longer properly biased. This observation emphasizes the need to use junctions with narrow linewidths; narrower linewidths than our present value of 2-3 μm, limited by the critical current density of about 5×10^3 A cm^{-2}, would be preferable. It should be noted, however, that the effect is ameliorated when the

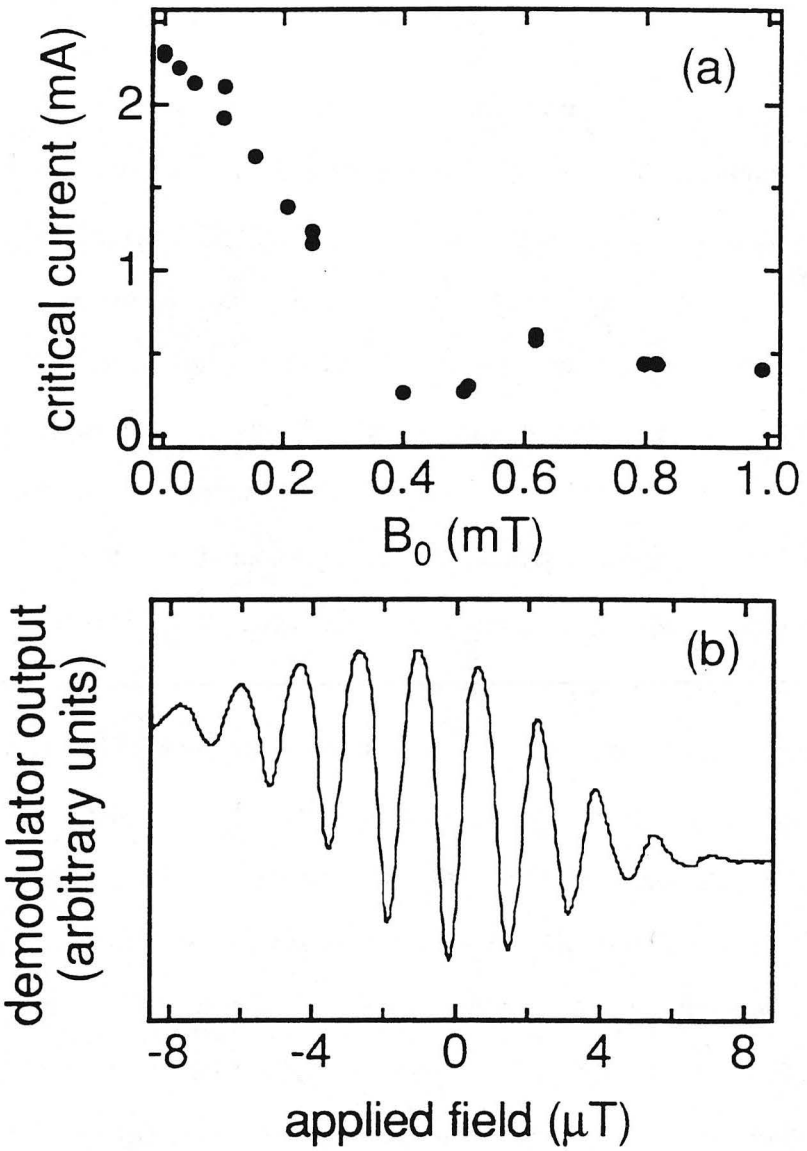

Fig. 6.5 (a) Critical current of the SQUID as a function of static cooling field, B_0. (b) Output of the SQUID box demodulator (mixer) vs. applied field for the SQUID cooled in $B_0 = 0.15$ mT.

SQUID is operated in a flux-locked loop, and that schemes to adjust the bias current automatically are available [HKM92].

Noise of High-T_c Devices in a Static Field

To measure their noise we operated our devices in a flux-locked loop with 100 kHz flux modulation (static bias current). Despite the reduction in critical current neither device showed an increase in white noise for $B_0 \leq 0.05$ mT. At higher fields, the white noise increased in a non-systematic way as shown in Fig. 6.6. Roughly, the variation of the white noise correlated with changes in the overall quality of the V-Φ transfer curve as judged by monitoring the mixer output, but no quantitative relationship could be found. At sufficiently low frequencies, both devices exhibited excess noise. In roughly one-third of the times that we cooled the samples we observed random telegraph signals (RTS) in which the SQUID output switched randomly between two values. This noise, generated by a single hopping event, was generally eliminated when we raised the device above its transition temperature and cooled it again. In the absence of RTS, the spectral density of the low-frequency noise was close to 1/f. Figure 6.7 shows the measured 1/f noise at 1 Hz versus B_0 for both devices for static bias current and for bias reversal at 2 kHz. In the case of the SQUID with a static bias current [Fig. 6.7(a)] S_Φ(1 Hz) is approximately constant for $B_0 \lesssim 0.2$ mT and increases at higher fields. With bias current reversal, on the other hand, S_Φ(1 Hz) is markedly reduced at the lower fields, and scales as B_0^m for $B_0 >$ 0.01 mT, where $m = 0.87 \pm 0.09$; the noise likely arises solely from vortex motion. Figure 6.7(b) shows ΔS_Φ(1 Hz), the difference in the two spectral densities in Fig. 6.7(a), vs. B_0. With the exception of one point ΔS_Φ(1 Hz) is roughly constant. Recall from chapter 1 that flux modulation with a static bias current removes the symmetric component of the critical current fluctuations of the two junctions, but not the antisymmetric component which produces a noisy circulating current in the SQUID. This

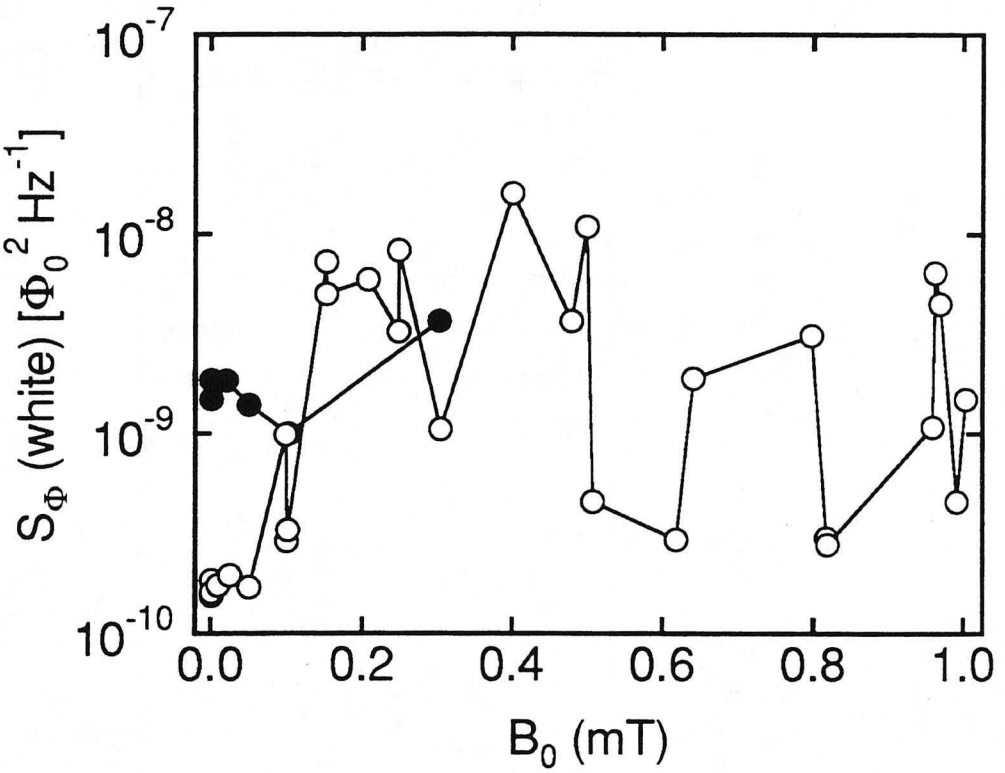

Fig. 6.6 White noise power with standard modulation (static bias current) for the SQUID (open circles) and the magnetometer (filled circles) vs. B_0.

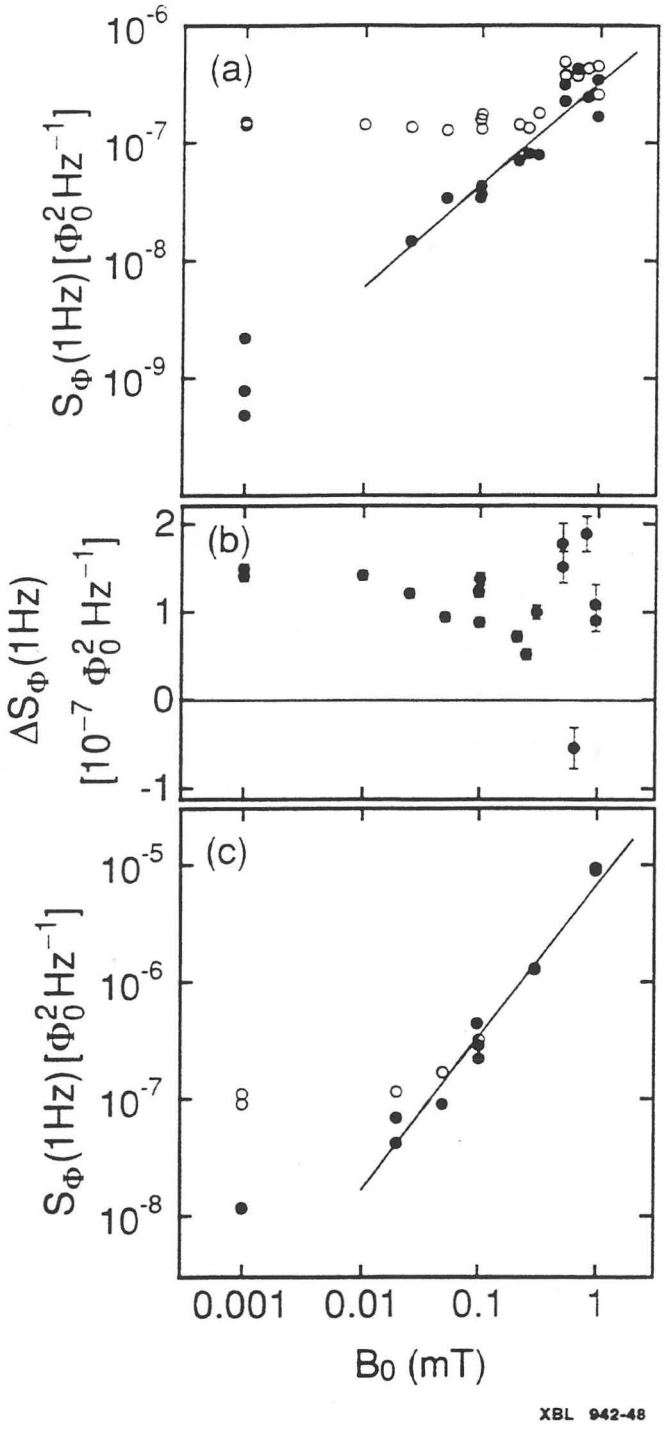

Fig. 6.7 (a) Spectral density of 1/f flux noise S_Φ(1 Hz) vs. B_0 for the SQUID at 77 K. Open circles are for static bias current, filled circles for bias reversal. "Zero-field" cooled data are shown at 0.001 mT. (b) Difference in S_Φ(1 Hz) for the SQUID measured with and without bias reversal. (c) S_Φ(1 Hz) vs. B_0 for the magnetometer. Lines in (a) and (c) are least squares fits to $S_\Phi(1\text{ Hz}) \propto B_0^m$ for $B_0 > 0.01$ mT.

latter component is removed by bias reversal. Thus, the noise difference $\Delta S_\Phi(1\ \text{Hz})$ in Fig. 6.7(b) should reasonably be expected to scale as $S_{Ic}L^2$ (where S_{Ic} is the spectral density of critical current noise), and should therefore be independent of changes in V_Φ with cooling field. For this device, the critical current fluctuations are approximately independent of B_0 up to 1 mT, despite the fact that the critical current is reduced by a factor of 8.

Figure 6.7(c) shows $S_\Phi(1\ \text{Hz})$ vs. B_0 for the magnetometer with and without bias reversal. In this case, the two noise levels are not very different because the flux noise is much higher than in the case of the bare SQUID. For the case of bias reversal, $S_\Phi(1\ \text{Hz})$ scales as B_0^m for $B_0 > 0.01$ mT, where $m = 1.3 \pm 0.1$. We emphasize that we cannot be sure if the flux noise is generated in the magnetometer itself or if it is due to fluctuations in the ambient field, for example, due to the motion of vortices trapped in the polycrystalline YBCO shield. On the other hand, the bare SQUID has a field sensitivity 230 times smaller than the magnetometer and should exhibit a noise power 54,000 times smaller if the noise were generated externally. Since $S_\Phi(1\ \text{Hz})$ for the SQUID is only 50 times less than that for the magnetometer, we can say with confidence that in this case it is intrinsic.

When cooled in 0.05 mT, the SQUID and magnetometer show increases in $S_\Phi(1\ \text{Hz})$ of about 21 and 12, respectively, over the zero field values. Furthermore, the noise in both devices at all fields is substantially higher than that of our quiet unpatterned YBCO film (Fig. 6.1). The higher level of noise may be due, at least in part, to the fact that the long, narrow lines containing the grain-boundary junctions enhance the sensitivity of the SQUID to the motion of a given vortex [FKW91]. It is also possible that damage at the patterned edges of the films provide copious weak flux pinning sites; edge pinning has been shown to be a dominant source of hysteresis in high-T_c devices [SGK93]. Improvements in the quality of the edges have greatly reduced this hysteresis [SGK93b], and may well also reduce the 1/f flux noise. However, even the unpatterned film showed an increase in $S_\Phi(1\ \text{Hz})$ of 15 when cooled in 0.05 mT, implying that excess flux noise is

likely to be an issue for devices operating in the Earth's field unless one can find a way to pin the flux more effectively in high quality thin films. An alternative practical solution to this problem may be found in the principle of the three-SQUID gradiometer [KRS93]; one could use a (nonsuperconducting) magnetometer and bucking coils to provide a low-field environment for the SQUIDs at all times, including the initial cooling process.

Chapter VII: A SQUID-based Voltmeter[1]

So far this dissertation has discussed only SQUIDs used for low-frequency magnetometry. This overlooks the great range of other uses which SQUIDs have found. Most commercial manufacturers of low-T_c SQUIDs will sell the user a SQUID with a superconducting input coil on it and two superconducting screw terminals to attach to a signal source. Thus, the SQUID can be used as a high-resolution detector of any signal which can be converted into a current. In this chapter I discuss an experiment to construct a high-resolution voltmeter out of high-T_c SQUIDs.

Basic SQUID Voltmeters

SQUID voltmeters made of low-T_c materials have existed for a long time.[2] In fact, the first practical device using Josephson tunnelling, the SLUG (superconducting low-inductance undulatory galvanometer), was originally conceived as a voltmeter [CLA66]. It is important to bear in mind, however, that a superconducting voltmeter is only competitive with more conventional amplifiers for a limited range of signal sources. Transistors and FETs operating at room temperature have outstanding performance when the voltage source is in the range of 1 kΩ to 1 MΩ. For example, the 2N5434 JFET, which is the preamplifier on our SQUID box electronics, at 100 kHz has a voltage noise of 0.5 nV $Hz^{-1/2}$ and a current noise of 5 fA $Hz^{-1/2}$ for an optimal noise temperature of 0.09 K, but only when looking at an optimal source impedance of 100 kΩ. At low source resistances, a small intrinsic voltage noise is desirable, and this can be achieved by using cooled transformers and resonant circuits. (See, for example, the recent work

---

[1]Believe it or not, this chapter has not yet been published. However, the results in it were presented previously at the 1994 March Meeting of the American Physical Society [MKL94].

[2]Even recently work has been done on low-T_c voltmeters, for example with a dc SQUID using additional positive feedback [PDK94].

published in ref. [LLB92].) However, this requires an input at a frequency of at least a few Hz. For small, quasistatic voltages coming from a low-impedance source, the SQUID voltmeter is the optimal choice. Examples of experiments of this nature are measurements of thermoelectric effects [RUM69], charge imbalance in superconductor junctions [CLA86], and flux creep in high-T_c superconductors [GSB91].

The voltmeter is shown schematically in Fig. 7.1(a). A voltage V_S from a source with resistance R_S is applied to a calibrated resistance R_0 in series with an input coil of inductance L_i and resistance R_i. This coil is coupled with a mutual inductance M_i to a high-T_c SQUID of inductance L. The SQUID, which I bias with either our standard modulation techniques or with double modulation, is flux modulated in the usual way. In principle one could record the flux in the SQUID and infer the input voltage knowing the impedances of each element in the input circuit. However, it is easier in practice to use the feedback network in the SQUID electronics to apply a current to the input circuit as shown in Fig. 7.1(a). In this mode, it is easiest to think of the circuit in terms of its Thevenin equivalent shown in Fig. 7.1(b). V_F represents a feedback voltage source with output impedance R_0 which is identically equal to $I_F R_0$ and which the SQUID adjusts to maintain zero current in the input coil. In this case, one has trivially $V_F = I_F R_0 = V_S$, so that one need only know R_0 to find V_S. Additionally, the use of feedback increases the resistance loading the voltage source substantially, to $R_\Sigma[1+G(f)]$ where $R_\Sigma = R_S + R_0 + R_i + i2\pi f L_i$ and G(f) is the open loop gain of the feedback loop. In order to reduce the noise of the input circuit (see below) one would like to keep R_i and R_0 as small as possible. However, it is clear from Fig. 7.1(a) that one cannot make R_0 too small compared with the rest of the input circuit or else the feedback electronics will not be able send current to the input coil. In particular R_0 must be real (i.e., not just an inductor) for operation with quasistatic voltages. Furthermore, this means that the input coil inductance cannot be too large, and for most of this work I will assume that $2\pi f L_i \ll R_S, R_0, R_i$.

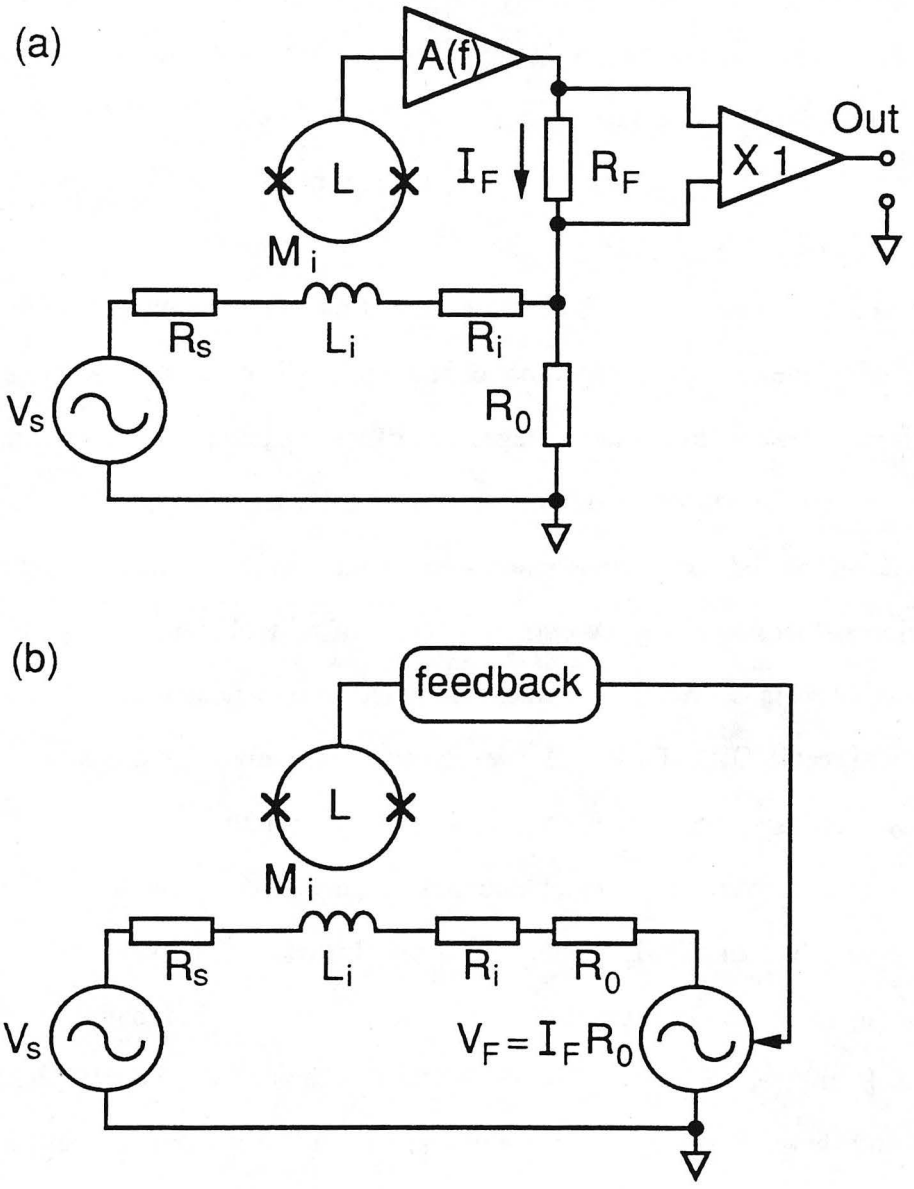

Fig. 7.1 (a) Block diagram of my high-T_c SQUID-based voltmeter. (b) Thevenin equivalent input circuit.

Design Considerations for High-T_c Voltmeters

Realizing this circuit with a high-T_c technology is not as straightforward as with low-T_c technology. In the latter case, it is relatively simple to bond thin Nb or Pb wires to a superconducting coil to produce a zero resistance input circuit. However, for a multiturn input coil made of high-T_c material the flux noise of the coil would degrade the resolution of the voltmeter in the same way as it does that of our flip chip magnetometers (chapter 4). Furthermore, even if a quiet superconducting input coil could be made, high-T_c wires are rather inflexible, and, to our knowledge, they cannot be bonded to a thin film of YBCO to produce a superconducting contact. Given that the leads and contacts to the coil are resistive, one is led to the conclusion that, at least in a certain resistance range, little resolution is lost in making the entire input coil of normal metal, but the relatively large resistance of metallic thin films makes it impractical to deposit a multiturn input coil on a square washer SQUID. Cu wire however has a relatively large cross-sectional area and thus a typical resistance at 77 K of ~1 mΩ per cm of length.

Of course, it is not reasonable to make a Cu-wire coil with dimensions of the order of our square washer SQUIDs (250 - 500 μm). Instead I chose to make a wire input coil which couples to the pickup loop of one of our directly coupled magnetometers shown in Fig. 7.2 [sample 5 of chapter 5 (#981)]. In this device, the SQUID inductance, L, is 40 pH and the pickup loop has a mean size of 7.5 mm × 7 mm and a 1 mm linewidth for an inductance of $L_p \approx 14$ nH [KET87]. In experiments of the type described in chapter 5 where the single-turn input coil of a very large area flux transformers was flip-chip coupled to the pickup loop of this magnetometer [KMD93], it was found that the mutual inductance between the input coil and the pickup loop was $\approx 0.7\ L_p$. Thus, for the voltmeter, I expect that the mutual inductance between the n-turn input coil and the pickup loop should be $\eta n L_p$ where $0.5 < \eta < 1$. Since for this directly coupled magnetometer the

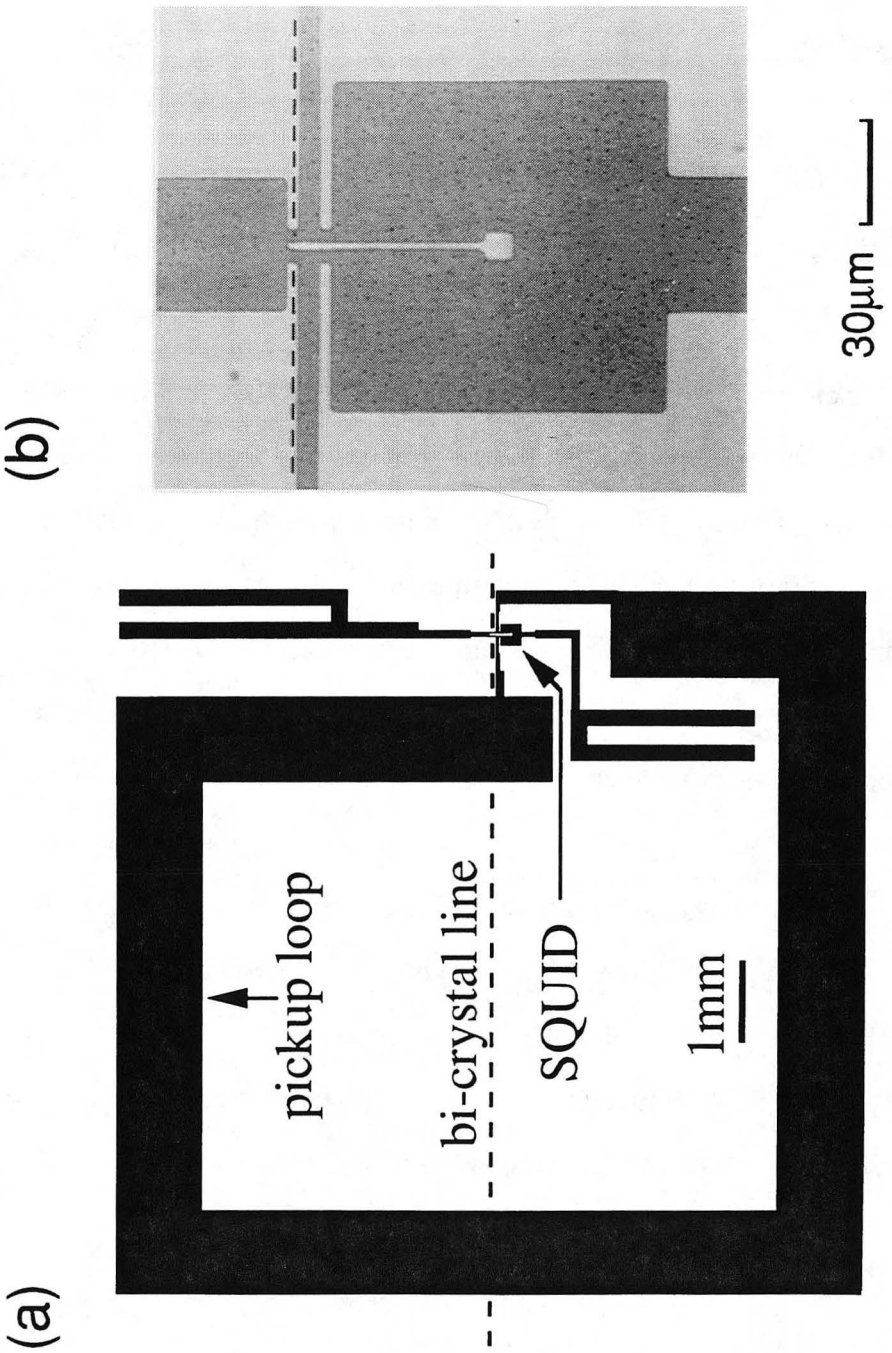

Fig. 7.2 (a) Scale drawing of a directly coupled magnetometer. (b) Photograph of 40 pH SQUID for the magnetometer.

Table 7.1. Summary of input coils used in voltmeter.

Coil (Device)	type	n	R_i (mΩ)	R_0 (mΩ)	M_i (pH)	M_i/nL
A	140 μm dia. Cu wire	7	51	30	150	0.54
B	100 μm dia. Cu wire	10	120	89	240	0.60
C (1055)	YBCO thin film	2	8.0	3.5	45	0.56

flux in the SQUID is measured to be $0.9\ L/L_p$ of that in the pickup loop [KML93], the net mutual inductance between the input coil and the SQUID is $M_i \approx 0.9\ \eta nL$. In practice I find M_i/nL varies between 0.54 and 0.60 (see Table 7.1) which is close to the expected value of 0.63 I find by taking $\eta = 0.7$. I note as well that the mutual inductance compares favorably with what we have measured in our multiturn, superconducting input coils flip-chipped onto SQUIDs; here we find M_i/nL lies between 0.5 and 0.85 [KOE94b]. However, it is important to remember that the coupling coefficient between the input coil and the SQUID inductance, $\alpha \equiv M_i/\sqrt{LL_i}$ is very low, typically 0.03, where I have assumed $L_i \approx n^2 L_p$.

I now discuss the noise and choice of component values for the voltmeter with a Cu-wire input coil. The noise theory of the voltmeter has been worked out in a number of fine references [CTG79, MAC85]. Here I present a less general treatment, applicable to the case at hand. Examining the Thevenin equivalent circuit in Fig. 7.1(b), one finds the spectral density of the voltage noise, referred to the source, is

$$S_V(f) = 4k_B T R_S + 4k_B T(R_0 + R_i) + S_\Phi(f)\frac{|R_\Sigma|^2}{M_i^2}, \qquad (7.1)$$

where T is the bath temperature, k_B is Boltzmann's constant and $S_\Phi(f)$ is the flux noise power of the SQUID. The first two terms are the Nyquist noise of the source resistor and

the resistors R_0 and R_i in the input circuit. The last term, which depends on the source resistance and which is analogous to the current noise present in all two-terminal amplifiers [ROB74], arises because some current must be fed back through the input coil to cancel the flux noise of the SQUID. When discussing the optimization of input circuits coupled to the SQUID, it is important to realize that in addition to the noise voltage at the output terminals of the SQUID there is also a noisy circulating current in the SQUID loop, the so-called "current noise" of the SQUID [TEC79, MAC86]. One does not see this current directly, but when the SQUID is tightly coupled to an input circuit, it will induce a noise voltage in the input coil which limits the resolution of the device. However, for the present case this noise source is negligible since $M_i^2 \ll LL_i$.

Using Eq. (7.1), I can introduce the noise temperature, $T_N(f)$, defined as the noise power added by the voltmeter normalized to the Nyquist noise of the source [ROB74, CTG79]:

$$\frac{T_N(f)}{T} = \frac{S_V(f) - 4k_BTR_S}{4k_BTR_S} = \frac{R_0 + R_i}{R_S} + \frac{S_\Phi(f)}{M_i^2}\frac{|R_\Sigma|^2}{4k_BTR_S}. \tag{7.2}$$

For a given coil, T_N/T has a shallow minimum about an optimum source resistance given by

$$R_s^2\Big|_{opt} = (R_0 + R_i)^2 + \frac{4k_BT(R_0 + R_i)}{S_\Phi(f)/M_i^2}. \tag{7.3}$$

Here I have explicitly assumed $2\pi fL_i \ll R_S + R_0 + R_i$. Alternatively, given a particular source resistance, one can use Eq. (7.3) to design a coil with the proper number of turns so as to be optimized for it. The reader should note that I have chosen a somewhat unusual way to define the noise temperature. For low-T_c voltmeters, with superconducting wire in the input circuit, the second term in Eq. (7.1) is negligible so that the only contribution to T_N comes from the SQUID itself [CLA77] (including the current noise [CTG79]). For this

case, however, with the input coil made of copper wire, R_i is not negligible. In fact, it is clear from Eq. (7.2) that the way to reduce T_N is to make R_i small while increasing M_i. However, with copper wire coils these two conditions are contradictory since R_i increases with the number of turns; therefore, one must keep both terms in Eq. (7.1) to balance these two trends. Once one has chosen R_s and set R_i and M_i to optimize the noise temperature, only R_0 remains. It should be as small as possible, but not so small that feedback loop fails to work as discussed above; I typically set $R_0 \lesssim R_i$, although the experience I gained while working with this experiment leads me to suspect that the feedback loop would function even with R_0 significantly less than R_i.

Measurements and Discussion

I constructed and tested voltmeters with two different Cu-wire input coils, A and B, coupled to the same SQUID (see Table 7.1). The coils were wound in the shape of a flat rectangular spiral and then pressed on top of the pickup loop as indicated in Fig. 7.3. For each coil, I completed the circuit with a range of source impedances surrounding the optimal value given above. The entire circuit was cooled in liquid nitrogen and magnetically shielded as described in chapter 1. I operated the SQUID with both standard modulation and bias reversal. I calibrated the voltmeter by sending a known, static current to the source resistor and recording the feedback current to R_0. I also sent a broadband noise signal to the source resistance and found that the response had a 3 dB high frequency roll-off at typically 10 to 15 kHz. For each source resistance I measured the noise and could thus calculate the noise temperature. Figure 7.4 shows the results in the white noise limit for both coil A (squares) and coil B (circles). The lines are the predictions of Eq. (7.2) using the parameters in Table 7.1 with $S_\Phi^{1/2} = 7.5\ \mu\Phi_0\ \mathrm{Hz}^{-1/2}$ and $8.5\ \mu\Phi_0\ \mathrm{Hz}^{-1/2}$, reflecting the observed variance in the SQUID white noise from run to run. The shallow minimum is evident in both cases. Regrettably, the minimum noise temperatures for these

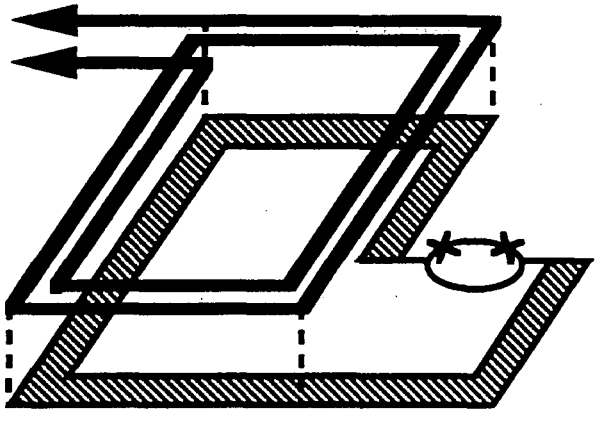

Fig. 7.3 Schematic drawing showing a flat rectangular spiral input coil pressed onto the pickup loop of a directly coupled magnetometer. Arrows point to rest of input circuit.

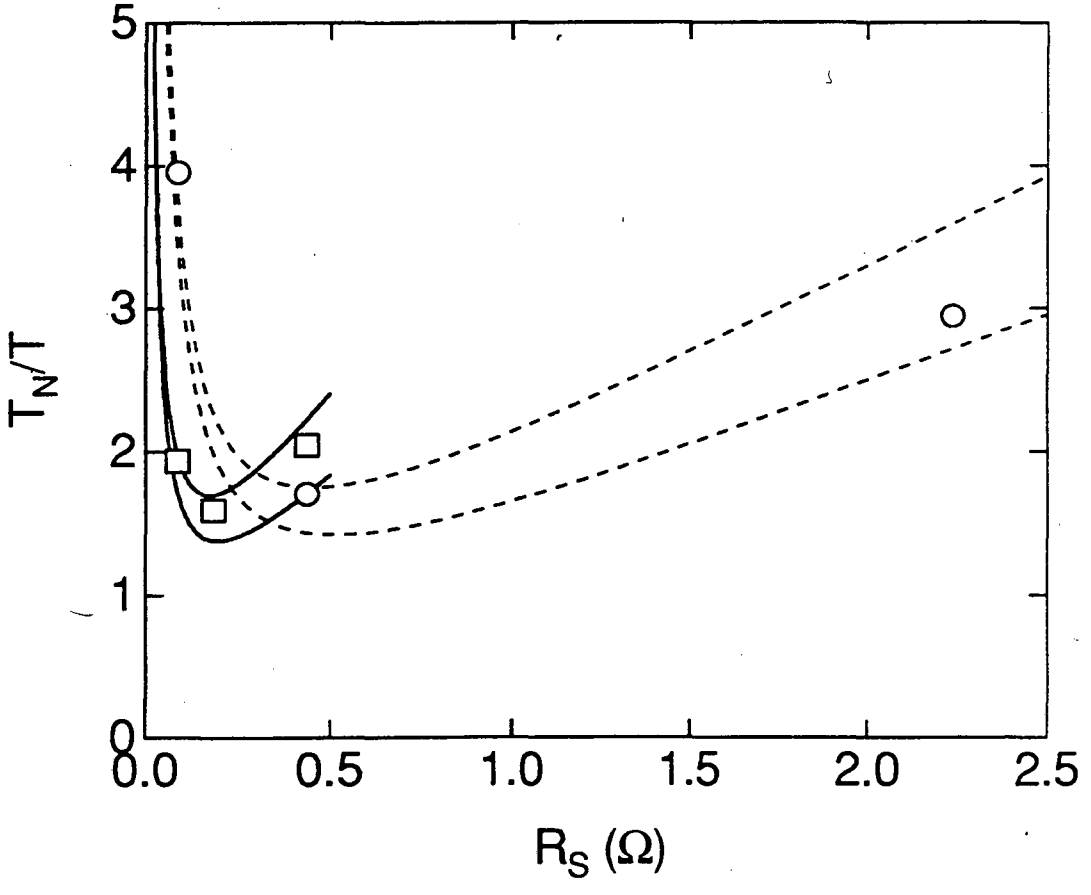

Fig. 7.4 Noise temperature relative to the bath temperature (77 K) for coils A (squares) and B (circles) measured with standard modulation in the white noise region. Lines are predictions of Eq. (7.2); solid lines for coil A, dashed lines for coil B.

two coils were 123 K and 132 K, respectively, reflecting the large input coil resistance and the relatively poor coupling to the SQUID with only a small number of turns.

The rms voltage resolution of the voltmeters is shown in Fig. 7.5 as a function of source resistance for both coil A (squares) and B (circles). The data here are from the white noise region with bias reversal which extends down to ~10 Hz. For both coils the measured resolutions fall in the range of 30 - 200 pV $Hz^{-1/2}$, increasing as the source resistance increases. The solid line is the Nyquist noise of the source resistor which sets the noise floor of the voltmeter. The size of the source resistor, however, is determined by the size of the input coil resistance as discussed above. At frequencies below a few Hz we often saw excess noise which could have been 1/f noise in the SQUID or drifts in the ambient field. The voltage resolutions at 1 Hz are plotted in Fig. 7.6. It is interesting to note that the excess noise was worse in the later experiments suggesting that some aging process in the SQUID was taking place.

In an attempt to achieve noise levels of a few pV $Hz^{-1/2}$ I made a third voltmeter, C, with a two-turn input coil patterned from a thin film of YBCO deposited on an MgO substrate. Contacts to the coil were made with bundles of seven Cu wires buried in In pads pressed onto an Ag film which had been deposited immediately following the YBCO deposition. One contact was placed inside the inner turn of the input coil so that no superconducting crossover was necessary. This coil was then flip-chipped to the pickup loop in the usual way. Contrary to my hopes, I found that each contact contributed ~3 mΩ of resistance over a contact area of about 1 mm^2. This may reflect a poor interface between the YBCO and the Ag (which was not annealed after deposition) or some reaction between the In and the Ag. I note that I had to remake the pressed In contacts several times over the course of a week as I adjusted the Cu wire leads to minimize stray coupling to the SQUID (see below). With bias reversal, the noise was 9.2 pV $Hz^{-1/2}$ at frequencies down to about 5 Hz, increasing to 24 pV $Hz^{-1/2}$ at 1 Hz. These data are shown on Figs. 7.5 and 7.6 as the triangles.

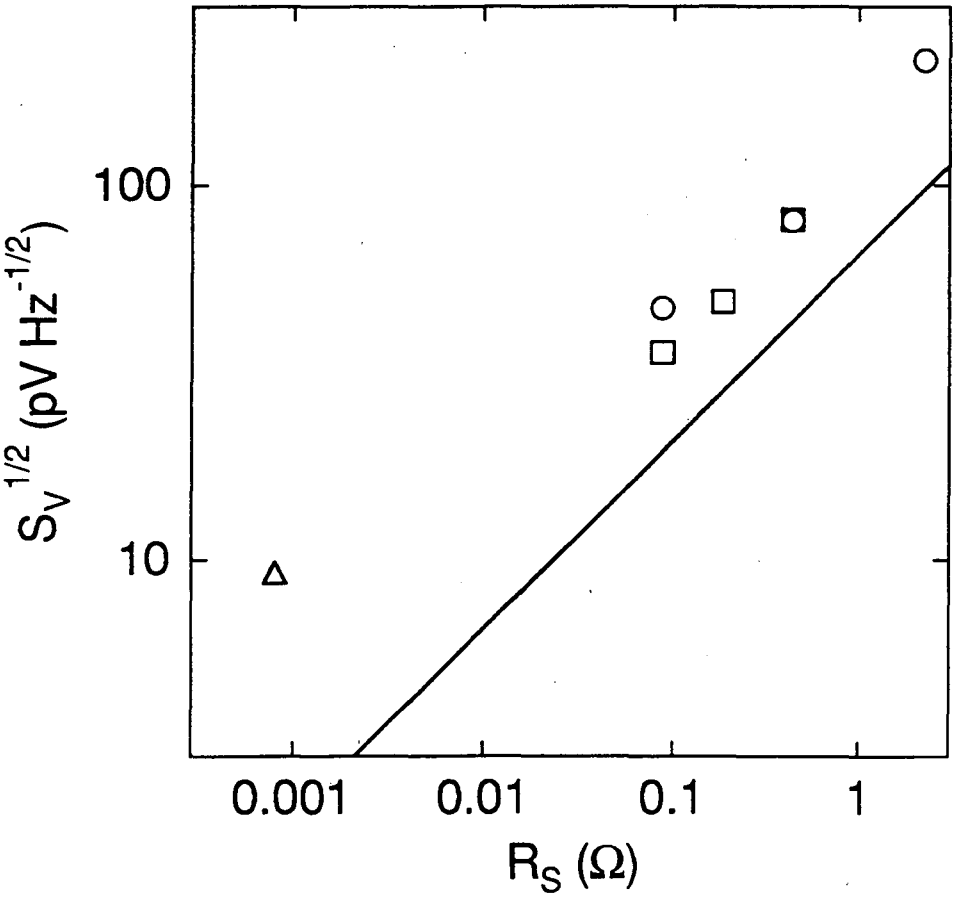

Fig. 7.5 Rms voltage resolution for the three voltmeters at T = 77 K, measured with double modulation, in the white noise limit: coil A (squares), coil B (circles), coil C (triangles). Solid line is the Nyquist noise of the source resistor.

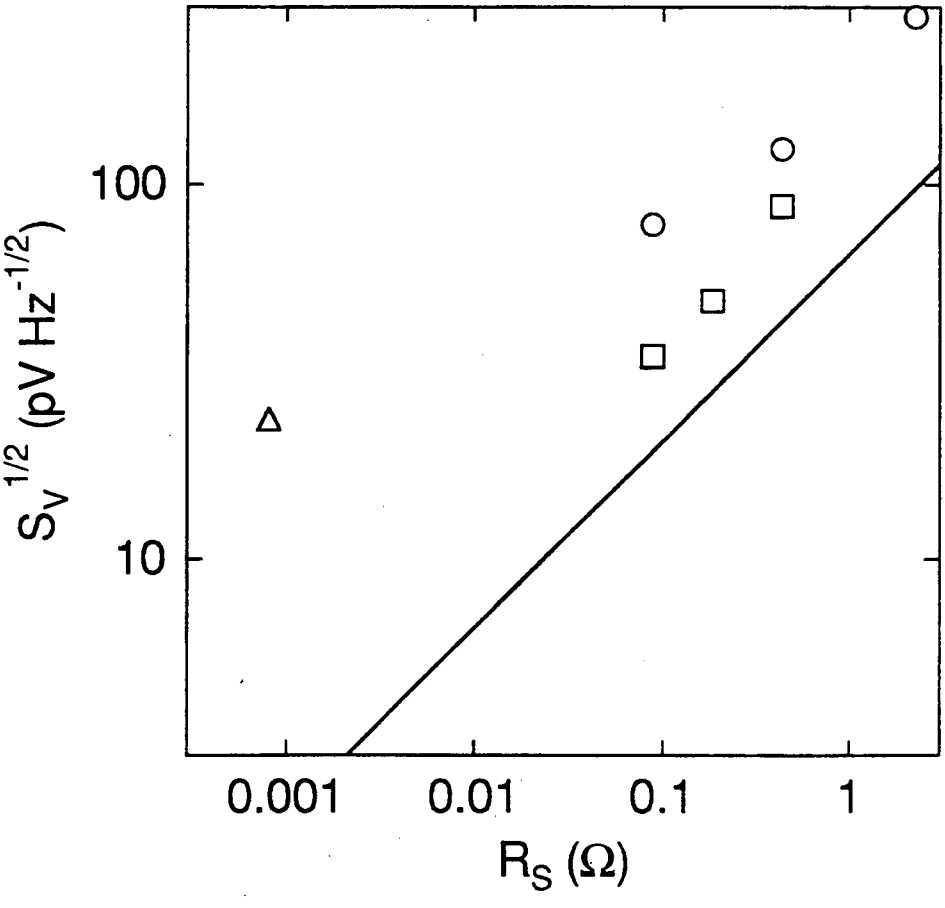

Fig. 7.6 Rms voltage resolution at 1 Hz with double modulation (T = 77 K). Symbols are as in Fig. 7.5.

For all three voltmeters there was stray coupling between the pickup loop and the current leads to both R_S and R_0. Since the feedback scheme assumes the only coupling to the SQUID is via the input coil, these stray mutual inductances cause an imbalance in the input coil and allow current to flow through it even when the feedback loop is closed, thus lowering the input impedance of the voltmeter. Also, any strays in the leads for the feedback current will cause a systematic error in the determination of the true voltage at the input. We correct for this here by using a calibrated source, but we cannot account for strays in the current leads to the source resistors. For all three coils the net effect was determined to be no larger than 5% from comparison of the fed-back currents with the known values of the source and feedback resistors. In practice, one would like to shield the SQUID by placing it in a superconducting tube, but this increases the length of the wire leads on chip and will thus probably require superconducting wires.

In the future I feel it should be possible with this technology to obtain a resolution of 3 pV $Hz^{-1/2}$. This will require a total series resistance in the input coil ≤ 2 mΩ which should be achievable (assuming the contact resistance can be made negligible with proper processing) by using thicker Cu wires in parallel bundles of 10 wires each. Also, the number of turns on the input coil will be increased to 20 to bring down the SQUID noise, in particular the low-frequency noise. This will, however, significantly increase the input coil inductance, and may pose a problem in frequency response. Finally, since the linewidths on the input coil will now be much smaller, it will probably be more difficult to get good coupling to the SQUID. In particular, the thickness of the wires will most likely preclude placing a pressed In contact on the inside of the turns of the input coil, requiring some type of normal metal crossover. Aluminium wirebonds may work, but one will need ~20 in parallel to make their resistance negligible.

Chapter VIII: Conclusions

There has certainly been tremendous progress over the past 6 years not only in the performance of high-T_c SQUIDs but in understanding what limits their performance. Looking back at the biepitaxial SQUIDs presented in chapter 2 and comparing them with our present best results for bicrystal SQUIDs (which I mention briefly in chapter 3) one sees an improvement in energy resolution at 1 Hz of 3 orders of magnitude, from 1.5×10^{-27} J Hz^{-1} in a device operating at 4.2 K to 1.5×10^{-30} J Hz^{-1} at 77 K. This latter device is approaching the benchmarks typically set for commercially available low-T_c SQUIDs operating at 4.2 K. So what's next? Here is my personal, and somewhat speculative, inventory of what does (and does not) need to be done to continue to make progress.

Junctions. The technology for making high-T_c junctions has stabilized to a large extent from the frenzied days following the first high-T_c films. It is clear now that if one is interested in making SQUIDs, and therefore needs only a dozen or so junctions on a chip, the bicrystal technology provides excellent results with little effort on the part of the film grower. The availability of prefabricated bicrystals means that anyone who can grow a thin film of YBCO can make quiet SQUIDs. Furthermore, these SQUIDs are made with a single mask step making them even easier than low-T_c technology. However, bicrystal GBJs still have more 1/f critical current noise than their low-T_c counterparts, and although this can be controlled by using bias reversal it is hard to say how much of the residual 1/f noise is due to critical current fluctuations. Furthermore, in a user-friendly system one would like not to have to do this. It does not appear, though, that anything else will challenge the bicrystals in the near future. The most promising work so far has been done with "break-type" junctions [DYY93, OBC91] where YBCO is deposited over a step cut into the substrate such that the step edge is not covered; the exposed a-b planes of the YBCO are then connected with a Ag or Au film. Preliminary results at BTi showed

SQUIDs with very low 1/f noise. Later work from NIST-Boulder reported single junctions with resistances of more than 10 Ω [RGO93], which would be ideal for low white noise SQUIDs, but as far as I know no noise measurements have been made on a SQUID made with this process.

Films with strong pinning. It has become a straight-forward matter to make single, unpatterned YBCO films with exceptionally low levels of 1/f flux noise when they are cooled in zero field. However, all of the samples studied by Mark Ferrari and Tim Shaw [FJW94], showed a marked increase in the noise when the films were cooled in a static magnetic field even as small as 0.1 mT (1 G). This will undoubtedly be a problem for high-T_c devices operated in the field as discussed in chapter 6. Clearly, one should find a way to put strong pinning defects into otherwise epitaxial films. There is a huge literature of work on putting strong pinning centers in bulk samples and wires, and some of this has been translated into thin films. However, the criteria here is usually high critical current density and not low flux noise. It is not clear that the same type of defects will satisfy both standards since it is conceivable that the potential well containing the vortex may have steep sides but a rough bottom with many shallow troughs in which the fluxon can hop around. One should bear in mind that whatever process is decided upon must be compatible with multilayer growth and processing, and should be relatively easy to implement if it is to be commercially successful.

Improved multilayer processing. Multilayer transformers will certainly be a necessity if high-T_c magnetometers are to compete with low-T_c devices in terms of field resolution and detector size, but there is clearly much work to be done in reducing the flux noise of patterned multilayer structures.

Finding a better dielectric substrate. $SrTiO_3$ is the material of choice for substrates and insulating layers because of its good lattice match to YBCO and because much is known about processing with it. Unfortunately, much that is known about it is bad; in particular its large dielectric constant and loss tangent make it a suspect material from the

start. We have known for some time [KML93] that the white noise power of our SQUIDs is about a factor of 4-10 higher than the predicted value, $16k_BTR/V_\Phi^2$. It is not known if this is some artifact of high-β SQUIDs (the result holds for $\beta = 1$) or if there is some unknown noise source in high-T_c junctions, but it is also possible that the $SrTiO_3$ substrate acts as a lossy conductor for currents at the Josephson frequency and thereby adds noise. Also, the high dielectric constant may cause unwanted resonances in structures with input coils fabricated on top of SQUIDs. Moreover, there are processing problems with this material: we in the Clarke group have found (as have other groups) that good films of $SrTiO_3$ are relatively impervious to oxygen diffusion, and that this makes it difficult to reoxygenate the lower YBCO layers of a multilayer structure. Of course, $SrTiO_3$ does have the advantage that we know we can grow very quiet films on it with a minimum of buffer layers, and this may yet prove to be the deciding factor.

Liquid nitrogen dewars. One of the major selling points for high-T_c technology, especially with regard to field work, is the low boil-off rate of liquid nitrogen. However, our experience with prototype field systems [DKM94] shows that liquid nitrogen dewars (and the cryostats that go in them) must be designed with at least as much care as their liquid helium counterparts if they are to achieve their expected holdtimes.

Computer Modeling. Although much work was done in past decades on modeling the behavior of low-T_c dc SQUIDs, most of this work focussed on a range of parameters which is inappropriate for our high-T_c devices. For example, Tesche and Clarke [TEC77] did extensive computer simulations of the signal and noise in dc SQUIDs, but they largely avoided the high critical current, low inductance, high temperature limits which are the case for high-T_c SQUIDs. One result of this is that we failed to anticipate the $1/L^2$ behavior of the SQUID transfer function at high inductances although recent extensions of the low-T_c SQUID computer models clearly show it to be there [ESK93, KOC93, KOC93b]. A thorough re-examination of the dc SQUID in the high-T_c limit may also help explain the excess white noise noted above. Furthermore, Ketchen [KET81] has discussed in detail

the coupling of a multiturn thin film flux transformer to a SQUID, but only in the limit in which the width of the lines of the input coil is large compared to their distance from the SQUID, an appropriate approximation presuming one can fabricate an integrated (monolithic) device with the SQUID and input coil on the same chip. For the case of our flip chip magnetometers it is clear that we do not always achieve as much coupling as we would like, and at present it is unclear if this is a result of the increased separation between the input coil and the SQUID, a problem associated with our films being too thin compared with the London penetration depth, an effect of the slits and slots patterned into our SQUID washers for the junctions, or something else entirely. It would speed up the development time considerably (and reduce the cost of trial and error) to produce computer code to solve the electromagnetic equations. One thing seems certain, though: the increased temperature of operation limits the inductance of the SQUID (which sets the scale for all other inductances in the problem) and this makes stray effects such as stripline inductances in the flux transformer input coil much more noticeable.

All of the aforementioned challenges will likely need to be met in the future if high-T_c SQUIDs are to achieve their full potential and begin to rival their low-T_c counterparts. However, for many commercial applications one does not need the full resolution of state-of-the-art low-T_c SQUIDs, and the simplifications afforded by using devices cooled with liquid nitrogen (or even single-stage cryocoolers) make high-T_c technology very attractive. A prime example of this is the 3-axis geophysical magnetometer described in chapter 5 [DKM94] which is soon to be marketed by Conductus, Inc. Also, the Superconducting Sensor Laboratory in Japan has been developing a 4-channel YBCO dc SQUID system for obtaining human magnetocardiograms [ITH93]. Another example is the high-T_c "scanning SQUID" developed by Fred Wellstood's group at the University of Maryland with bicrystal SQUIDs supplied by our group at Berkeley. This has been used to obtain two-dimensional magnetic field images of materials such as ferromagnetic inks [BMW93], and also eddy-current images of defects in normal metals [BWD94] similar to corrosion in aircraft wings.

It seems reasonable to suggest that in the near future high-T_c SQUIDs will carve out a niche for themselves in the marketplace, thus becoming the first commercially viable high-T_c technology.

References

[ABA91] N. McN. Alford, T. W. Button, M. J. Adams, S. Hedges, B. Nicholson, and W. A. Phillips, "Low surface resistance in $YBa_2Cu_3O_x$ melt-processed thick films," Nature **349**, 680 (1991)

[ABS65] Milton Abramowitz and Irene A. Stegun, eds., *Handbook of Mathematical Functions with Formulas, Graphs, and Tables*, 9th printing, (Dover, New York, 1965).

[AHK91] A. I. Ahonen, M. S. Hämäläinen, M. J. Kajola, J. E. T. Knuutila, O. V. Lounasmaa, J. T. Simola, C. D. Tesche, and V. A. Vilkman, "Multichannel SQUID systems for brain research," IEEE Trans. Magn. **27**, 2786 (1991).

[AMH69] Vinay Ambegaokar and B. I. Halperin, "Voltage due to thermal noise in the dc Josephson effect," Phys. Rev. Lett. **22**, 1364 (1969).

[BAR92] A. Barone, ed., *Principles and Applications of Superconducting Quantum Interference Devices*, (World Scientific, Singapore, 1992).

[BAW91] T. W. Button, N. McN. Alford, F. Wellhofer, T. C. Shields, J. S. Abell, and M. Day, "The processing and properties of high T_c thick films," IEEE Trans. Magn. **27**, 1434 (1991).

[BEM86] T. G. Bednorz and K. A. Müller, "Possible high T_c superconductivity in the Ba-La-Cu-O system," Z. Phys. B **64**, 189 (1986).

[BMW93] R. C. Black, A. Mathai, F. C. Wellstood, E. Dantsker, A. H. Miklich, D. T. Nemeth, J. J. Kingston, and J. Clarke, "Magnetic microscopy using a liquid nitrogen cooled $YBa_2Cu_3O_7$ superconducting quantum interference device," Appl. Phys. Lett. **62**, 2128 (1993).

[BWD94] R. C. Black, F. C. Wellstood, E. Dantsker, A. H. Miklich, J. J. Kingston, D. T. Nemeth, and J. Clarke, "Eddy current microscopy using a 77-K superconducting sensor," Appl. Phys. Lett. **64**, 100 (1994).

[CCG91] K. Char, M. S. Colclough, S. M. Garrison, N. Newman, and G. Zaharchuk, "Bi-epitaxial grain boundary junctions in $YBa_2Cu_3O_7$," Appl. Phys. Lett. **59**, 733 (1991).

[CCL91] K. Char, M. S. Colclough, L. P. Lee, and G. Zaharchuk, "Extension of the bi-epitaxy Josephson junction process to various substrates," Appl. Phys. Lett. **59**, 2177 (1991).

[CGC83] J. Clarke, T. D. Gamble, W. M. Goubau, R. H. Koch, and R. F. Miracky, "Remote-reference magnetotellurics: equipment and procedures," Geophysical Prospecting **31**, 149 (1983).

[CGL93] S. Casciardi, C. Del Gratta, S. Di Luzio, G. L. Romani, V. Foglietti, A. Pasquarelli, V. Pizzella, and G. Torrioli, "11 channel magnetometer for

biomagnetic measurements in unshielded environments," IEEE Trans. Appl. Sup. **3**, 1894 (1993).

[CHA81] W. H. Chang, "Numerical calculation of the inductances of a multi-superconductor transmission line system," IEEE Trans. Magn. **MAG-17**, 764 (1981).

[CLA66] J. Clarke, "A superconducting galvanometer employing Josephson tunnelling," Phil. Mag. **13**, 115 (1966).

[CLA77] John Clarke, "Superconducting quantum interference devices for low frequency measurements," in *Superconductor Applications: SQUIDs and Machines*, Brian B. Schwartz and Simon Foner, eds., (Plenum, New York, 1977), pp. 67-124.

[CLA83] John Clarke, "Geophysical applications of SQUIDs," IEEE Trans. Magn. **MAG-19**, 288 (1983).

[CLA86] John Clarke, "Experiments on charge imbalance in superconductors," in *Nonequilibrium Superconductivity*, D. N. Langenberg and A. I. Larkin, eds., (Elsevier, 1986), pp. 1-63.

[CLA93] John Clarke, "SQUIDs: Theory and practice," in *The New Superconducting Electronics*, H. Weinstock and R. Ralston, eds., NATO ASI Series, Vol E 251, (Kluwer, Dordrecht, Boston, London, 1993), pp. 123-180.

[CLF69] J. Clarke and T. A. Fulton, "Origin of low-voltage structure and asymmetry in the I-V characteristics of multiply-connected superconducting junctions," J. Appl. Phys. **40**, 4470 (1969).

[CTG79] John Clarke, Claudia Tesche, and R. P. Giffard, "Optimization of dc SQUID voltmeter and magnetometer circuits," J. Low Temp. Phys. **37**, 405 (1979).

[DCM88] D. Dimos, P. Chaudhari, J. Mannhart, and F. K. LeGoues, "Orientation dependence of grain-boundary critical currents in $YBa_2Cu_3O_{7-\delta}$ bicrystals," Phys. Rev. Lett. **61**, 219 (1988).

[DCM90] D. Dimos, P. Chaudhari, and J. Mannhart, "Superconducting transport properties of grain boundaries in $YBa_2Cu_3O_{7-x}$ bicrystals," Phys. Rev. B **41**, 4038 (1990).

[DCP91] D. Drung, R. Cantor, M. Peters, T. Ryhänen, and H. Koch, "Integrated dc SQUID magnetometer with high dV/dB," IEEE Trans. Magn. **27**, 3001 (1991).

[DDF93] O. Dössel, B. David, M. Fuchs, J. Krüger, K.-M. Lüdeke, and H.-A. Wischmann, "A modular 31-channel SQUID system for biomagnetic measurements," IEEE Trans. Appl. Sup. **3**, 1883 (1993).

[DDH79] P. Dutta, P. Dimon, P. M. Horn, "Energy scales for noise processes in metals," Phys. Rev. Lett. **43**, 646 (1979).

[DKM94] E. Dantsker, D. Koelle, A. H. Miklich, D. T. Nemeth, F. Ludwig, John Clarke, J. T. Longo, and V. Vinetskiy, "High T_c three-axis dc SQUID magnetometer for geophysical applications," (submitted to Rev. Sci. Instr., 1994).

[DUH81] P. Dutta, P. M. Horn, "Low-frequency fluctuations in solids: 1/f noise," Rev. Mod. Phys. **53**, 497 (1981).

[DUT81] T. Van Duzer and C. W. Turner, *Principles of Superconductive Devices and Circuits*, (Elsevier, New York, 1981).

[DYY93] M. S. DiIorio, S. Yoshizumi, K-Y. Yang, M. Maung, J. Zhang, and B. Power, "Low-noise high-T_c dc SQUIDs at 77 K," IEEE Trans. Appl. Sup. **3**, 2011 (1993).

[EHL81] S. N. Erné, H.-D. Hahlbohm, and H. Lübbig, eds., *Biomagnetism*, (Walter de Gruyter, Berlin, New York, 1981).

[ESK93] K. Enpuku, Y. Shimomura, and T. Kisu, "Effect of thermal noise on the characteristics of a high T_c superconducting quantum interference device," J. Appl. Phys. **73**, 7929 (1993).

[FDV93] G. Friedl, G. Daalmans, M. Vildić, D. Uhl, F. Bömmel, B. Roas, B. Hillenbrand, B. Stritzker, and H. E. Hoenig, "Noise properties of YBaCuO step edge dc-SQUIDs with different inductance," IEEE Trans. Appl. Sup. **3**, 2018 (1993).

[FER91] M. J. Ferrari, "Magnetic flux noise in copper oxide superconductors," Ph. D. thesis, University of California, Berkeley, 1991.

[FJW94] M. J. Ferrari, Mark Johnson, F. C. Wellstood, J. J. Kingston, T. J. Shaw, and John Clarke, "Magnetic flux noise in copper oxide superconductors," J. Low Temp. Phys. **94**, 15 (1994).

[FKW91] M. J. Ferrari, John J. Kingston, Frederick C. Wellstood, and John Clarke, "Flux noise from superconducting $YBa_2Cu_3O_{7-x}$ flux transformers," Appl. Phys. Lett. **58**, 1106 (1991).

[FPP93] V. Foglietti, A. Pasquarelli, V. Pizzella, G. Torrioli, G. L. Romani, S. Casciardi, W. J. Gallagher, M. B. Ketchen, A. W. Kleinsasser, and R. L. Sandstrom, "Operation of a hybrid 28-channel neuromagnetometer," IEEE Trans. Appl. Sup. **3**, 1890 (1993).

[GCK90] R. Gross, P. Chaudhari, M. Kawasaki, and A. Gupta, "Scaling behavior in electrical transport across grain boundaries in $YBa_2Cu_3O_{7-\delta}$ superconductors," Phys. Rev. B **42**, 10735 (1990).

[GGC79] T. D. Gamble, W. M. Goubau, and J. Clarke, "Magnetotellurics with a remote magnetic reference," Geophysics **44**, 53 (1979).

[GRM91] R. Gross and B. Mayer, "Transport processes and noise in $YBa_2Cu_3O_{7-\delta}$ grain boundary junctions," Physica C **180**, 234 (1991).

[GRO46] Frederick W. Grover, *Inductance Calculations: Working Formulas and Tables*, (D. Van Nostrand, New York, 1946).

[GSB91] P. L. Gammel, L. F. Schneemeyer, and D. J. Bishop, "SQUID picovoltometry of $YBa_2Cu_3O_7$ single crystals: evidence for a finite-temperature phase transition in the high-field vortex state," Phys. Rev. Lett. **66**, 953 (1991).

[HDB91] H. E. Hoenig, G. M. Daalmans, L. Bär, F. Bömmel, A. Paulus, D. Uhl, H. J. Weisse, S. Schneider, H. Seifert, H. Reichenberger, and K. Abraham-Fuchs, "Multi channel dc SQUID sensor array for biomagnetic applications," IEEE Trans. Magn. **27**, 2777 (1991).

[HHM93] S. G. Hammond, Y. He, C. M. Muirhead, and P. Wu, "Noise properties of biepitaxial HTS junctions," IEEE Trans. Appl. Sup. **3**, 2319 (1993).

[HKM92] M. Hotta, H. Kado, K. Makie, and K. Okajima, "A new method of adjusting bias currents of neuromagnetometers," in *Superconducting Devices and Their Applications*, Springer Proceedings in Physics, Vol. 64, H. Koch and H. Lübbig, eds., (Springer-Verlag, Berlin, Heidelberg, 1992), pp. 529-532.

[ITH93] H. Itozaki, S. Tanaka, N. Harada, T. Adachi, T. Komuro, H. Toyoda, K. Okajima, T. Nagaishi, and H. Kado, "Four channel YBCO dc-SQUID," presented at the 4th International Superconductive Electronics Conference, Boulder, CO, August 11-14, 1993 (unpublished).

[JAM81] J. M. Jaycox and M. B. Ketchen, "Planar coupling scheme for ultra low noise dc SQUIDs," IEEE Trans. Magn. **MAG-17**, 400 (1981).

[KCD91] H. Koch, R. Cantor, D. Drung, S. N. Erné, K. P. Matthies, M. Peters T. Ryhänen, H. J. Scheer, and H. D. Hahlbohm, "A 37 channel dc SQUID magnetometer system," IEEE Trans. Magn. **27**, 2793 (1991).

[KCG83] Roger H. Koch, John Clarke, W. M. Goubau, J. M. Maritnis, C. M. Pegrum, and D. J. Van Harlingen, "Flicker (1/f) noise in tunnel junction dc SQUIDs," J. Low Temp. Phys. **51**, 207 (1983).

[KCG92] M. Kawasaki, P. Chaudhari, and A. Gupta, "1/f noise in $YBa_2Cu_3O_{7-\delta}$ superconducting bicrystal grain-boundary junctions," Phys. Rev. Lett. **68**, 1065 (1992).

[KCN91] M. Kawasaki, P. Chaudhari, T. H. Newman, and A. Gupta, "Submicron $YBa_2Cu_3O_{7-\delta}$ grain boundary junction dc SQUIDs," Appl. Phys. Lett. **58**, 2555 (1991).

[KET81] M. B. Ketchen, "dc SQUIDs 1980: The state of the art," IEEE Trans. Magn. **MAG-17**, 387 (1981).

[KET87] M. B. Ketchen, "Integrated thin-film dc SQUID sensors," IEEE Trans. Magn. **MAG-23**, 1650 (1987).

[KFR94] R. H. Koch, V. Foglietti, J. R. Rozen, K. G. Stawiasz, M. B. Ketchen, D. K. Lathrop, J. Z. Sun, W. J. Gallagher, "The effects of radio frequency radiation on the dc SQUID," presented at the 1994 March Meeting of the American Physical Society, Pittsburgh, PA, March 21-25, 1994 (unpublished).

[KFS94] R. H. Koch, V. Foglietti, J. Z. Sun, J. R. Rozen, R. L. Sandstrom, W. J. Gallagher, "Using SQUIDs in real-world environments," presented at the OE/LASE '94 Conference, Los Angeles, CA, January 23-29, 1994 (unpublished).

[KGK85] Mark B. Ketchen, W. J. Gallagher, A. W. Kleinsasser, S. Murphy, and John R. Clem, "dc SQUID flux focuser," in *SQUID '85 - Superconducting Quantum Interference Devices and their Applications*, H. D. Hahlbohm and H. Lübbig, eds., (Walter de Gruyter, Berlin, New York, 1985), pp. 865-871.

[KMD93] D. Koelle, A. H. Miklich, E. Dantsker, F. Ludwig, D. T. Nemeth, John Clarke, W. Ruby, and K. Char, "High performance dc SQUID magnetometers with single layer $YBa_2Cu_3O_{7-x}$ flux transformers," Appl. Phys. Lett. **63**, 3630 (1993).

[KML93] D. Koelle, A. H. Miklich, F. Ludwig, E. Dantsker, D. T. Nemeth, and John Clarke, "dc SQUID magnetometers from single layers of $YBa_2Cu_3O_{7-x}$," Appl. Phys. Lett. **63**, 2271 (1993).

[KOC93] Roger Koch (private communication).

[KOC93b] R. H. Koch, presented at the 4th International Superconductive Electronics Conference, Boulder, CO, August 11-14, 1993 (unpublished).

[KOE94] D. Koelle, "High-T_c dc SQUID magnetometers," presented at the OE/LASE '94 Conference, Los Angeles, CA, January 23-29, 1994 (unpublished).

[KOE94b] D. Koelle, A. H. Miklich, E. Dantsker, D. T. Nemeth, F. Ludwig, and J. Clarke, "Coupling issues in optimizing the performance of high-T_c dc SQUID magnetometers," presented at the 1994 March Meeting of the American Physical Society, Pittsburgh, PA, March 21-25, 1994 (unpublished).

[KRS93] R. H. Koch, J. R. Rozen, J. Z. Sun, and W. J. Gallagher, "Three SQUID gradiometer," Appl. Phys. Lett. **63**, 403 (1993).

[KUG87] R. H. Koch, C. P. Umbach, G. J. Clark, P. Chaudhari, and R. B. Laibowitz, "Quantum interference devices made from superconducting oxide thin films," Appl. Phys. Lett. **51**, 200 (1987).

[KWL90] John J. Kingston, Frederick C. Wellstood, Philippe Lerch, Andrew H. Miklich, and John Clarke, "Multilayer $YBa_2Cu_3O_x$ - $SrTiO_3$ - $YBa_2Cu_3O_x$ films for insulating crossovers," Appl. Phys. Lett. **56**, 189 (1990).

[KWQ91] J. J. Kingston, F. C. Wellstood, Du Quan, and John Clarke, "Photolithographically patterned thin-film multilayer devices of $YBa_2Cu_3O_{7-x}$," IEEE Trans. Magn. **27**, 974 (1991).

[LDN94] F. Ludwig, E. Dantsker, D. T. Nemeth, D. Koelle, A. H. Miklich, and John Clarke, "Fabrication issues in optimizing $YBa_2Cu_3O_{7-x}$ flux transformers for low 1/f noise," (submitted to Supercond. Sci. Technol., 1994).

[LHW93] J. Lin, T. W. Huang, J. J. Wang, H. B. Lu, S. L. Tu, S. J. Yang, and S. E. Hsu, "YBCO dc SQUID on MgO bicrystal substrate with flux transformer," IEEE Trans. Appl. Sup. **3**, 2438 (1993).

[LLB92] J. Lepaisant, M. Lam Chok Sing, and D. Bloyet, "Low-noise preamplifier with input and feedback transformers for low source resistance sensors," Rev. Sci. Instrum. **63**, 2089 (1992).

[LPU90] A. G. Likhachev, V. N. Polushkin, S. V. Uchaikin, and B. V. Vasiliev, "Magnetocardiometer based on a single-hole high-T_c SQUID," Supercond. Sci. Technol. **3**, 148 (1990).

[MAC85] John M. Martinis and John Clarke, "Signal and noise theory for a dc SQUID amplifier," J. Low Temp. Phys. **61**, 227 (1985).

[MAC86] John M. Martinis and John Clarke, "Current noise measured in the dc SQUID," J. Low Temp. Phys. **65**, 459 (1986).

[MCC92] A. H. Miklich, John Clarke, M. S. Colclough, and K. Char, "Flicker (1/f) noise in biepitaxial grain boundary junctions of $YBa_2Cu_3O_{7-x}$," Appl. Phys. Lett. **60**, 1899 (1992).

[MCU68] D. E. McCumber, "Effect of ac impedance on dc voltage-current characteristics of superconductor weak-link junctions," J. Appl. Phys. **39**, 3113 (1968).

[MKD93] A. H. Miklich, D. Koelle, E. Dantsker, D. T. Nemeth, J. J. Kingston, R. F. Kromann, and J. Clarke, "Bicrystal YBCO dc SQUIDs with low noise," IEEE Trans. Appl. Sup. **3**, 2434 (1993).

[MKL94] A. H. Miklich, D. Koelle, F. Ludwig, D. T. Nemeth, E. Dantsker, and J. Clarke, "A high-T_c SQUID picovoltmeter operating in liquid nitrogen," presented at the 1994 March Meeting of the American Physical Society, Pittsburgh, PA, March 21-25, 1994 (unpublished).

[MKS93] A. H. Miklich, D. Koelle, T. J. Shaw, F. Ludwig, D. T. Nemeth, E. Dantsker, John Clarke, Neil McN. Alford, Tim W. Button, and M. S. Colclough, "1/f noise of dc SQUIDs in YBCO shields and its dependence on the stabilized magnetic field," presented at the 4th International Superconductive Electronics Conference, Boulder, CO, August 11-14, 1993 (unpublished).

[MKS94] A. H. Miklich, D. Koelle, T. J. Shaw, F. Ludwig, D. T. Nemeth, E. Dantsker, John Clarke, Neil McN. Alford, Tim W. Button, and M. S.

Colclough, "Low-frequency excess noise in $YBa_2Cu_3O_{7-x}$ dc superconducting quantum interference devices cooled in static magnetic fields," (submitted to Appl. Phys. Lett., 1994).

[MKS94b] A. H. Miklich, D. Koelle, T. J. Shaw, F. Ludwig, D. T. Nemeth, E. Dantsker, J. Clarke, N. McN. Alford, T. W. Button, and M. S. Colclough, "Performance of $YBa_2Cu_3O_{7-x}$ superconducting quantum interference devices cooled in static magnetic fields," presented at the OE/LASE '94 Conference, Los Angeles, CA, January 23-29, 1994 (unpublished).

[MKW91] A. H. Miklich, J. J. Kingston, F. C. Wellstood, John Clarke, M. S. Colclough, K. Char, and G. Zaharchuk, "Sensitive $YBa_2Cu_3O_{7-x}$ thin-film magnetometer," Appl. Phys. Lett. **59**, 988 (1991).

[MLB93] B. H. Moeckly, D. K. Lathrop, and R. A. Buhrman, "Electromigration study of oxygen disorder and grain-boundary effects in $YBa_2Cu_3O_{7-\delta}$ thin films," Phys. Rev. B **47**, 400 (1993).

[MUC94] M. Mück, "High-T_c rf SQUID magnetometers," presented at the OE/LASE '94 Conference, Los Angeles, CA, January 23-29, 1994 (unpublished).

[MWK91] A. H. Miklich, F. C. Wellstood, J. J. Kingston, John Clarke, M. S. Colclough, K. Char, and G. Zaharchuk, "Thin-film YBCO magnetometer," Nature **352**, 482 (1991).

[MWK91b] A. H. Miklich, F. C. Wellstood, J. J. Kingston, J. Clarke, M. S. Colclough, A. H. Cardona, L. C. Bourne, W. L. Olson, and M. M. Eddy, "High-T_c thin-film magnetometer," IEEE Trans. Magn. **27**, 3219 (1991).

[NMC88] E. A. Nichols, H. F. Morrison, and J. Clarke, "Signals and noise in measurements of low-frequency geomagnetic fields," J. Geophys. Res. **93**, 13 743 (1988).

[OBC91] R. H. Ono, J. A. Beall, M. W. Cromar, T. E. Harvey, M. E. Johansson, C. D. Reintsema, and D. A. Rudman, "High-T_c superconductor - normal metal - superconductor Josephson microbridges with high-resistance normal metal links," Appl. Phys. Lett. **59**, 1126 (1991).

[OKN93] H. K. Olsson, R. H. Koch, P-Å. Milsson, and E. A. Stepantsov, "dc-SQUIDs with low noise and large β_L-values on $(Y)ZrO_2$ bicrystal substrate," IEEE Trans. Appl. Sup. **3**, 2426 (1993).

[PDK94] V. Polushkin, D. Drung, and H. Koch, "A broadband picovoltmeter based on the direct current superconducting quantum interference device with additional positive feedback," (submitted to Rev. Sci. Instrum., 1994).

[RBC91] Peter A. Rosenthal, M. R. Beasley, K. Char, M. S. Colclough, and G. Zaharchuk, "Flux focusing effects in planar thin-film grain-boundary Josephson junctions," Appl. Phys. Lett. **59**, 3482 (1991).

[RCZ91] S. J. Rosner, K. Char, and G. Zaharchuk, "Microstructure of biepitaxial grain boundary junctions in $YBa_2Cu_3O_{7-x}$," Appl. Phys. Lett. **60**, 1010 (1992).

[RGO93] P. A. Rosenthal, E. N. Grossman, R. H. Ono, and L. R. Vale, "High temperature superconducting - normal metal - superconductor Josephson junctions with high characteristic voltages," Appl. Phys. Lett. **63**, 1984 (1993).

[RLM90] S. E. Russek, D. K. Lathrop, B. H. Moeckly, R. A. Buhrman, D. H. Shin, and J. Silcox, "Scaling behavior of $YBa_2Cu_3O_{7-\delta}$ thin-film weak links," Appl. Phys. Lett. **57**, 1155 (1990).

[RMK90] D. Robbes, A. H. Miklich, J. J .Kingston, Ph. Lerch, F. C. Wellstood, and John Clarke, "Josephson weak links in thin films of $YBa_2Cu_3O_{7-x}$ induced by electrical pulses," Appl. Phys. Lett. **56**, 2240 (1990); Erratum published Appl. Phys. Lett. **57**, 1169 (1990).

[ROB74] F. N. H. Robinson, *Noise and fluctuations in electronic devices and circuits*, Oxford Monographs in Electrical and Electronic Engineering, (Oxford University Press, London, 1974).

[ROM89] Gian Luca Romani, "The use of SQUIDs in the study of biomagnetic fields," in *Superconducting Electronics*, H. Weinstock and M Nisenoff eds., NATO ASI Series, Vol. F 59, (Springer-Verlag, Berlin, Heidelberg, 1989), pp. 149-174.

[RSI89] Tapani Ryhänen, Heikki Seppä, Risto Ilmoniemi, and Jukka Knuutila, "SQUID magnetometers for low-frequency applications," J. Low Temp. Phys. **76**, 287 (1989).

[RUM69] E. Rumbo, "Measurements of thermoelectric power at low temperatures," Phil. Mag. **19**, 689 (1969).

[SAS68] A. R. Sass and W. C. Stewart, "Self and mutual inductances of superconducting structures," J. Appl. Phys. **39**, 1956 (1968).

[SGC93] J. Z. Sun, W. J. Gallagher, A. C. Callegari, V. Foglietti, and R. H. Koch, "Improved process for high-T_c superconducting step-edge junctions," Appl. Phys. Lett. **63**, 1561 (1993).

[SGK93] J. Z. Sun, W. J. Gallagher, and R. H. Koch, "Non-linear hysteresis in thin film SQUID magnetometers," IEEE Trans. Appl. Sup. **3**, 2022 (1993).

[SGK93b] J. Z. Sun, W. J. Gallagher, and R. H. Koch, "Improved magnetic hysteresis in thin film high-T_c SQUIDs," presented at the 4th International Superconductive Electronics Conference, Boulder, CO, August 11-14, 1993 (unpublished).

[STE68] W. C. Stewart, "Current-voltage characteristics of Josephson junctions," Appl. Phys. Lett. **12**, 277 (1968).

[SYZ89] O. G. Symko, W. J. Yeh, D. J. Zheng, and S. Kulkarni, "Magnetic shielding and relaxation characteristics of superconducting $YBa_2Cu_3O_7$ tubes," J. Appl. Phys. **65**, 2142 (1989).

[TEC77] Claudia Tesche and John Clarke, "dc SQUID: Noise and optimization," J. Low Temp. Phys. **29**, 301 (1977).

[TEC79] Claudia D. Tesche and John Clarke, "dc SQUID: current noise," J. Low Temp. Phys. **37**, 397 (1979).

[TGK91] Mohammed E. Tidjani, Ronald Gronsky, John J. Kingston, Frederick C. Wellstood, and John Clarke, "Heteroepitaxial $YBa_2Cu_3O_{7-x}$ - $SrTiO_3$ - $YBa_2Cu_3O_{7-x}$ trilayers examined by transmission electron microscopy," Appl. Phys. Lett. **58**, 765 (1991).

[VBB93] J. Vrba, K. Betts, M. Burbank, T. Cheung, A. A. Fife, G. Haid, P. R. Kubik, S. Lee, J. McCubbin, J. McKay, D. McKenzie, P. Spear, B. Taylor, M. Tillotson, D. Cheyne, and H. Weinberg, "Whole cortex, 64 channel SQUID biomagnetometer system," IEEE Trans. Appl. Sup. **3**, 1878 (1993).

[WAT87] M. K. Wu, J. R. Ashburn, C. J. Torng, P. H. Hor, R. L. Meng, L. Gao, Z. J. Huang, Y. Q. Wang, and C. W. Chu, "Superconductivity at 93 K in a new mixed-phase Y-Ba-Cu-O compound system at ambient pressure," Phys. Rev. Lett. **58**, 908 (1987).

[WEN69] Cheng P. Wen, "Coplanar waveguide: a surface strip transmission line suitable for nonreciprocal gyromagnetic device applications," IEEE Trans. Micro. Theory Tech. **MTT-17**, 1087 (1969).

[WIK81] S. J. Williamson and L. Kaufman, "Biomagnetism," J. Magnetism Magnet. Mat. **22**, 129 (1981).

[WKC90] Frederick C. Wellstood, John J. Kingston, and John Clarke, "Superconducting thin-film multiturn coils of $YBa_2Cu_3O_{7-x}$," Appl. Phys. Lett. **56**, 2336 (1990).

[WKC94] F. C. Wellstood, J. J. Kingston, and John Clarke, "Thin-film multilayer interconnect technology for $YBa_2Cu_3O_{7-x}$," (submitted to Appl. Phys. Rev., 1994).

[WKF90] F. C. Wellstood, J. J. Kingston, M. J. Ferrari, and J. Clarke, "Superconducting thin-film flux transformers of $YBa_2Cu_3O_{7-x}$," Appl. Phys. Lett. **57**, 1930 (1990).

[WKF91] F. C. Wellstood, J. J. Kingston, M. J. Ferrari, and J. Clarke, "Thin-film flux transformers of $YBa_2Cu_3O_{7-x}$," IEEE Trans. Magn. **27**, 2569 (1991).

[YMM93] S. Yamasaki, T. Morooka, N. Matsuda, J. Kawai, N. Mizutani, K. Tsukada, G. Uehara, and H. Kado, "Design and fabrication of multichannel dc SQUIDs for biomagnetic applications," IEEE Trans. Appl. Sup. **3**, 1887 (1993).

[ZIM71] J. E. Zimmerman, "Sensitivity enhancement of superconducting quantum interference devices through the use of fractional-turn loops," J. Appl. Phys. **42**, 4483 (1971).

[ZMH93] Y. Zhang, M. Mück, K. Herrmann, J. Schubert, W. Zander, A. I. Braginski, and C. Heiden, "Sensitive rf-SQUIDs and magnetometers operating at 77 K," IEEE Trans. Appl. Sup. **3**, 2465 (1993).

Appendix A: Calculating the SQUID Inductance

One of the more important problems in designing planar SQUIDs and evaluating their performance is determining their self-inductance. This is a particularly nettlesome issue because unlike the critical current or the junction resistance, there is no straightforward way to measure the inductance of a SQUID. In principle one can pattern an extra set of leads so as to pass a current through the SQUID body (but not crossing the junctions) and then measure the period of SQUID voltage modulation. However, this method suffers from several drawbacks. First, you only measure part of the SQUID inductance. In particular, you don't measure the inductance in the narrow bridges containing the junctions, and this can be considerable for SQUID inductances of 40 pH or less. Second, you have to have a second set of leads to the SQUID which is impossible to do in hindsight. Finally, the mutual inductance from the leads to the SQUID can be as much as 10 or 20% of the total SQUID inductance.

In light of this, it would be useful to have a method of calculating the SQUID inductance given just the geometry and the penetration depth of the material. Surprisingly, the problem does not seem to be of enough general interest to have generated much activity, and I have not found a good example in the literature on how to approach this. Most of what is available has been devoted to the situation where one has a set of parallel-plane transmission lines tightly coupled to one another which can be assumed to be infinitely long (i.e., the spacing between the transmission lines is much smaller than the characteristic length over which they change path). In this case the problem can be reduced to two dimensions by considering a cross section of the striplines. Chang [CHA81] found a fast method of solving this problem through a finite element technique based on an energy minimization algorithm. Unfortunately, this does not address the issue of a planar washer such as a SQUID. Sass and Stewart [SAS68] show that the problem can be reduced to solving Poisson's equation for the superconducting phase, but they do not suggest an

efficient method for solving it (except, again, for the case of superconducting striplines over a ground plane).

In light of this, I have adopted the following rather crude approach to calculating inductances. The idea is to divide a SQUID into several parts each of which has a simple geometry. The inductance for each part is calculated separately using simple analytical formulas and then the results are added together to obtain the total inductance. No attempt is made to account for the effect of one part of the SQUID on the other parts. I note that all of the SQUIDs we make here are variations on the square washer design; i.e., a square superconductor with a square hole in it, possibly with a long slit running down the middle to the hole from the junctions as in the type A SQUID in chapter 3. Any such design can be broken down into geometrical primitives belonging to the following three categories.

Category I: The square washer. I assume that the hole in the center of the SQUID contributes an inductance of $1.25\ \mu_0 d$ where d is the width of the inner hole. This formula is arrived at from numerical calculations performed by Jaycox and Ketchen [JAM81] for a superconducting square washer with no junctions in the limit that the outer diameter is much larger than the inner diameter. For a type B SQUID as defined in chapter 3, an inner hole is well-defined and this formula should apply. For the case of the type A SQUID, where the junctions are on the outside, the inner hole is often not much larger than the width of the slot running up to the junction bridges. In this case the formula is assumed to account for the inductance arising from the circulating currents as they go around the corner at the end of the SQUID.

Category II: Parallel wide strips. This is what one usually has for the upper half of a type A SQUID where the slot runs up to the junctions. For this I use a formula from C. P. Wen [WEN69] for the inductance of normal metal coplanar waveguides at radio frequencies, $L = [K(m)/K'(m)]\mu_0 l$ where K and K' are complete elliptical integrals of the first kind, l is the length of the transmission line, and $m = 1/(1+2b/c)^2$ where b is the width of a single strip and c is the width of the slot between them. K and K' can be evaluated

numerically (see Table 17.3 of ref. [ABS65]) and one finds that K/K' is a slowly varying function of m. For b = 120 μm and c = 10 μm (which are typical values for a 250 μm O.D. type A SQUID) we find K/K' ≈ 1/2.92. I typically use this number for quick calculations of parallel lines with b/c anywhere from 4 to 25. I note, however, that in some earlier published papers the inductance of the slot was estimated using the formula $L = 0.5\mu_0 l$ which was derived by Mark Colclough from an unreferenced source; thus there may be some discrepancies of 20% or so between earlier and later reported values for the inductances of similar objects. (Note in particular the biepitaxial SQUID discussed in chapters 2 and 4 (#K91-109-1SQ3) was reported [MKW91] to have an inductance of 110 pH using the earlier method, whereas now I estimate it to be 96 pH.)

Category III: Parallel narrow strips. For strips whose width is less than the width of the slot, I use an approximation given to me by D. Drung, $L = (\mu_0/\pi) \ln[(4d/w)-(w/d)]\, l$, where l is the length of the strips, d is the distance between the middle of the strips, and w is the width of the strips. This is useful for the inductance of the long, narrow bridges containing the junctions in our bicrystal SQUIDs.

More complicated expressions that yield similar results for the structures in categories II and III can also be found in ref. [GRO46].

LAWRENCE BERKELEY LABORATORY
UNIVERSITY OF CALIFORNIA
TECHNICAL INFORMATION DEPARTMENT
BERKELEY, CALIFORNIA 94720